ABSTRACT

Title of Dissertation: FROM RIBOSOMAL ROTATION TO AUTISM AND CANCER

Sergey O. Sulima, Doctor of Philosophy, 2013

Dissertation Directed by: Professor Jonathan D. Dinman
Department of Cell Biology and Molecular Genetics

The ribosome transits between two main conformational states – non-rotated and rotated - as it progresses through the translation elongation cycle. How this transition is controlled is not known. Here, we present evidence that the essential ribosomal protein L10 regulates this process in yeast ribosomes through a flexible loop located within 13 Å of the peptidyltransferase center. While deletion of the entire loop is lethal, viable mutants in this region were found to promote opposing effects on the natural equilibrium between the two conformational states of the ribosome. Mutants causing rotational disequilibria show defects in essential ribosomal processes including ligand binding, peptidyltransfer, decoding, reading frame maintenance, and gene expression. Large-scale chemical modification analyses of rRNA of the mutant ribosomes identified networks of near-, medium-, and long-range allosteric interactions involved in coordinating intersubunit rotation. These allosteric pathways map from L10 in the core of the large subunit and propagate outward through both subunits, linking all of the functional centers of the ribosome. Mutants of ribosomal protein L3 promoting opposing structural effects suppress the effects of the L10 mutants by re-establishing the correct rotational

equilibrium. This loop is also involved in recruitment of the biogenesis factor Sdo1p as part of a quality control mechanism in which pre-60S subunits undergo a "test drive" before maturation. This suggests that the correct rotational status is important for ensuring late-stage maturation of the large subunit, indicating that the L10 loop is a key regulator of ribosome function throughout the ribosomal life cycle. A model is presented describing how the unidirectionality of translation and ribosomal rotation are powered by this intrinsic mobile loop. Additionally, mutants in this element have been identified in a fraction of T-cell acute lymphoblastic leukemia patients, and these mutants were found to also favor the rotated state. This suggests that a rotational disequilibrium is at the heart of this disease, and a mechanistic model is presented that describes how a ribosomal mutation can lead to cancer, and identifies new treatments. Moreover, analysis of mutations in the essential C-terminal end of L10 linked with autism has provided functional insight into the mechanism of this disorder.

FROM RIBOSOMAL ROTATION TO AUTISM AND CANCER

By

Sergey O. Sulima

Dissertation submitted to the Faculty of the Graduate School of the
University of Maryland, College Park, in partial fulfillment
of the requirements for the degree of
Doctor of Philosophy
2013

Advisory Committee:
Professor Jonathan D. Dinman, Chair
Associate Professor Volker Briken
Professor James N. Culver
Associate Professor Jason D. Kahn
Associate Professor Douglas A. Julin, Dean's Representative

Preface

There is poetry in the real world. Science is the poetry of reality.

-Richard Dawkins

Acknowledgements

I would like to thank my advisor Dr. Dinman for years of mentorship, friendship, and particularly the insight to have a plastic bag in his car. A big thank you to all members of the Dinman lab, past and present, for a fun and cooperative work experience, especially the lab grandma. A special thank you goes to my parents for the nature and the nurture.

Table of Contents

List of Tables

List of Figures

List of Abbreviations

1M7	1-methyl-7-nitroisatoic anhydride
5-FOA	5-Fluoroorotic acid
aa-tRNA	Aminoacyl tRNA
AF	Assembly factor
ARS	Aminoacyl-tRNA synthetase
ATP	Adenosine triphosphate
CP	Central protuberance
Cryo-EM	Cryogenic electron microscopy
DBA	Diamond-Blackfan anemia
DC	Decoding center
EF	Elongation factor
eEF	Eukaryotic elongation factor
eIF	Eukaryotic initiation factor
eRF	Eukaryotic release factor
GAC	GTPase-associated center
GDP	Guanosine diphosphate
GEF	Guanine exchange factor
GGQ	Glycine-glycine-glutamine motif
GTP	Guanosine triphosphate
HIV-1	Human immunodeficiency virus type 1
IF	Initiation factor
IRES	Internal ribosomal entry site

LSU	Large ribosomal subunit
m^7G	7-methylguanosine
mRNA	Messenger RNA
NGD	No-go decay
NMD	Nonsense mediated decay
NRD	Non-functional ribosomal decay
ORF	Open reading frame
PABP	Poly-A binding protein
Pol	Polymerase
Poly A	Poly-adenosine
PRF	Programmed ribosomal frameshifting
PTC	Peptidyltransferase center & premature termination codon
RF	Release factor
RP	Ribosomal protein
RRF	Ribosomal recycling factor
rRNA	Ribosomal RNA
SARS	Severe acute respiratory syndrome
Sec	Selenocysteine
SHAPE	Selective 2'-hydroxyl acylation analyzed by primer extension
snoRNAs	Small nucleolar RNAs
SRL	Sarcin-ricin loop
SSU	Small ribosomal subunit
T-ALL	Acute T-cell lymphoblastic leukemia

tRNA   Transfer RNA

YPAD   Yeast media containing: yeast extract, peptone, adenine sulfate, dextrose

Chapter 1

Introduction

Faithful conversion of genomic information into functional proteins is central to life. In all domains of life, this is accomplished by the largest RNA-protein complex in the cell, the ribosome, in a process called "translation". The ribosome translates the information contained in messenger RNAs (mRNAs) into polypeptide chains with tremendous speed and accuracy, linking the nucleic acid and protein worlds. There are significant differences in both the assembly and structure of eukaryotic ribosomes as compared to their bacterial counterparts: these are the basis for approximately half of our current arsenal of antibiotics. However, given the rapid emergence of antibiotic resistance, increasing our understanding of ribosome mechanics is critical. From a mechanistic point of view, the ribosome can be viewed as a model "nanomachine." In addition to rational drug development, studies of the wiring and workings of the machine provide a platform for the understanding of macromolecular assembly and function. Defects associated with this nanomachine and canonical translation have broad impacts on human health including birth defects, cancer, heart and lung diseases, connective tissue disorders, and mental retardation. Viruses, immune to antibiotics and reliant on ribosomes, have evolved ways to subvert canonical translation strategies. Despite all this, ribosomal molecular mechanics and dynamics, as well as mechanisms of quality control of ribosome assembly, are not well understood. Understanding of these important areas will provide the foundation for the design of new classes of anti-bacterial and anti-viral drugs, nanodevices, and treatment of translation-linked diseases.

Ribosome History and Anatomy

The ribosome is thought to have originated in the pre-biotic world where it evolved to bridge the realms of RNAs and proteins and was first detected approximately 3.5 billion years later as a "small particle" by Albert Claude in the early 1940s [1,2]. It was not until the 1950s that these so-called "microsomes", operationally defined in terms of sedimentation, optical inspection, and chemical composition, became linked on experimental grounds to protein synthesis [3–6]. Purification of microsomes was the major breakthrough in allowing development of cell-free protein synthesis systems in 1955. Around the same time, through the novel technique of transmission electron microscopy George Palade was able to obtain images of the microsome in the cytoplasm as well as on the endoplasmic reticulum, for which he won the Nobel Prize in 1974 [7,8]. These images provided the first insights into the structure of these small particles, and similar techniques were the basis for the very first strikingly accurate 3D models developed by James Lake and shown in Figure 1. After a few transient aliases including "deoxycholate-insoluble" and "ribonucleoprotein particle", Howard Dintzis coined the term "ribosome" for purified microsomes in 1958 based on the presumed role of the particle's large RNA content (rRNA) [9]. This was also the year of the first ribosome symposium. The following "golden age of translation" of the 1960s saw the discovery of mRNA, the dissection of the ribosome into its components, and the resolution of the translational process into partial functions. Much of this golden age, as well as the myriad breakthroughs in the field between the 1970s and the 1990s, will be referred to in later sections and chapters.

30S
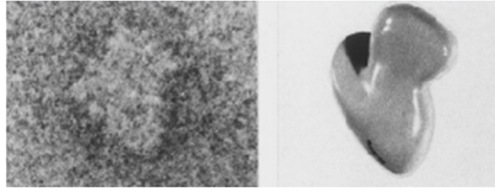
50S
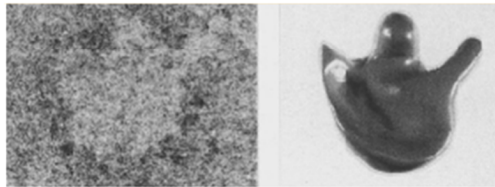
70S
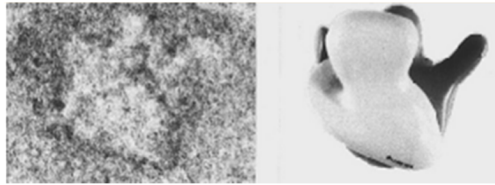
Figure 1. Electron microscopy images of bacterial ribosomes.
Electron microscopy images from 1973 reveal the shape of the ribosomal subunits. These images were used by James Lake to construct the very first ribosome models on the right. Parts of the image obtained from Wittman [10].

More recently, the major focus in the field has shifted to high resolution structural analyses. At the turn of the century the combined efforts of several groups resulted in the elucidation of eubacterial ribosomal structures at the atomic level, revealing in detail this complex macromolecule and its discrete functional centers [11,12,13]. This work was awarded the Noble Prize in chemistry in 2009. Shortly after, ribosomal X-ray crystallographic structures at the atomic level became available for the yeast *Saccharomyces cerevisiae* [14,15]. As of 2013, lower resolution structures obtained through cryogenic electron microscopy exist for complete fruit fly and human ribosomes [16], as well as for the small subunit of rabbit ribosomes [17]. The ribosome consists of two

subunits defined by the sedimentation coefficient S: the large subunit (LSU, 50S in prokaryotes and 60S in eukaryotes) and the small subunit (SSU, 30S in prokaryotes and 40S in eukaryotes). These subunits have distinct functions, but must also interact with one another along with numerous *trans*-acting factors to form a holoenzyme that coordinates a complex series of events. The secondary and tertiary structures of the ribosomal core (the "proto-ribosome"), including the active site, are well conserved across all domains of life. However, the eukaryotic ribosome is much larger and more complex, containing additional RNA in the form of so-called expansion segments as well as many additional proteins or protein extensions. As a result, its construction is fundamentally different in many key ways. Mitochondrial ribosomes, consisting of 28S and 39S subunits, structurally more closely resemble prokaryotic ribosomes – one of the strongest supports for the endosymbiotic theory of cellular evolution [18,19].

Compared with the 4500 nucleotides of rRNA and 54 proteins of the bacterial 70S ribosome, the yeast 80S ribosome contains 5500 nucleotides of rRNA (SSU: 18S rRNA; LSU: 5S, 5.8S, 25S rRNA) and 79 proteins (LSU and SSU proteins are prefixed with "L" or "S" respectively). The structural landscape of the 3.6 MDa yeast ribosome is shown in Figure 2. The SSU contains the mRNA decoding center (DC), a region responsible for reading the mRNA to ensure proper acceptance of transfer RNAs (tRNAs), and the tunnel through which mRNA moves. The most salient structural feature in the SSU is the flexible "head" domain. The LSU harbors the catalytic peptidyltransferase center (PTC) at its core, the exit tunnel for the growing polypeptide chain, three tRNA binding pockets and a single binding site that must distinguish between elongation and release factors in response to specific circumstances. The main structural features of the 60S include the

stalk which consists of proteins L7 and L12 and is required for factor binding, and the central protuberance (CP) which consists of L11 and 5S rRNA.

The yeast ribosome is an RNA-protein complex and has an approximate 1:1 RNA to protein mass ratio. It is the largest and most abundant natural ribozyme, and is also the only natural RNA-based polypeptide polymerase. Ribosomal RNA is highly modified, containing over 100 modifications including base methylations, ribose 2'-hydroxyl methylations, and the most common nucleotide modification – pseudouridylations. Mice and humans with impaired pseudouridylation develop cancer and dyskeratosis congenita [20,21]. Moreover, out of the 25 non-canonical basepair types, 20 are present in the ribosome [22]. A balance between flexibility and rigidity is achieved through a plethora of structural RNA elements and motifs including tetraloops, E-loops, U- and K-turns, purine stacks, coaxial stacking, ribose zippers, and most commonly – the A-minor motif [23]. Most ribosomal proteins contain globular portions that tend to localize to the solvent sides of the two subunits, as well as non-globular solvent-inaccessible and flexible extensions or "tails" interacting with the rRNA core. Historically, it was first thought that ribosomal proteins were the central players in ribosome function while rRNA was relegated to a minor, scaffolding function. As understanding of the ribosome progressed and it was established that catalysis occurs in an entirely RNA-based environment, these perceived roles were almost completely reversed. However, more recently ribosomal proteins have begun to be appreciated as being more than just the structural glue: it has been shown that over half are essential, and a small set of ribosomal proteins are even required for catalytic activity [24,25]. Thus, the 1:1 RNA to protein mass ratio is likely also indicative of the contribution of each to ribosomal structure and function.
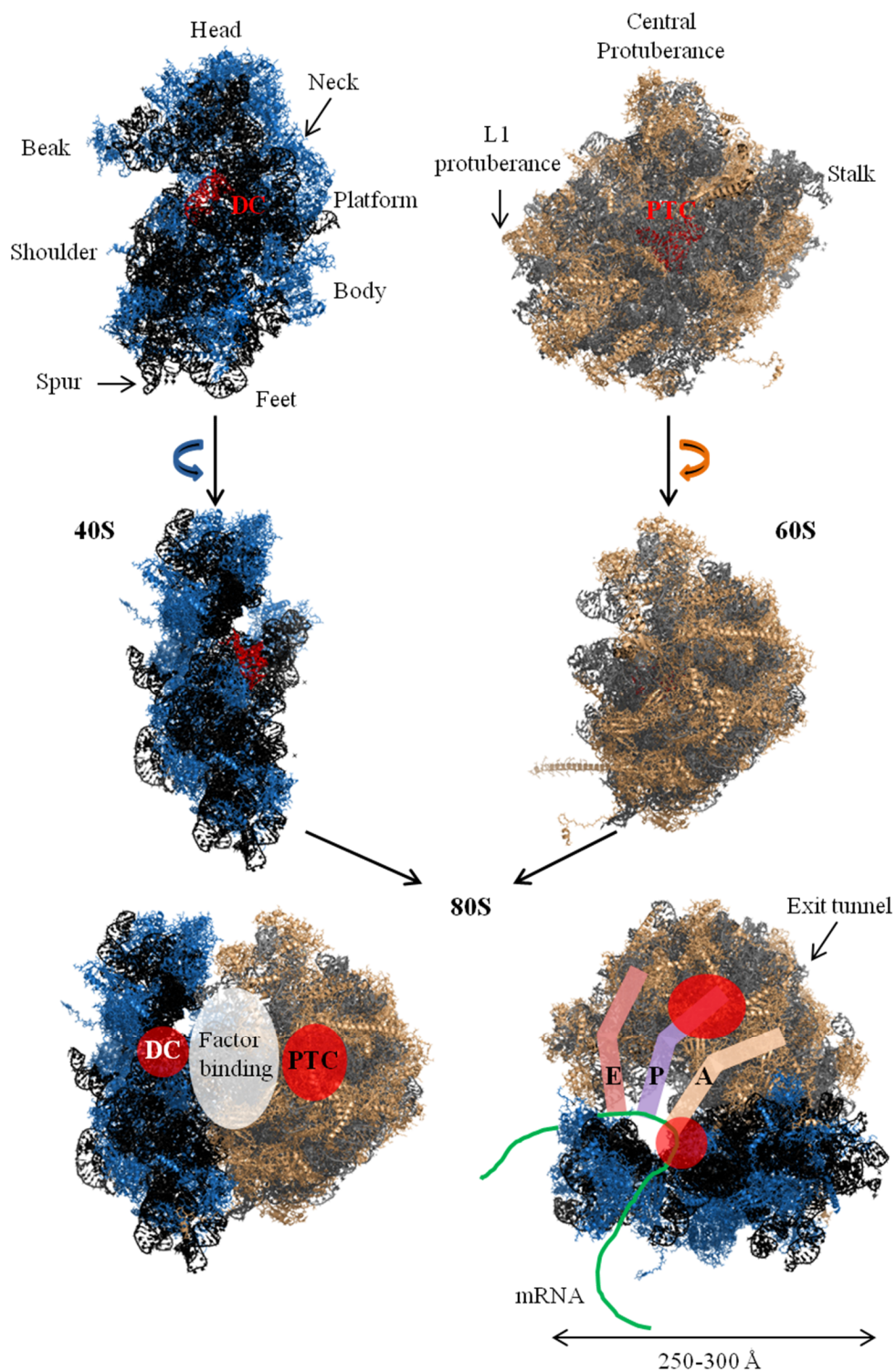
Figure 2. Yeast ribosome structure.

Subunits are shown from the intersubunit face view (top), side (middle) and in the 80S context (bottom). Proteins = blue/brown; rRNA = black/grey. Generated from 3 Å crystallography structures using PyMOL (PDB code: 3U5B/C/D/E) [26].

The 80S ribosome must function as one unit. To this end, the interaction surface between the two subunits contains 17 connecting intersubunit bridges to provide communication pathways and structures [15]. These bridges consist of RNA:RNA, protein:protein, and RNA:protein interactions and are shown in Figure 3. Because the two subunits must dynamically interact with one another as the ribosome undergoes global conformational rearrangements during translation, some of these intersubunit bridges (such as B3) consist of strong permanent interactions, while others (such as B7a) are malleable in composition and can thus break and reform throughout translation.
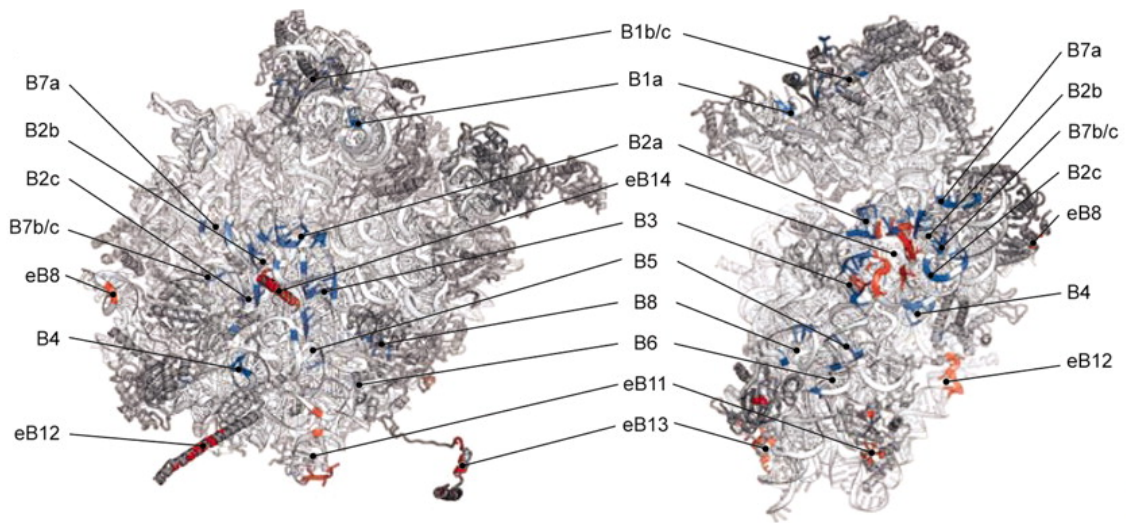
Figure 3. Location of ribosomal intersubunit bridges.
Out of the 17 intersubunit bridges, B1b/c is the only protein:protein bridge, while all others are RNA:protein or RNA:RNA. Image from Ben-Shem [15].

Precise subunit interactions are necessary to guide tRNAs through the ribosome. The job of the 20 tRNAs, each 75-90 nucleotides long and carrying one specific amino acid, is to provide the ribosome with building blocks for protein synthesis. Transfer RNAs are the most modified RNA molecules: 80 modifications out of a total of 95 reported have been observed in tRNAs [27]. The secondary and tertiary tRNA structure is shown in Figure 4. Based on base complementarity, the secondary structure of a tRNA can be drawn as a cloverleaf containing 4 stems. Five regions of the tRNA are not base paired: the CCA acceptor stem, the D-loop and T-loop, the anticodon loop and the variable "extra arm". These structural elements result in an L-shaped molecule upon folding and allow tRNAs to interact with both the mRNA in the SSU (the anticodon) and the PTC in the LSU (3' CCA end). As tRNA molecules interact with the ribosome they move through a distinct path through functional sites on the ribosomes. There are well defined tRNA binding sites along this path: the A- and P- sites, where the aminoacyl- and peptidyl-tRNAs reside before peptide bond formation, and the E-site, from which deacylated or "used" tRNAs exit the ribosome [28]. While high resolution structures of yeast ribosomes bound with tRNAs do not exist, such structures have been resolved in the bacterium *T. thermorphilus*, shown in Figure 5.
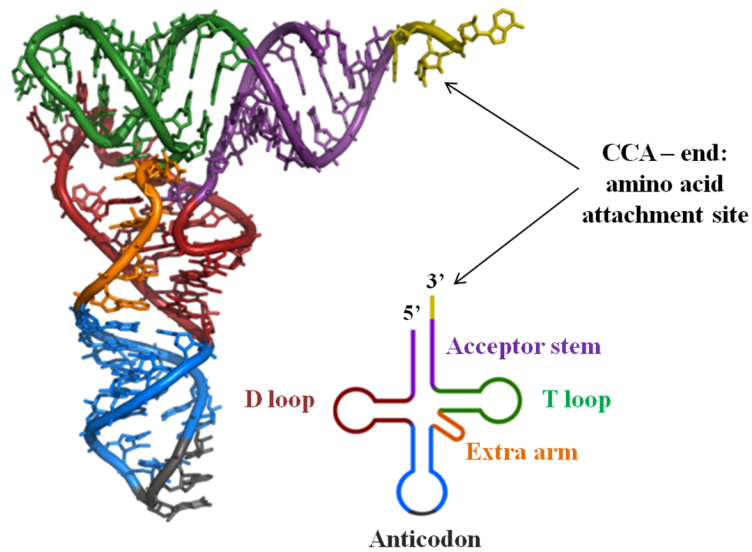
Figure 4. tRNA structure.

Non base-paired regions form the 4 shown loops. The anticodon interacts with the decoding center in the SSU, while the acceptor stem is covalently linked to the appropriate amino acid and interacts with the PTC in the LSU. Image modified from Griffiths-Jones [29].
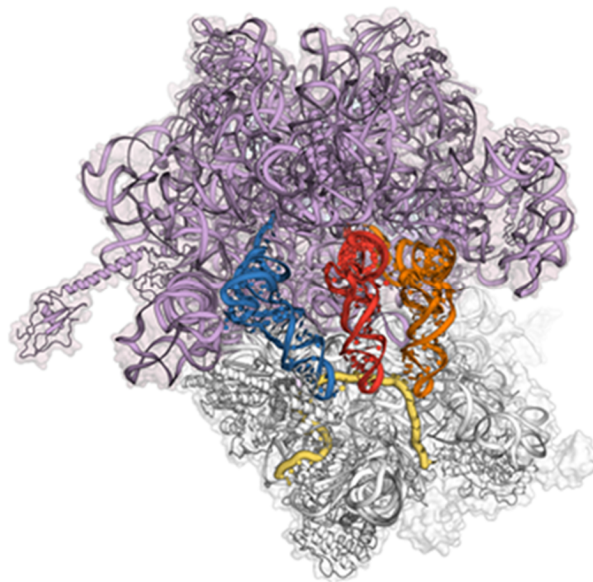
Figure 5. Position of tRNAs on the 70S ribosome.

tRNAs in A, P and E sites are orange, red and blue, respectively, and mRNA is yellow. Image from Yusupov [28].

Ribosome Biogenesis and Disease

Healthy yeast cells contain approximately 200,000 ribosomes distributed throughout the cytoplasm as well as bound to the endoplasmic reticulum (the "rough" part of it), where proteins of the intra-cellular transport system are translated [30]. Up to 2000 ribosomes are produced per minute per cell to keep up with such a demand. Impaired ribosome assembly is the underlying cause of the set of pathological conditions known as ribosomopathies. As such, accurate piece by piece ribosome assembly and subsequent quality check are essential components of ribosome biogenesis.

Ribosome Assembly Overview

Ribosomes must be assembled from rRNA and proteins in a complicated and energetically demanding process taking place in both the nucleus and cytoplasm of cells. In prokaryotes, *in vitro* reconstitution of functional ribosomal subunits from purified or *in vitro* transcribed rRNAs and ribosomal proteins has been demonstrated, and assembly maps for both subunits have been constructed [31–34]. Ribosome assembly in eukaryotes is much more complex, and reconstitution such as seen in bacteria has never been achieved. Most of the knowledge pertaining to eukaryotic ribosome biogenesis comes from studies in yeast. Unlike in prokaryotes, in which ribosome biogenesis is determined and driven by the intrinsic properties of its rRNA and proteins and follows an established assembly gradient, yeast ribosome assembly involves transient association of ~200 essential accessory proteins, *trans*-acting assembly factors that do not form part of the mature ribosome structure [35,36]. These proteins include GTPases, ATPases, kinases, helicases and chaperones and promote essential functions such as rRNA processing, modification and

folding, and assembly of ribosomal proteins. Eukaryotes also bear the added burden of exporting immature ribosomal subunits from the nucleus to the cytoplasm. A summary of the subunit processing pathway including known factors is given in Figure 6.

In yeast, the assembly process begins in the nucleolus, a specialized subcompartment of the nucleus that is organized around the rDNA transcription units. 18S, 25S and 5.8S rRNA are transcribed in the nucleolus as a 35S polycistronic precursor rRNA by RNA polymerase I. This pre-rRNA undergoes a series of endonucleolytic cleavages and exonucleolytic trimmings, along with extensive modifications by ~70 small nucleolar RNAs and protein co-factors into the final 18S, 25S and 5.8S rRNAs, which serve as the catalytic core of the ribosome [37]. The 5S rRNA is transcribed by RNA polymerase III in the nucleoplasm, undergoes maturation in the cytoplasm, and is transported to the nucleolus in complex with L5 and L11 [38]. Similarly, ribosomal protein mRNAs are transcribed by RNA polymerase II in the nucleoplasm, translated into mature proteins in the cytoplasm, after which they are transported back to the nucleolus for additional processing steps. These steps consist of the formation of numerous assembly intermediates, including a 90S pre-ribosome that begins to fold and associate with ribosomal proteins, cleavage steps resulting in 43S and 66S preribosomal particles, and their transport from the nucleolus into the nucleus and subsequently the cytoplasm for final rRNA processing and protein assembly events [39]. Both subunits are exported with a small complement of non-ribosomal *trans*-acting factors, some of which (Nmd3) facilitate export while others (Tif6) prevent the premature interaction of the ribosomal subunits. These factors must be released in the cytoplasm and shuttled back to the nucleus for subsequent rounds of maturation and export. After this recycling step, the

11

fully assembled and mature subunits can interact to form translationally active 80S ribosomes.

While the sequence of events constituting 40S cytoplasmic maturation is largely unknown, the recently established order of 60S cytoplasmic maturation steps is shown in Figure 7 [40]. Maturation is initiated by the ATPase Drg1 which facilitates the replacement of Rlp24 by Rpl24, which in turn recruits Rei1. Together with Jjj1 and Ssa1/Ssa2, Rei1 enables the release of the export receptor Arx1, freeing up the polypeptide exit tunnel. Concurrently, Yvh1 enables replacement of Mrt4 with P0 to form the foundation upon which the ribosome stalk is constructed. At this point the last component that is part of the final mature subunit, ribosomal protein L10, is incorporated. This is followed by the recruitment of the Efl1:Sdo1 complex and the subsequent Sdo1-induced GTP hydrolysis by Efl1 to release the anti-association factor Tif6 from the subunit joining face of the subunit. The release of Tif6 leads to activation of Lsg1 to release the export adaptor Nmd3 from the joining face - the last step of 60S maturation.
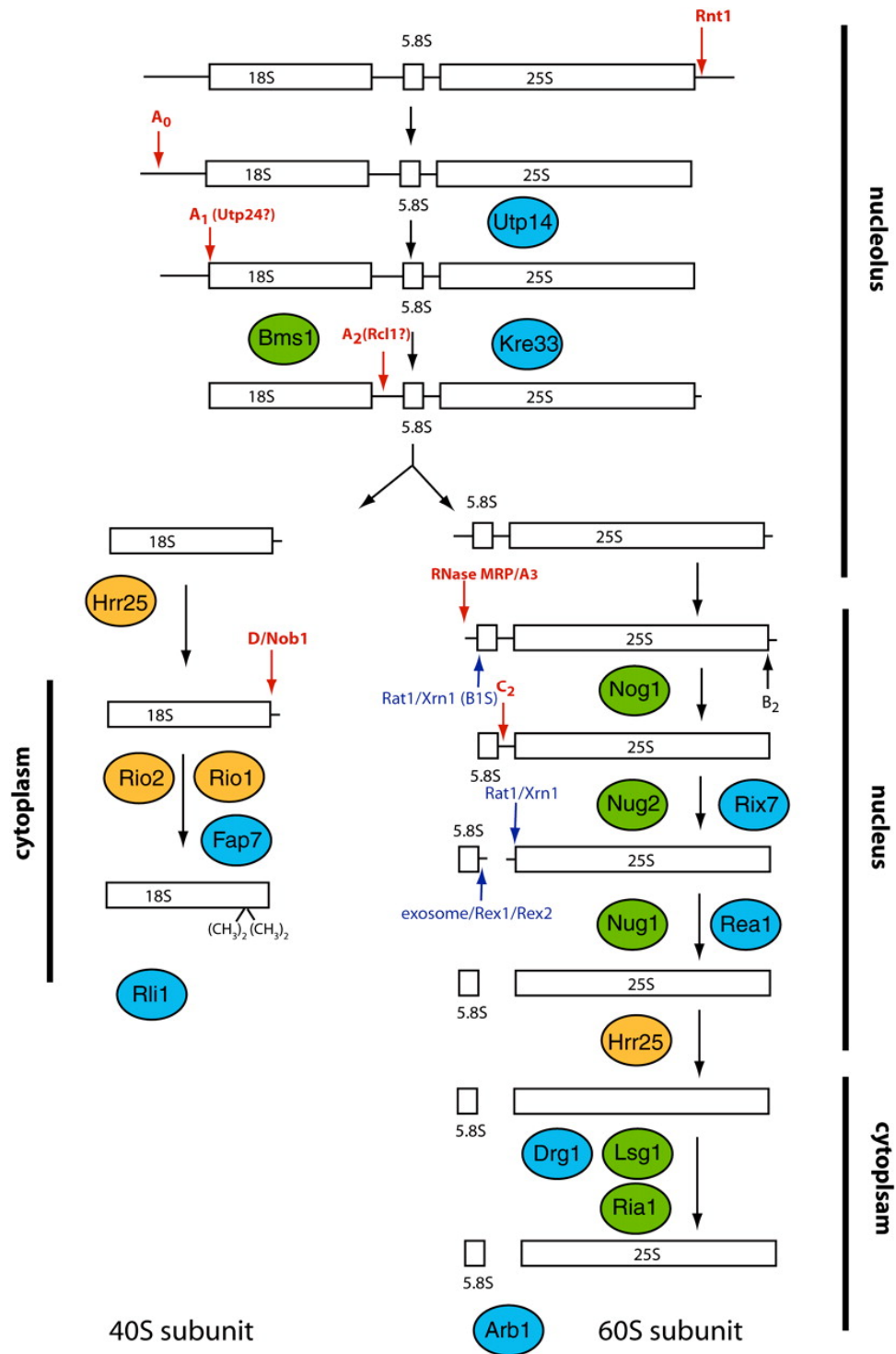
Figure 6. Ribosomal subunit biogenesis summary.

Red arrows = endonucleolytic steps; blue arrows = exonucleolytic steps; cyan = ATPases; green = GTPases; orange = kinases. Figure is from Strunk [41].
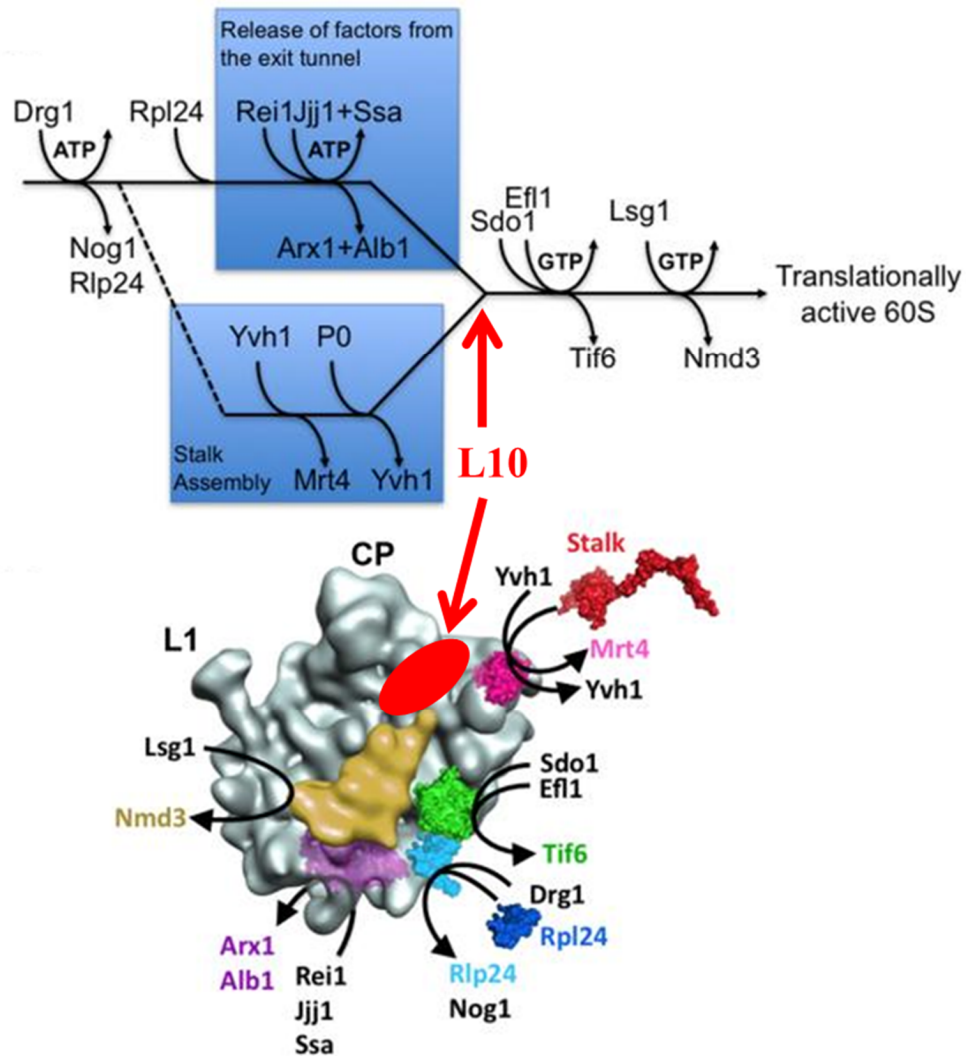
Figure 7. Pathway of 60S maturation in the cytoplasm.

The ribosomal stalk is assembled in the cytoplasm which, along with incorporation of L10, enables the recruitment of the G-protein Efl1 in complex with Sdo1. This results in the GTP hydrolysis induced dissociation of Tif6 and Nmd3 and a mature 60S subunit. Figure modified from Lo [40].

In addition to central roles in cell viability, ribosome biogenesis and protein synthesis are two of the most energy consuming processes in a growing cell. Thus it is critical for cells to have evolved a surveillance system for monitoring proper assembly of the translational machinery. It was recently demonstrated that pre-40S subunits undergo a proofreading step late during their cytoplasmic maturation [42]. This involves a translation-like cycle, whereby mature 60S subunits join pre-40S subunits in an eIF5B (eukaryotic initiation factor 5B)-dependent manner. However, the resulting 80S-like ribosomes are not translationally active, as they do not contain mRNA or initiator tRNA. Rather, this translation-like cycle serves as a final quality control step in which major functions of the maturing small subunit, such as binding to 60S subunits and to translation factors, are tested. Along the same lines, a "test drive" of immature 60S subunits has recently been reported by our lab and will be discussed in more detail in chapter 2.

Ribosome Assembly Defects

Given the essential role ribosomes play in the central dogma of biology, it is likely that defects in translation would result in wide-spread deleterious phenotypic effects. However it was not until recently that disorders of ribosome dysfunction, collectively called ribosomopathies, were described [43]. In 1999, recurrent mutations in the ribosomal protein gene *RPS19* were reported in patients with Diamond-Blackfan anemia (DBA), a rare congenital bone marrow failure syndrome [44]. Since then, mutations in a number of ribosomal proteins have been identified in up to 50% of patients with DBA. Moreover, other congenital syndromes have been linked to non-RP related ribosomal

defects and include Schwachman-Diamond syndrome, X-linked dyskeratosis congenita, cartilage hair hypoplasia, and Treacher Collins syndrome [45]. In addition, the 5q− syndrome, a subtype of myelodysplastic syndrome, is caused by a somatically acquired deletion of chromosome 5q, which leads to haploinsufficiency of the ribosomal protein S14 and an erythroid phenotype highly similar to Diamond-Blackfan anemia [46]. The genetic abnormalities in all of these disorders cause defects in a step in ribosome biogenesis, shown in Figure 8, and lead to a higher incidence of cancer.

A precise mechanism of ribosome biogenesis impairment has recently been described for Schwachman-Diamond syndrome (SDS), an inherited bone marrow failure syndrome [47]. SDS has an incidence estimated at 1 in 50 000 births and is characterized by a strong predisposition to leukemia, with bone marrow transplantation as the only definitive therapy. Approximately 90% of SDS cases are caused by mutations in the *SBDS* (Shwachman-Bodian-Diamond syndrome) gene. The SBDS protein functions in a late step in the cytoplasmic maturation of 60S subunits by promoting the release of eIF6 (eukaryotic initiation factor 6) from pre-60S subunits. This *trans*-acting factor keeps the nascent 60S subunit in a functionally inactive state during cytoplasmic 60S assembly, but needs to be released for final 60S maturation. Much like its yeast homolog Sdo1, SBDS appears to promote the release of eIF6 by stimulating the GTPase activity of Efl1. The mutant form of the protein in SDS patients is unable to release eIF6 as efficiently and hence stalls 60S maturation.

The causes of the hypo-proliferative clinical symptoms of most ribosomopathies, such as anemia and dystosis, have recently been linked to the tumor-suppressor protein p53 [48]. This protein is known to play a fundamental role in the surveillance of protein

translation, and recent studies show that it can be activated by ribosome dysfunction. The HDM2 protein (Human Double Minute 2) can bind many ribosomal proteins and is a central regulator of p53, acting as a ubiquitin ligase that leads to p53 degradation, thereby providing a link between ribosome biogenesis and the p53 pathway: a disruption in ribosome biogenesis leads to an accumulation of free ribosomal proteins binding HDM2, the inhibition of HDM2 activity, and the consequent accumulation of p53 and apoptosis [49]. However, how clinically *hypo*-proliferative diseases can also cause *hyper*-proliferation (cancer) is unclear and will be addressed in Chapter 3.
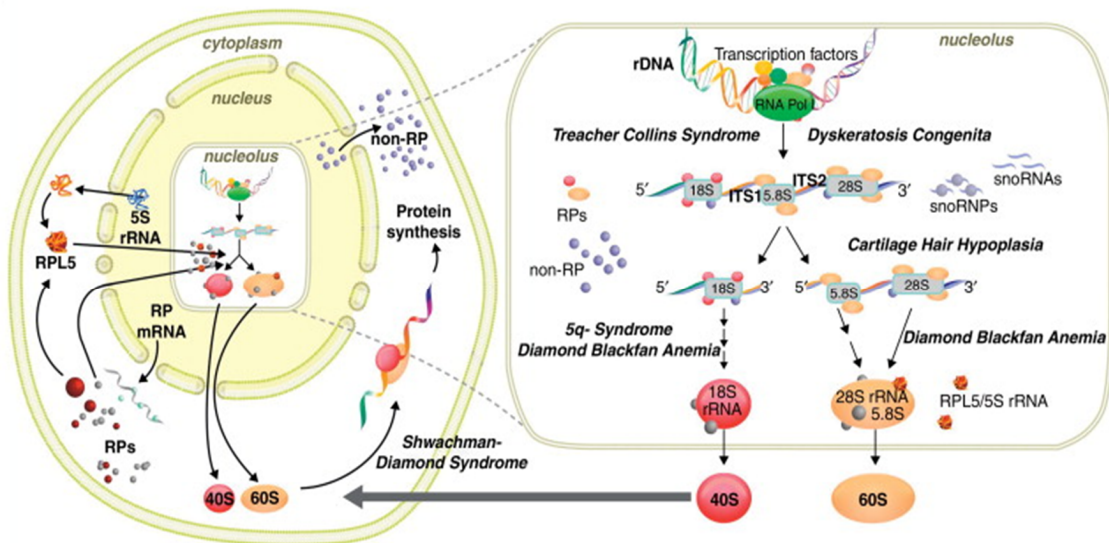
Figure 8. Ribosome biogenesis and disease.
The step in ribosome biogenesis that is thought to be affected by each ribosomopathy is depicted. Image from Teng [50].

Ribosome Function

<u>Translation</u>

Once properly assembled, ribosomes can begin synthesizing polypeptides. Protein synthesis is remarkably fast: elongation of the polypeptide chain by one amino acid occurs in approximately 60 ms [51]. It is also highly accurate, making approximately 1 error every 10^3 - 10^4 codon reads [52]. Several ribosomes may translate a single mRNA molecule at the same time, resulting in a "polysome" which is shown in Figure 9. As with other polymerization reactions, the translational process is divided into the phases of initiation, elongation, and termination and is assisted by a multitude of essential *trans*-acting factors. A fourth less understood phase comprises ribosome recycling. During initiation the 80S ribosome is assembled on the mRNA and is guided to a start codon, marking the beginning of the protein product. The bulk of translation happens during elongation, when new amino acids are continuously added to the growing polypeptide chain as the ribosome moves one triplet codon at a time along the mRNA. Upon reaching a stop codon, the full-length protein is released by specialized release factors during the termination phase of translation. The 80S complex may either be recycled back to the beginning of the message for another round of translation or dissociate to begin translation of another message.
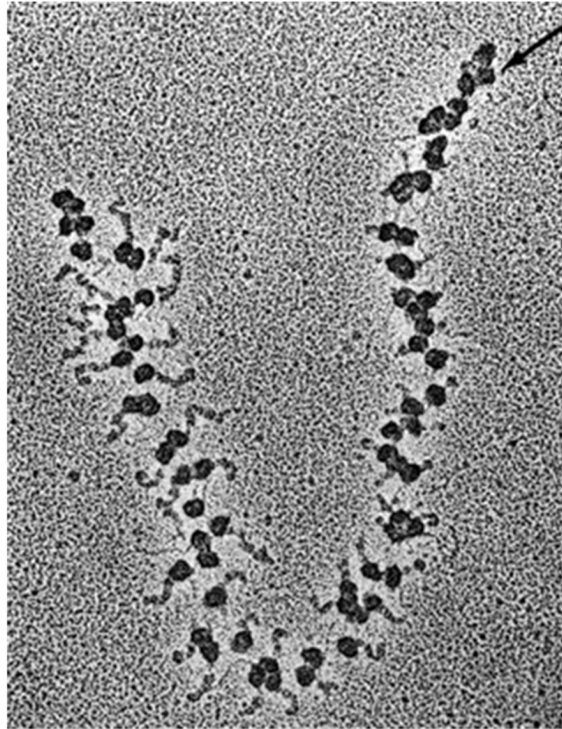
Figure 9. Electron micrograph of a polysome chain.
The beginning of the mRNA is to the right (at the arrow) and the end is to the left. The synthesized polypeptide can be seen growing longer and longer, the further along the ribosome is positioned along the message. Image obtained from the official website of the Nobel Prize Foundation [53].

Initiation

Initiation is a major rate-limiting step of translation, and is thus the principal target for regulation [54]. In eukaryotes, this process involves a series of initiation factors (eIFs) and is depicted in Figure 10. The starting point for assembly of the initiation complex is the production of free small subunits. Binding of eIF1A and eIF3 to the SSU prevents premature association with 60S [55]. The initiator methionine tRNA (Met-tRNA$_i^{Met}$) is delivered to the SSU in an initiation ternary complex containing eIF2 coupled with GTP. The eIF1A and eIF3 stimulate binding of the ternary complex to form

a 43S pre-initiation complex [56]. Before mRNAs can be bound by this complex they must first interact with several factors. Particularly, the 3' poly-A tail of the message is recognized by the Poly-A Binding Protein (PABP), while the 5' 7-methylguanosine cap (m^7G) is bound by eIF4E. The scaffold factor eIF4G interacts with both these components, linking the 5' and 3' ends of the mRNA thereby circularizing the message [57]. This results in a translationally competent "closed loop" message which is able to interact with the 43S pre-initiation complex. The eIF4G facilitates 43S binding near the 5' cap by interactions with eIF3, resulting in a 48S pre-initiation complex. Powered by ATP hydrolysis of eIF4A, this complex begins scanning the mRNA towards the 3' direction in search of a start codon. Pairing of the anticodon of Met-tRNA$_i^{Met}$ with the AUG start codon in the ribosomal P-site triggers GTP hydrolysis by eIF2, stimulated by the concerted action of the GTPase activating protein eIF5 and the 40S itself [58–62]. All the initiation factors are subsequently released, and the 60S is able to associate with the 40S complex, with the Met-tRNA$_i^{Met}$ stably occupying the ribosomal P-site. The eIF2-GDP is recycled to the eIF2-GTP by the guanine exchange factor (GEF) eIF2B to enable the reassembly of the ternary complex. Rare eukaryotic initiation from the ribosomal A-site has also been described, suggesting that the repertoire of translation initiation may be greater than anticipated [62].
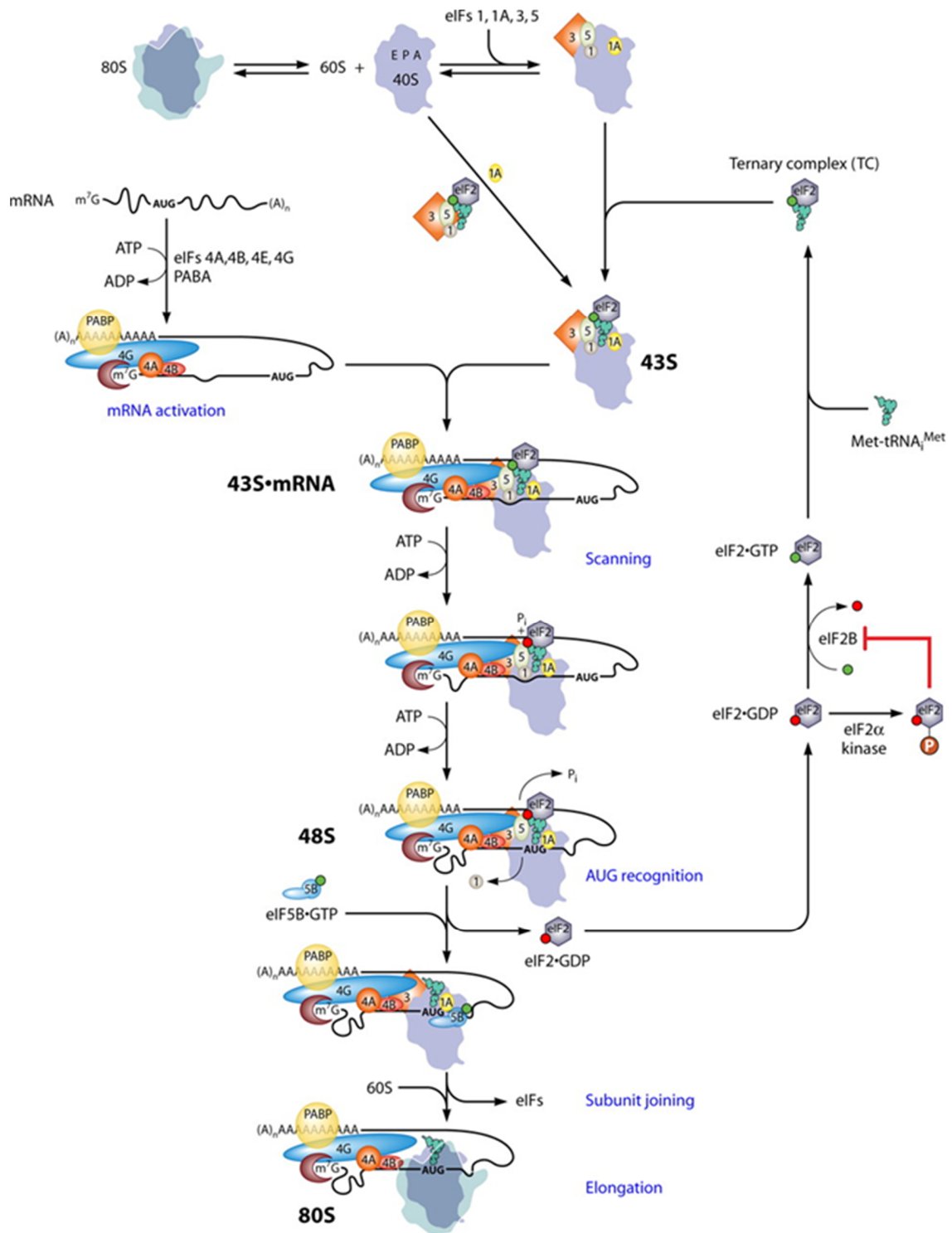
Figure 10. Eukaryotic initiation summary.

Known steps and factors are indicated. The GEF eIF2B is inhibited by the phosphorylation of eIF2 of its α subunit by various kinases, activated by different kinds of stress. Image from Hinnenbusch [63].

As discussed above, successful initiation is reliant on the formation of the "closed loop" structure that results from mRNA circularization, shown in Figure 11. Many viruses have evolved unique methods to fulfill the need for features of translationally competent eukaryotic mRNAs. For example, flu viruses can obtain their own 5' m^7G caps through a cap-snatching endonuclease [64]. This results in the capping and translational activation of viral mRNAs, while simultaneously rendering cellular mRNAs inactive. In another approach, picornaviruses covalently attach a VPg (viral protein genome-linked) protein to the 5' ends of their mRNA. The VPg mimics a 5' cap and is able to interact with initiation factors, thereby fulfilling the function of the cap [65,66]. Another successful viral initiation strategy bypasses the need for a 5' cap and other cellular mRNA features altogether. Instead, some viruses have evolved Internal Ribosomal Entry Site elements (IRES elements) [67,68]. These are special secondary structures located at the 5' end of viral mRNAs, some mimicking tRNAs and interacting with initiation factors, which can recruit ribosomes and direct them to initiate internally. Many IRES elements of various shapes and sizes have been described, and some are shown in Figure 12. The key for viruses is to lure the ribosome onto its message and to overcome the rate-limiting step of initiation. More recently, such IRES elements have also been described in eukaryotes [69,70,71]. IRES-mediated cellular translation appears to be favored under circumstances when cap-dependent translation is compromised, such as starvation conditions [72].
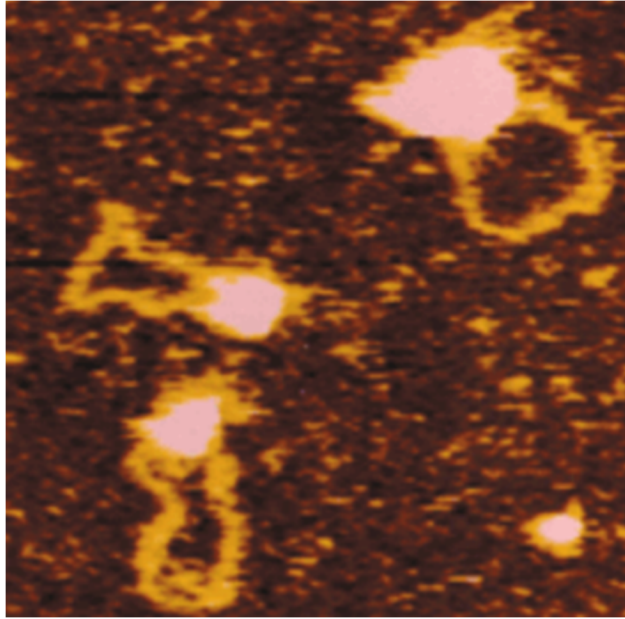
Figure 11. The "closed loop" mRNA structure.

Atomic force microscopy reveals complexes formed on circularized, translationally active mRNAs. Image from Mendez [73].
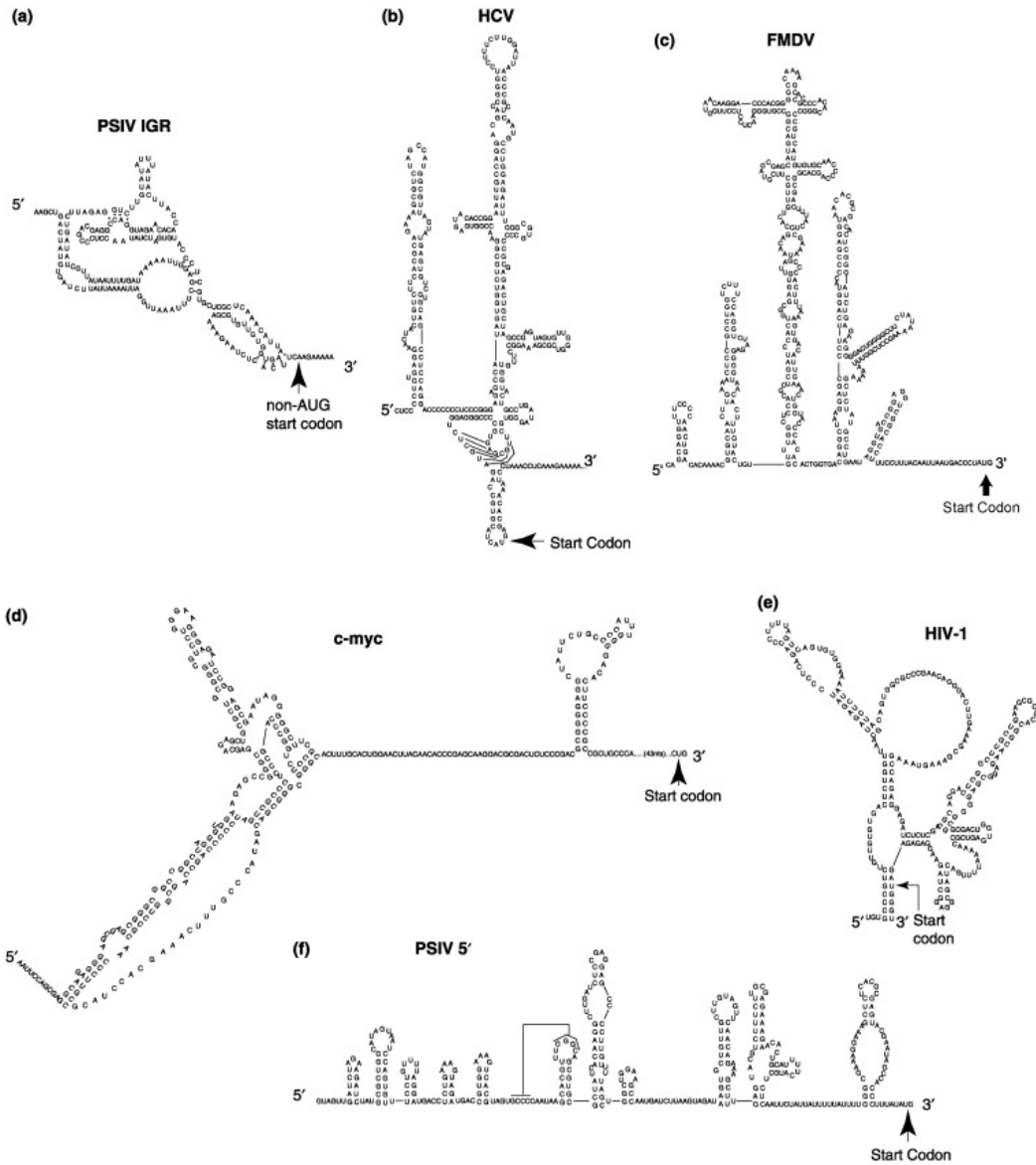
Figure 12. Examples of viral and cellular IRES secondary structures.
IRES elements in Plautia stali intestine, Hepatitis C, Foot-and Mouth Disease, and Human Immunodefiency virus genes are shown, as well as in the human proto oncogene c-Myc. Image from Filbin [74].

Once stably established on the mRNA during initiation, the ribosome elongates the polypeptide chain by reading one codon at a time and relying on tRNAs and elongation factors (eEFs) to supply the correct amino acid at each codon. This is when the bulk of protein synthesis occurs and is the fastest phase of translation.

tRNA charging, selection and accommodation

The first step in elongation is to bind a tRNA carrying an amino acid to the ribosomal A-site. Before this can happen, tRNAs need be activated or "charged" - covalently linked with an amino acid by a class of enzymes called aminoacyl-tRNA synthetases (ARS). Although codon:anticodon is the key interaction directing translation, the correct recognition of and aminoacylation of the tRNA by its cognate synthetase is of comparable importance and can be regarded as a second genetic code. Mis-charging of tRNAs can lead to the incorporation of the wrong amino acid and production of an aberrant protein product. Every cell requires an ARS for each of the 20 amino acids of the genetic code. Correct aminoacylation depends on the selection of two appropriate substrates by the corresponding ARS: the tRNA and the amino acid. While tRNAs are large and specific and can be easily distinguished, amino acids must be distinguished solely by the nature of their side chains. The aminoacylation reaction which takes place at a site of the enzyme called "the synthetic site" occurs in two steps [75]. The amino acid is first activated by ATP-driven adenylation and is then transferred to the CCA end of the cognate tRNA. Steric exclusion of amino acids with larger side-chains and recognition of specific properties of each amino acid generally make this synthetic site specific enough

so that only the correct amino acid can be activated and transferred. However, amino acids having similar properties to and a smaller size than the cognate amino acid can be mis-activated at frequencies that are too high to maintain an unambiguous code. As a consequence, enzymes facing this problem have evolved a second active site for proofreading called "the editing site", where mis-activated amino acids or mis-acylated tRNAs are hydrolyzed [76–79]. The presence of two catalytic sites with different activities led to the "double-sieve" model of fidelity and is shown below in Figure 13.
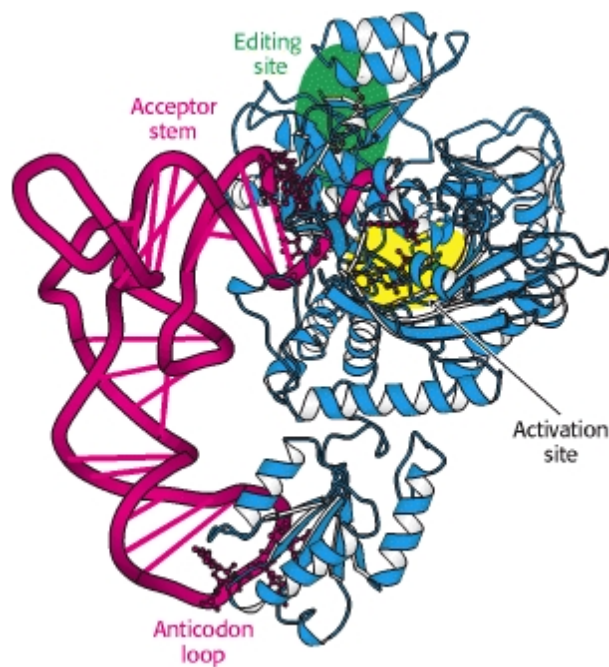
Figure 13. Structure of a tRNA synthetase complex.
The L-shaped structure of the tRNA allows the tRNA synthetase to bind both the acceptor stem and the anticodon loop. Charging of the cognate amino acid is further ensured through the proofreading editing site. Image from Berg [80].

Properly charged tRNAs are delivered to the ribosome in an elongation ternary complex with eEF1A and GTP. The interaction of this ternary complex and the ribosome follows distinct steps shown in Figure 14, and culminates in either acceptance (accommodation) or rejection of the tRNA [81–83]. First, initial binding of the ternary complex results in a labile interaction with the A-site, in which the anticodon of the tRNA is positioned in the decoding center. Cognate and near-cognate ternary complexes are stabilized by the following codon-recognition step, which is governed by codon-anticodon Watson-Crick base-pairing stability. Non-cognate ternary complexes are quickly and efficiently rejected at this first selection stage. Upon accurate tRNA selection, yeast 18S bases A1755, A1756, and G577 (*E. coli* A1492, A1493, G530) flip out from a *syn* to an *anti* conformation stabilizing the mini-helix formed from cognate codon-anticodon interactions [84,85]. This stabilization induces conformational changes in the ribosome that triggers the GTPase activity of eEF1A [86,87,88]. Near-cognate tRNAs fail to stimulate rearrangement of the three 18S rRNA bases, and thus fail to stimulate GTP hydrolysis by eEF1A. The conformational change of eEF1A to the GDP-bound form results in loss of its affinity for the tRNA and the ribosome. Once released from eEF1A, the aa-tRNA relocates to the LSU portion of the A-site in the process of accommodation. This is also accompanied by the release of the tRNA from the E-site.

The efficiency of the initial selection step is not sufficient to distinguish between the cognate and near-cognate ternary complexes, because the differences in the rate constants of the backward reaction (k_{-2} in Figure 14) and the forward reaction (k_3 in Figure 14) between cognate and near-cognate complexes are not large enough [89–91]. Therefore, most of the discrimination of near-cognate aa-tRNA is accomplished only

after GTP hydrolysis during the stage of selection known as "proofreading." This step is much less understood than the selection step during decoding. However, recent evidence suggests that recognition of the canonical geometry of the codon-anticodon helix in the DC induces stabilization of the entire anticodon loop by rRNA from both ribosomal subunits with involvement of magnesium ions [92]. This triggers fixation of the anticodon stem through a cascade of rearrangements in 25S rRNA and ribosomal proteins. The latter strengthen the binding of cognate tRNA on the ribosome via their flexible tails while concurrently stimulating positioning of the acceptor end in the PTC. An induced-fit mechanism in such a closed system of interactions as in the ribosome, in which the accommodation step is accomplished by the surrounding of cognate tRNA by dynamic layers of rRNA and proteins from both subunits, seems entirely reasonable. The kinetic data indicate that cognate aa-tRNA is faster in A-site accommodation and peptide bond formation [93]. As such, this "proofreading" step is unlike analogous functions of other macromolecules such as tRNA synthetases discussed above or DNA polymerases. Rather, this is a "kinetic proofreading" step. Together, the two selection strategies ensure that cognate aa-tRNAs are bound to the ribosome more stably, and are faster in "productive" forward reactions of GTP hydrolysis and A-site accommodation than near- and non-cognate tRNAs.
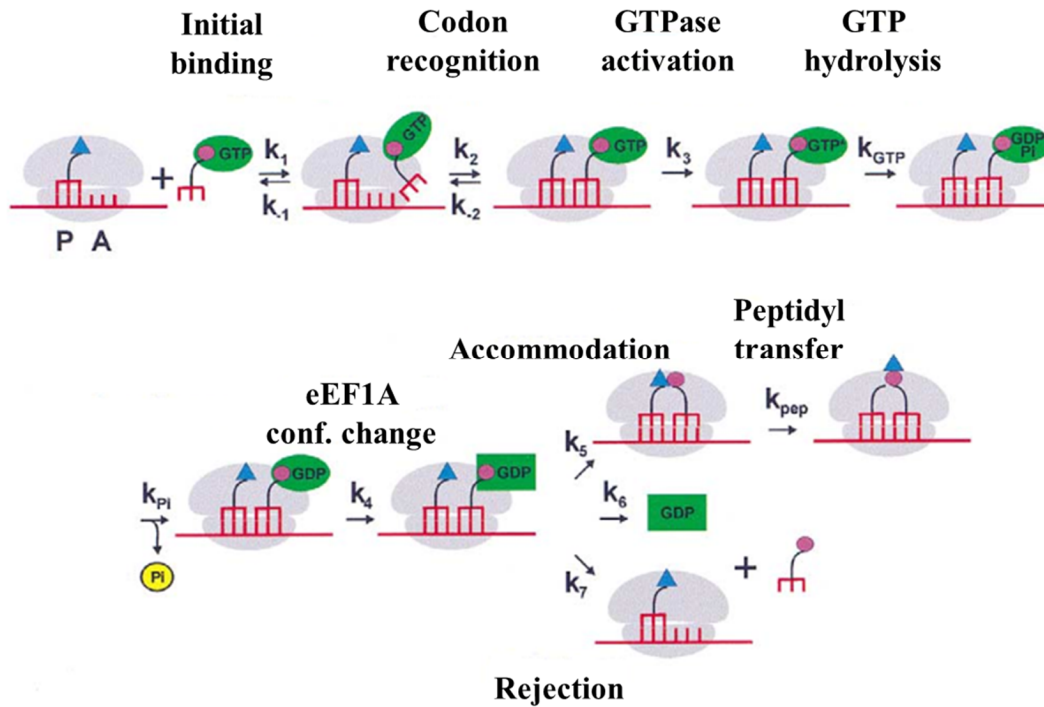
Figure 14. Scheme of tRNA selection at the ribosomal A-site.

The initial binding step in tRNA selection, governed by the rate constants k_1 and k_{-1}, is a codon-independent reaction between the ternary complex and the ribosome, while the following codon-recognition step is codon dependent. The active site of the elongation factor undergoes a conformational change during GTPase activation. This step is pivotal for establishing the irreversible step essential to proofreading and appears to limit the rate of GTP hydrolysis. During the proofreading stage after factor dissociation the tRNA either moves into the A-site (accommodation) for peptidyltransfer or dissociates from the ribosome (rejection). Accommodation is regulated by the rate constant k_5 and depends on codon-anticodon interactions.

Peptidyltransfer

The catalytic core of the ribosome is composed entirely of rRNA, with the nearest protein component approximately 13 Å away [15]. Peptidyltransfer is mediated solely by the LSU, and it alone can synthesize peptide bonds as rapidly as the full ribosome. Upon accommodation, the 3' CCA end of the aminoacyl-tRNA is stabilized by the 25S rRNA and positioned directly in the PTC resulting in almost instantaneous peptidyltransfer. The ribosome PTC catalyzes the aminolysis of an ester bond and is shown in Figure 15. The α-amino group of A-site aminoacyl tRNA nucleophilically attacks the P-site peptidyl tRNA at the carbonyl carbon of the ester bond that links the peptide to the tRNA, resulting in the deacylation of the P-site tRNA and the transfer of the growing polypeptide chain to the A-site tRNA. Amines react intrinsically fast with esters to form peptide bonds ($\sim 10^{-4}$ M^{-1} s^{-1} at room temperature), and the ribosome accelerates this reaction by $\sim 10^6$ -to 10^7 -fold [94]. This acceleration is achieved by lowering the entropy of activation, whereas the enthalpy of activation is the same for the reaction on the ribosome and in solution. Thus, the ribosome seems to rely on entropic catalysis as the mechanism of peptide-bond formation [94,95]. Recent evidence suggests that the correct binding of substrates induces structural rearrangements in the PTC resulting in an orientation suitable for catalysis. In particular, this includes the involvement of conserved active site residues in substrate positioning, desolvation, and organization of an electrostatic environment via a hydrogen network that stabilizes the reaction intermediates and allows appropriate proton shuttling [96].
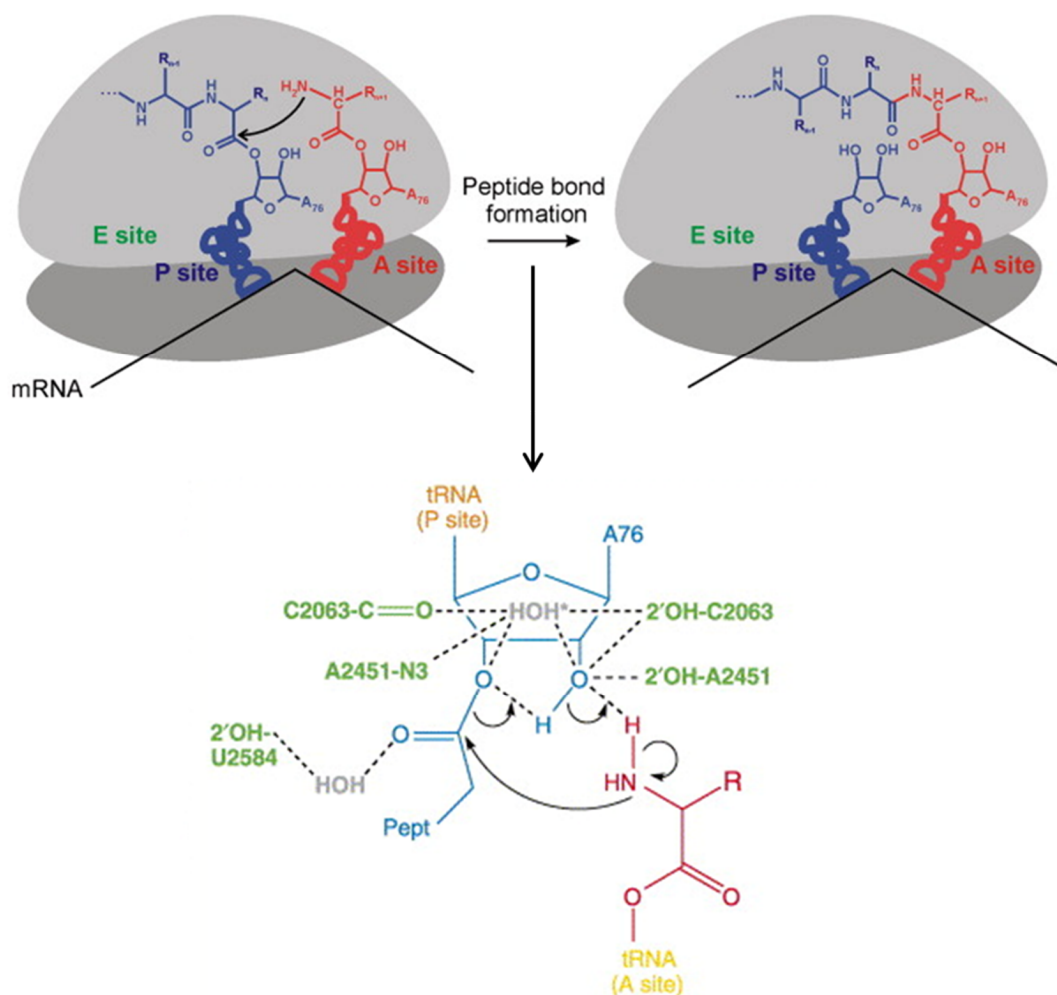
Figure 15. Mechanism of peptidyltransfer.

The α-amino group of aminoacyl tRNA in the A site attacks the carbonyl carbon of the peptidyl-tRNA in the P site. The universally conserved bases in green, among others, promote electrostatic shielding and a concerted proton-shuttle mechanism resulting in stabilization of a six-membered transition state and facilitating catalysis. Figure modified from Rodnina [96,97].

The ribosomal reaction rate acceleration is much less efficient compared to many protein enzymes, which use chemical catalysis and accelerate reactions by up to 10^{23}. Moreover, the intrinsic rate of peptidyltrasfer is estimated to be >300 s^{-1} and is much faster than the approximate 10 s^{-1} rate of accommodation [87,98]. Thus it seems that evolution has favored the increase in speed and fidelity of the rate-limiting steps of protein synthesis which do not involve chemistry, such as ternary complex binding described above, rather than peptide-bond formation itself. As a result, the catalytic core has retained its structure and mechanism of action during the course of the evolution from a pre-biotic ribozyme into a modern ribosome, and is one of the most conserved elements in all of life [99,100].

Translocation and ribosomal rotation

In order for translation to continue after a single round of peptidyltransfer, the A-site must be emptied to allow binding of a new ternary complex. For this to happen, the polypeptide-containing tRNA in the A-site needs to move into the P-site, while the "empty" deacylated tRNA needs to move from the P-site into the E-site. This is fueled by GTP and eEF2 in a process called translocation and results in ligand repositioning shown in Figure 16. Immediately after peptidyltransfer, the classically positioned P/P- and A/A site tRNAs (nomenclature signifies the position of tRNAs in the SSU/LSU) adopt a "hybrid" P/E and A/P conformation [101,102,103]. Adoption of this state is not possible before deacylation of the P-site tRNA, possibly due to the anchoring effect of the polypeptide chain in the exit tunnel [104]. The movement of the P-site tRNA into the hybrid state involves large motions in the whole body of the molecule, while adoption of the hybrid

state of the A-site tRNA only involves the shifting of the CCA-end into the P-site. This hybrid state conformation can bind the ternary complex mimic eEF2, which interacts with both subunits to promote translocation through GTP hydrolysis and the transition back to a classical state [105,106]. This is accompanied by a ribosomal shift in the 3'direction by one codon and the transfer of the tRNAs from the SSU P- and A-sites to the E- and P-sites.
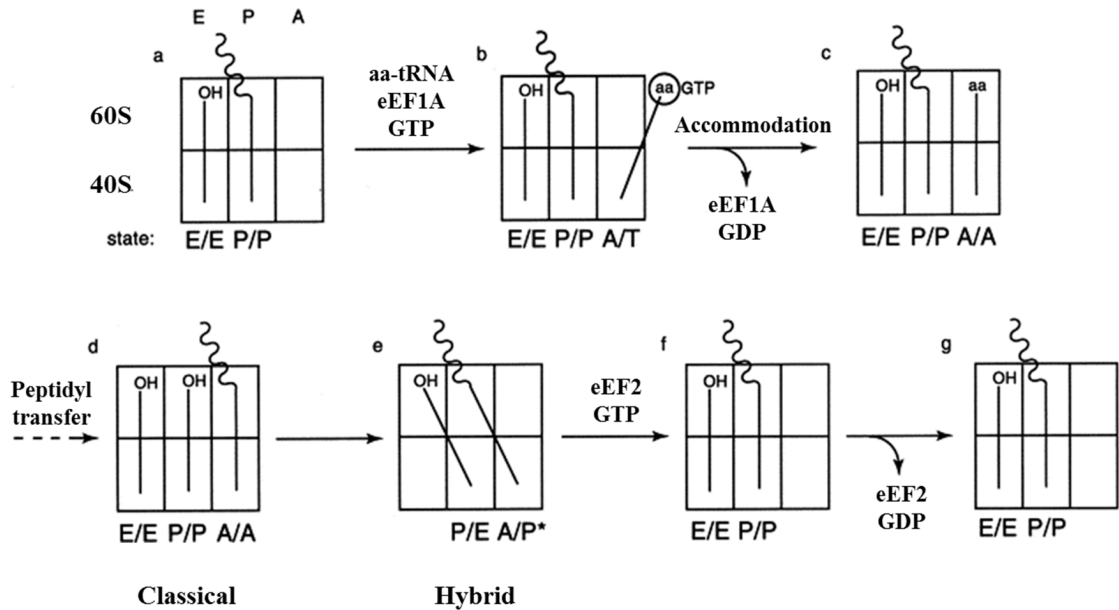
Figure 16. Positions of tRNAs during translation.

The relative position of tRNAs during classical, hybrid, and pre-accommodation states. Figure modified from Noller [107].

The transition between the classical and hybrid states above is accompanied by dramatic rearrangements in the structure of the whole ribosome. These are embodied by the rotation (previously referred to as "ratcheting") of the SSU by approximately 6° in a counterclockwise motion relative to the LSU, as shown in Figure 17 [108–112]. The hybrid state corresponds to the rotated conformation, while the classical state corresponds to a non-rotated conformation. In the rotating SSU, the head region is the most mobile element, rotating at the neck by 14° which translates to a movement of up to 25 Å. Corresponding structural changes in LSU are far less well known, and will be discussed in detail in the next chapter. The transition to a rotated state results in the disruption of several non-centrally located intersubunit bridges including B7a and B2b/c.
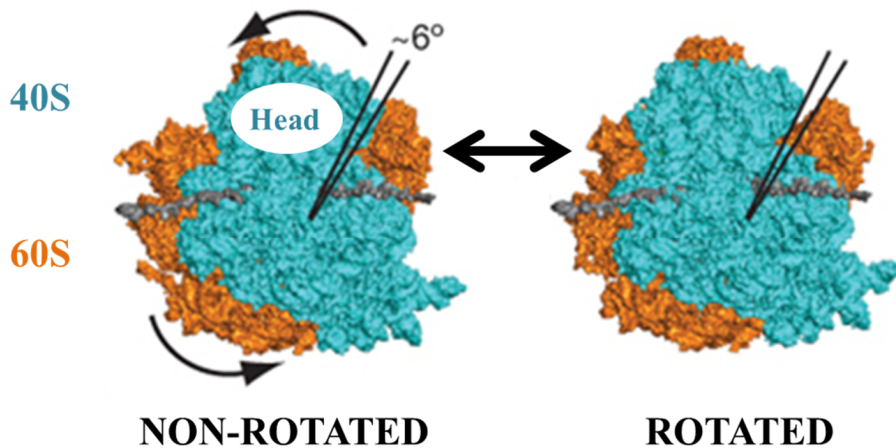
Figure 17. Ribosomal intersubunit rotation.
Subtle rotation of the SSU relative to the LSU during translation. Image modified from Schmeing [85]. The "head" domain of the SSU is indicated.

The recently adopted term "rotation" in place of "ratcheting" more accurately reflects the more continuous and fluid movements involved in the process: there may be up to 50 intermediate conformational states, with the fully rotated and fully non-rotated states representing the two extremes [101]. As such, the ribosome transits between these two conformational states as it progresses through the translation elongation cycle. Recent evidence suggests that ternary complex binding and peptidyltransfer occur primarily in the context of a non-rotated ribosome, while eEF2 binding and translocation occur in a rotated ribosome [113,114,115]. A summary of this process is shown in Figure 18.
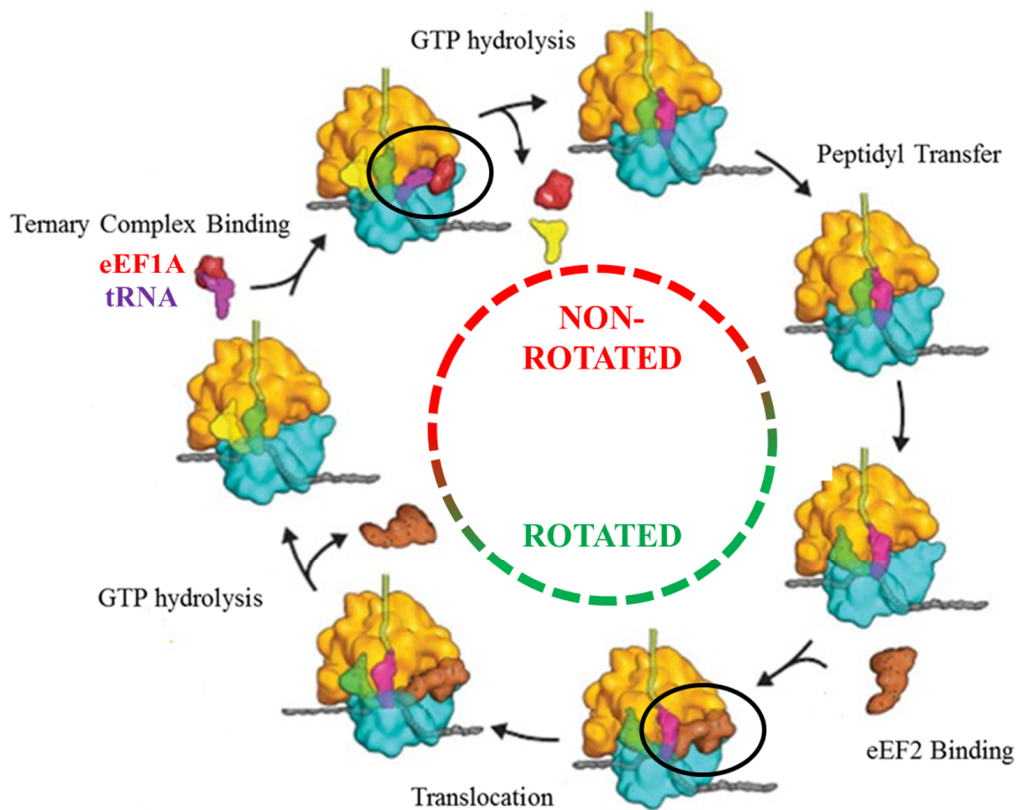
Figure 18. The elongation cycle of translation.
Ribosomal intersubunit rotation drives the elongation cycle and ligand binding. Image modified from Schmeing [85].

Termination

There are 3 stop codons, also known as nonsense codons (UGA, UAG, and UAA), which mark the end of the protein product. There are no cognate tRNAs for stop codons. Instead, protein factors called release factors (RFs) bind to the A-site when it is positioned over one of the stop codons and trigger a hydrolysis reaction in the ribosome active site, resulting in the release of the polypeptide chain from the P-site tRNA. Eukaryotes have one omnipotent class I RF (eRF1), which decodes all three stop codons. It associates with the class II RF (the GTPase eRF3) in the cytoplasm and binds to the ribosome as another ternary complex, resulting in GTP hydrolysis by eRF3 and subsequent activation of eRF1 [116,117]. Because eRF1 and aminoacyl tRNAs interact with the same ribosomal structural elements of the A-site, this release factor may also act as a functional tRNA mimic [118] (Figure 19.) Binding of release factors to the A site induces conformational changes similar to those for peptidyltransfer during translation elongation. Indeed, the mechanism of peptide release resembles the mechanism of peptide bond formation, differing only in the identity of the nucleophile and the requirement for protein factors. While an amine is the functional nucleophile during elongation, a water molecule plays that role in peptide release; the two mechanisms are compared in Figure 20. During elongation, a particular arrangement of the PTC excludes water from the active site to avoid premature peptide hydrolysis. During termination, the high conserved GGQ (glycine-glycine-glutamine) motif of eRF1 interacts with the PTC in a manner analogous to the 3' CCA ends of tRNAs, and helps position an attacking water molecule properly for reaction [119–121].
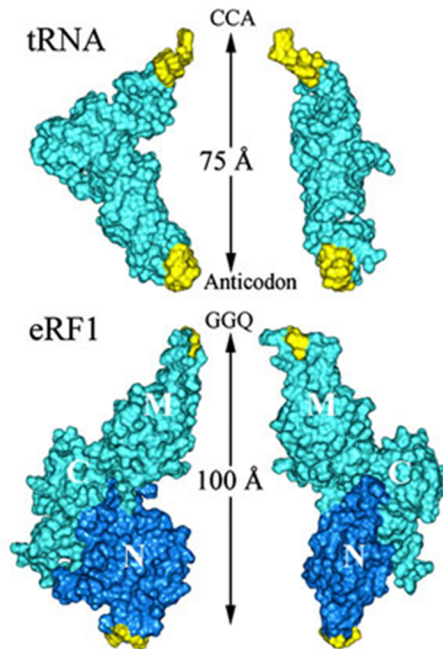
Figure 19. Eukaryotic release factor is a structural tRNA mimic.
The similarity of the structures is shown by a side view (left) and a front view (right). The N-terminal (N) domain mimics the anticodon arm, the middle (M) domain is equivalent to the amino acid acceptor arm and the C-terminal (C) domain is responsible for interaction with eRF3. Image modified from Chavatte [122].

Peptide release leaves the 80S ribosome still bound to the mRNA with deacylated tRNA in its P-site and eRF1 in its A-site, all of which need to be disassembled and released from the mRNA to allow further rounds of translation. While in bacteria subunit and factor dissociation is accomplished by the crowbar-shaped ribosome recycling factor (RRF), no such eukaryotic factors have been found [123]. However, though the mechanism of action remains enigmatic, it has recently been shown that the ATPase ABCE1 can promote ribosome splitting in combination with eRF1 [124]. The ABCE1 protein is also required to recycle stalled ribosomes in the eukaryotic mRNA surveillance pathways no-go decay (NGD) and no-stop decay (NSD). The protein Dom34 and its interaction partner the GTPase Hbs1 are paralogs of the eRF1-eRF3 system and are similarly recruited as a

ternary complex to the ribosomal A-site of stalled ribosomes. This assembly in turn recruits ABCE1, culminating in ribosome splitting and recycling [124,125]. Another possible post-termination and ribosome recycling model includes eIF3 induced separation of the subunits [126]. Lastly, a subunit dissociation step may not be needed at all. A linkage between termination and initiation is possible due to an interaction between eRF3 and PABP in the closed loop mRNA structure. As such, in some circumstances eRF3-guided ribosomes are able to move right back to the beginning of the message along the circularized mRNA. Translation is in fact strongly inhibited upon disruption of the eRF3-PABP interaction [127].
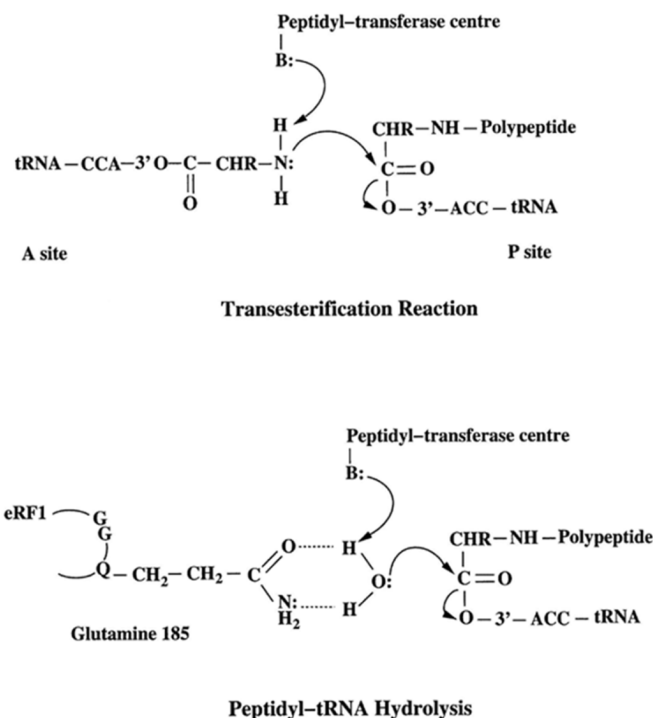
Figure 20. Mechanisms of peptidyltranfer and peptide release.
Both reactions occur in the same active site and begin with the same ground state complex, where the labile P-site ester linkage sits in the PTC. In eRF1 induced hydrolysis, the C-terminus of the polypeptide chain attached to the P-site tRNA undergoes nucleophilic attack at the ester carbon by a water molecule, stabilized by the glutamine of the GGQ motif, leading to release of the newly synthesized polypeptide.

Antibiotics and Ribosome Inhibition

Because of the central role of translation in the cell, as well as the structural differences between prokaryotic and eukaryotic ribosomes, protein synthesis inhibitors have been the most successful clinical antibiotics to date. Because the ribosome exceeds the size of an average antibiotic by four orders of magnitude, it provides a multitude of targets: approximately 50% of all existing antibiotics impair translation. The emergence of high resolution ribosomal structures in this decade has led to insights into the mode of antibiotic interactions and exact mechanisms of action [128–133].

There are several general classes of ribosomal antibiotics, most of which are obtained from natural producers such as *Streptomyces,* that can be grouped based on their structures and modes of action [134]. Antibiotics interfering with almost every step of translation are clinically available, some shown in Figure 21. For example, orthosomycins and pactamycin bind to the 50S and 30S subunits, respectively, preventing formation of the initiation complex. Kasugamycin also prevents initiation by binding in the path of mRNA in the 30S subunit and inhibiting initiator tRNA interactions. Affecting elongation, sparsomycin blocks tRNA binding at the 60S A-site while tetracyclins prevent tRNA accommodation. Aminoglycosides such as paromomycin can bind to the decoding center leading to stabilization of codon:anticodon mismatches and subsequent mistranslation. Pulvomycin prevents the binding of aa-tRNA to the eEF1A-homolog EF-Tu and hence ternary complex formation, while kirromycin prevents the conformational changes of EF-Tu required for GTP hydrolysis. Many types of antibiotics interfere with the catalytic activity in the PTC. Puromycin mimics the CCA end of an aa-tRNA, enters the ribosomal A-site and gets incorporated into the nascent polypeptide

chain triggering premature peptide release. Chloramphenicol blocks the peptide exit tunnel, leading to an obstruction referred to by Nobel Laureate Thomas Steitz as "molecular constipation". Fusidic acid prevents conformational changes required for dissociation of the eEF2-homolog EF-G after GTP hydrolysis, thus trapping the factor on the ribosome and stalling translation at the translocation step. Ribotoxins and thiopeptides block the binding of EF-G and its structural homologs such as the ternary complex and release factors.

The oxazolidinone class of synthetic antibiotics represents the first new class of drug to enter the antibiotic market in over 20 years [135]. While their precise mode of action is not known, these antibiotics appear to interact with the 50S subunit and inhibit initiation or early stages of elongation [136]. Interestingly, partial translation of full proteins is more detrimental to bacterial cells than complete translational shut down. As a result, more powerful antibiotics actually allow a fraction of proteins to escape inhibition. These "resistant" proteins stall biochemical pathways and result in toxic intermediates [137]. Because of the increasingly alarming rate of the development of bacterial resistance and cross-resistance to antibiotics, advancing our understanding of the precise mechanisms of ribosomal function and drug interactions is crucial to outpace the rapidly evolving pathogenic strains.
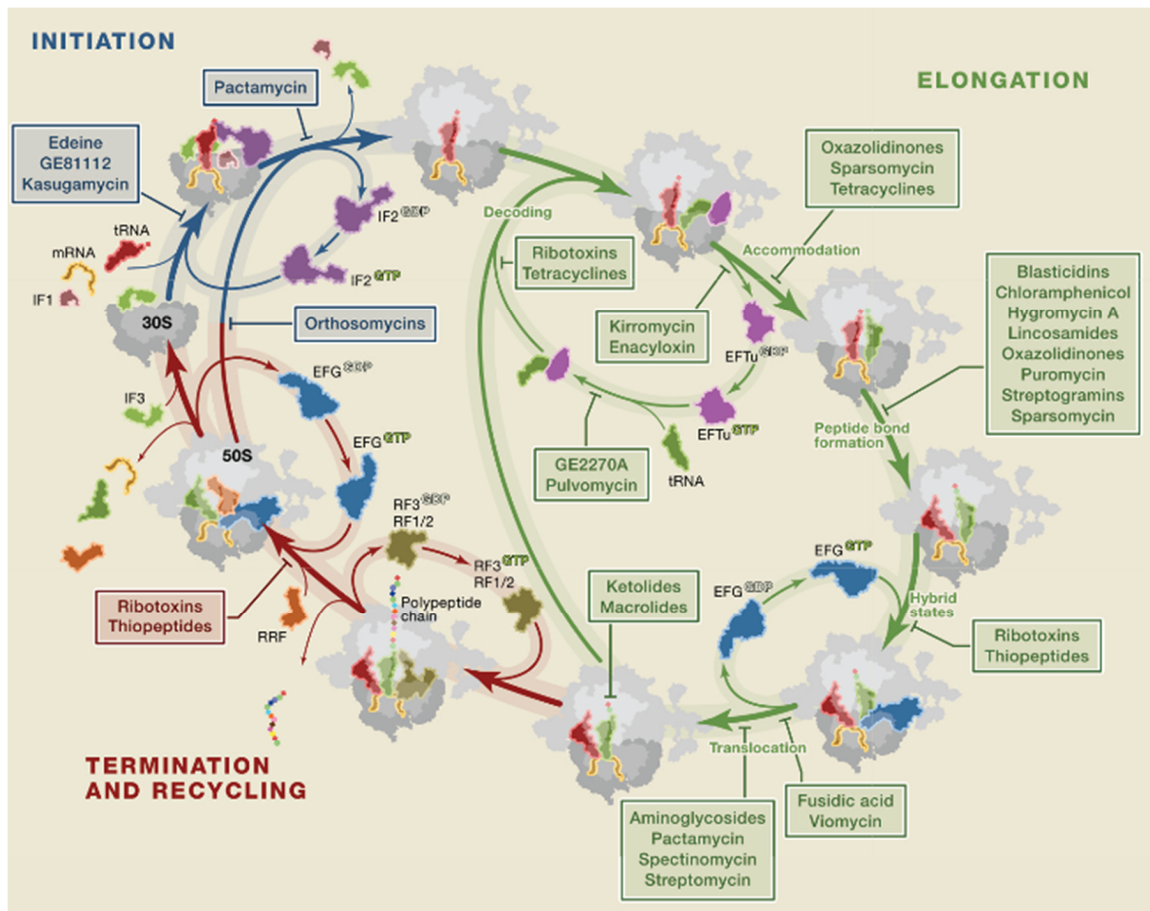
Figure 21. Steps of antibiotic inhibition of translation.

The prokaryotic life cycle of the ribosome is impaired by a variety of clinical drugs at the indicated steps. This image is from Sohmen [138].

<u>Translational Recoding</u>

As discussed above, canonical translation initiates at a start codon, proceeds uninterrupted along an open reading frame (ORF) one triplet codon at a time, and terminates at a stop codon yielding a single protein product. However, translation can also proceed through a variety of non-canonical pathways, generically referred to as translational recoding. While recoding events are intrinsically rare (10^{-4} – 10^{-5} events per codon) [139], they can be induced to occur at higher rates at specific sequences by *cis*-acting elements on mRNAs. Such exceptions to translational rules include shifting ribosomes into an alternate reading frame during elongation, directing ribosomes to alternate start sites during initiation, and suppression or recoding of stop codons [140]. Although originally identified in viruses, many of such recoding signals have since been documented in both prokaryotic and eukaryotic organisms [141].

Programmed -1 Ribosomal Frameshifting

A programmed -1 ribosomal frameshifting (-1 PRF) event induces a particular fraction of elongating ribosomes to "slip" back on the message, and out of the original ORF, by one nucleotide in the 5' direction. This results in the establishment of a new ORF and is followed by the continuation of elongation in the new reading-frame. Thus, a -1 PRF signals allows the synthesis of multiple proteins from a single, unaltered RNA template. This is a genome condensation strategy that allows viruses, all of which are limited by the size of their nucleocapsids, to maximize genomic coding space while maintaining genome integrity. -1 PRF was first identified in the Rous Sarcoma Virus, and is utilized by a plethora of other RNA viruses including those causing Acquired

Immunodeficiency Syndrome (HIV-1) and Severe Acute Respiratory Syndrome (SARS CoV) [142–145]. The large number of well-characterized viral -1 PRF signals has allowed the definition of the parameters and rules governing - 1 PRF efficiency in at least one class of signals, shown in Figure 22. A typical -1 PRF signal consists of 3 important elements: a "slippery site" of 7 nucleotides over which the ribosomal shift in frame actually takes place; a short spacer region of less than 12 nucleotides; and a strong stimulatory structure downstream, which is usually a pseudoknot [146–149].
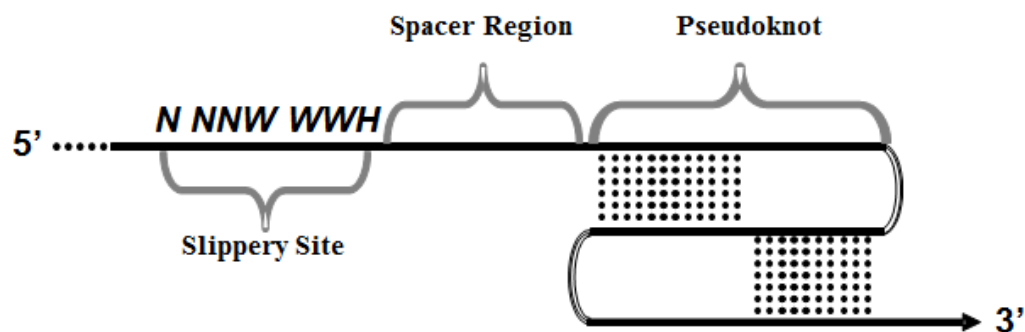
Figure 22. Structure of a typical -1 PRF signal.

The slippery site, where the A- and P-site tRNAs are positioned and the shift in frame occurs, is denoted by IUPAC notation (*N*=any 3 identical nucleotides, *W*=A or U, and *H*≠G). 22 functional slippery sites are known. While a pseudoknot is the most common type of stimulatory element, other mRNA structures are capable of filling that role as well.

A model of the mechanism of a -1 PRF event is shown in Figure 23. Generally it is thought that the function of the pseudoknot is to stall the ribosome and position it over the slippery site, making the "slip" more likely and biologically relevant. The nature of the slippery sequence enables re-pairing of the non-wobble bases of both the aa- and peptidyl-tRNAs with the -1 frame codons. As this is occurring, the energetic barrier of the pseudoknot is overcome by the ribosome, and elongation can continue in the newly established reading frame. Frameshift "attenuators" consisting of hairpin structures upstream of the slippery site have been shown to influence rates of frameshifting as well [150]. A number of models have been presented addressing the exact time point and mechanism of the shift in frame. More recently, the "many pathways model" has unified previous competing models by demonstrating that -1 PRF products merely represents an endpoint accessible by at least three different kinetic pathways [151].

In addition to enrichment of genomic content, -1 PRF is also used by viruses to ensure production of viral gene products in their correct stoichiometric ratios and is shown in Figure 24. For example, the L-A virus of yeast has a simple icosahedral structure of T=1. In Euclidian solid geometry, the simplest sphere (T=1) is composed of 60 identical subunits and resembles a traditional soccer ball. Translating this structure to viruses, these subunits are the capsid proteins (also called Gag for ''Group specific antigen'') which typically self-assemble to form the viral capsid [152]. The only other component required for L-A virus propagation is a single molecule of an enzyme capable of replicating the genome, the viral replicase, or polymerase. Thus, the ideal ratio of capsid to replicase is 60:1. The L-A viral -1 PRF signal has evolved to shift ribosomes from the Gag open reading frame to the Pol open reading frame at a rate of 1.8%, thus

producing the desired 60:1 ratio of capsid to replicase proteins [153]. Changing this rate by mutations in the frameshift signal, mutations in the host translational apparatus, or with small molecule inhibitors alters this important stoichiometric ratio and proper virion assembly [154]. This general concept applies to many other viruses as well, with specific -1 PRF efficiencies ranging 1-10%. Because the correct frameshift structure and function are necessary for viral propagation, targeted altering of these parameters may open up new avenues for anti-viral treatments.

Many functional -1 PRF signals have also been identified in eukaryotic systems where their role appears to be quite different from the viral context [155–158]. Over 95% of ''cellular'' -1 PRF events direct elongating ribosomes into premature termination codons, including in humans, leading to an inverse relationship between -1 PRF efficiency and mRNA half-lives. Studies using endogenous -1 PRF signals from yeast demonstrated that these can function as mRNA destabilizing elements through both the nonsense-mediated decay (NMD) and the No-Go decay pathways [159,160]. In unpublished studies from our laboratory, we have shown that endogenous -1 PRF signals from human genes also function as mRNA destabilizing elements in mammalian cells through NMD, play an important role in regulation of the immune response, and that frameshifting efficiency can be regulated through miRNAs. In addition, it was recently demonstrated that levels of -1 PRF directly correlate with telomere length in yeast [161]. Thus, it is now clear that -1 PRF is much more widespread and versatile than originally thought, is employed by organisms representing every branch in the tree of life, and presents a powerful new method of gene regulation.
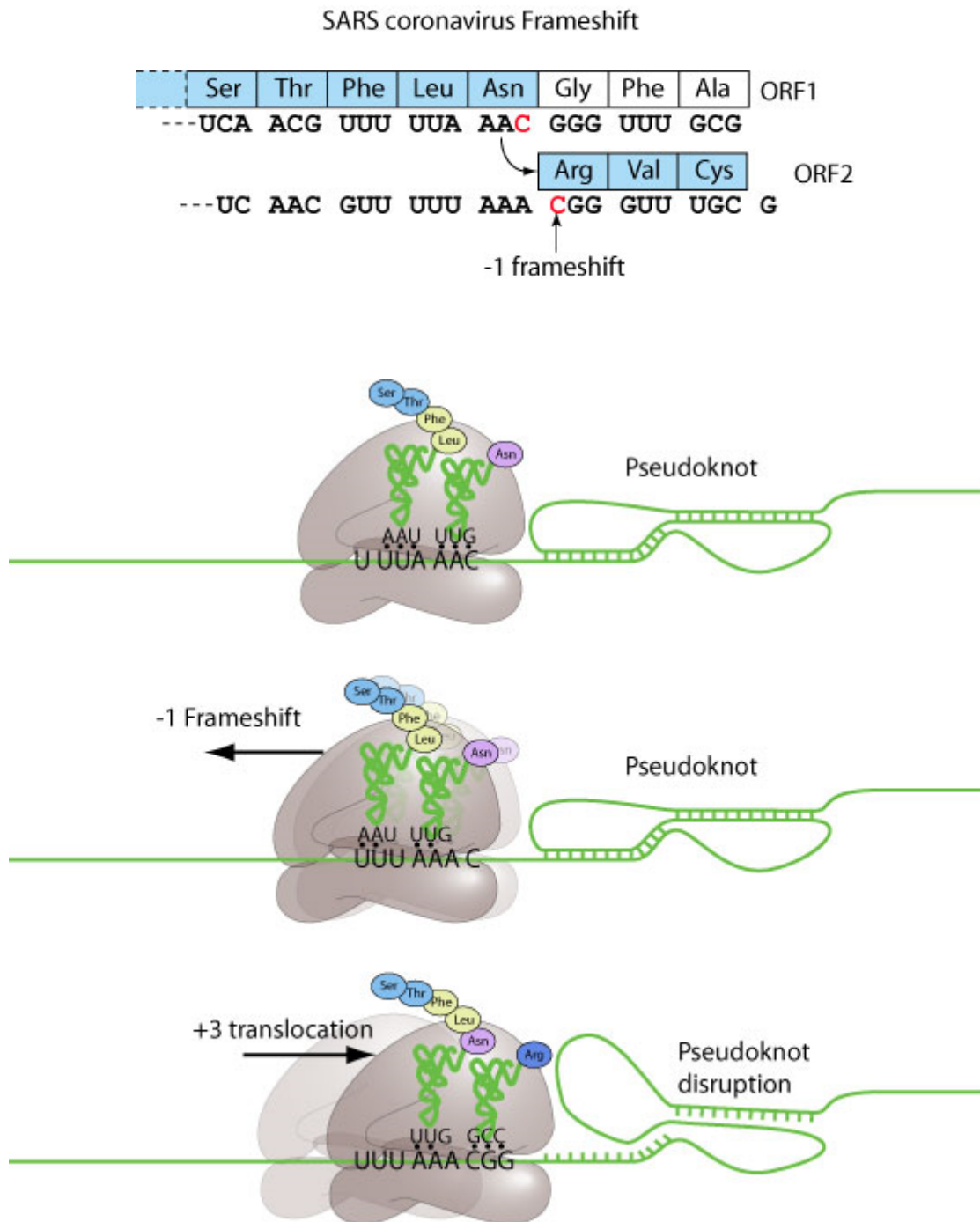
Figure 23. The mechanism of -1 PRF.

The SARS coronavirus -1 PRF signal is used as an example. An mRNA pseudoknot forces elongation ribosomes to pause over the slippery site which induces a shift by 1 base in the 5' direction and the subsequent repairing of A- and P-site tRNAs with the new -1 frame codons. The pseudoknot is eventually denatured, and elongation in the new ORF continues. Image obtained from ViralZone [162].
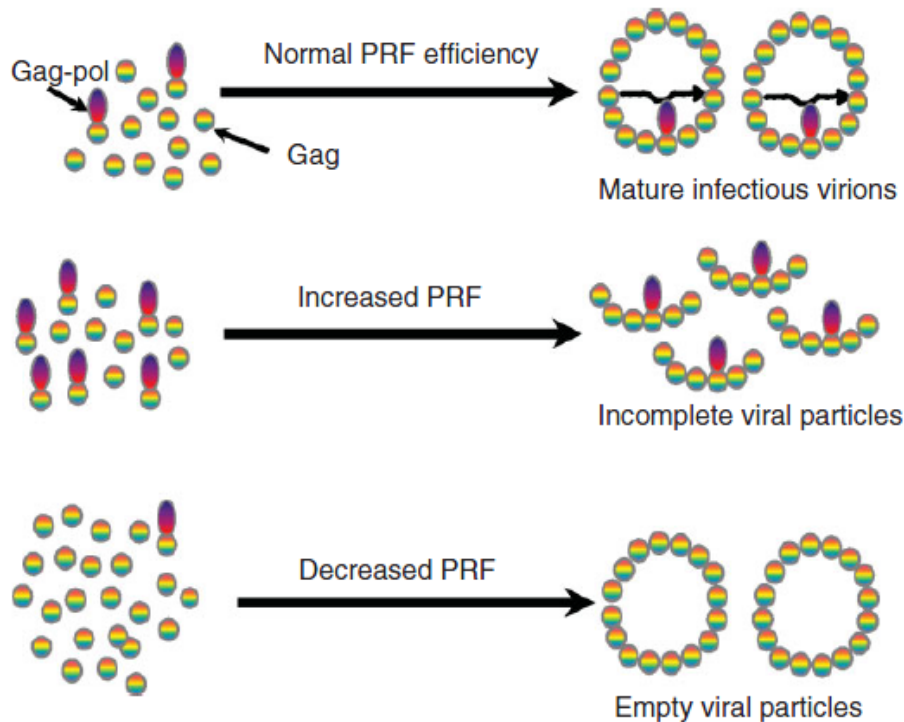
Figure 24. Effects of -1 PRF on viral propagation.

The correct ratio of structural to enzymatic proteins is achieved by a -1 PRF signal in the viral genome directing ribosomes into an alternate reading frame at a set rate, resulting in the production of the Gag-pol fusion protein. No shift in frame yields the Gag protein product. Increase/decrease in the frameshifting rate results in improper virion assembly and a non-functional virus. Image adapted from Dinman [154].

Programmed +1 Ribosomal Frameshifting

A less widespread and understood example of a recoding event is programmed +1 ribosomal frameshifting (+1 PRF). Like -1 PRF, this mechanism utilizes *cis*-acting mRNA elements, is employed by viruses and transposable elements to regulate the synthesis of structural and enzymatic proteins, and has been found in human, mouse, bacteria, and yeast genomes [163–166]. Unlike -1 PRF however, +1 PRF induces elongating ribosomes to bypass one nucleotide in the 3' direction. A slippery site is required for this,

while a downstream stimulatory structure is not. Rather, in bacteria ribosomal pausing is caused by a low abundance of a particular tRNA or release factor 2 (RF2) as the ribosome is positioned over the slippery site [167]. While there is only one generally well-understood type of -1 PRF signal, +1 PRF signals appear to be case-specific, with different mechanisms for different signals. However, recent modeling of *E. coli* +1 PRF signals revealed that the mechanism is influenced by distinct kinetic parameters: 1) destabilization of deacylated tRNA in the E-site, 2) rearrangement of peptidyl tRNA in the P-site, and 3) availability of cognate aminoacyl tRNA at the A-site. While all three parameters are important for efficient +1 PRF, a rate constant of $\sim$1.9 sec^{-1} for slippage of the P-site tRNA by one downstream nucleotide appears to be the driving force of this mechanism [168]. It is also greatly enhanced by the presence of a "hungry codon" in the A-site decoding a low abundance tRNA or RF2.

Missense and Nonsense Suppression

In addition to reading frame maintenance, translational fidelity can also be assessed by missense suppression (the rate at which near- or non-cognate tRNAs are mistakenly accommodated), and nonsense suppression (the rate at which suppressing tRNAs are incorporated at stop codons, thereby reading through the codon). Nonsense suppression is found to be a translational strategy in a number of viruses, often used to produce *gag-pol* fusion proteins as a result of *cis*-acting elements on mRNAs not unlike in PRF [169–171]. Similarly, the incorporation of the essential 21st amino acid selenocysteine (Sec), the major biological form of the element selenium, occurs through an induced nonsense suppression mechanism in all three kingdoms. This requires specific *trans-*

acting factors and secondary structures in the mRNA to actively recode an in-frame UGA from a stop codon to Sec sense codon [172,173]. While the human genome only encodes 25 selenoproteins, variations in these Sec-containing proteins or their synthetic machinery is linked to a range of human disorders including cancer. The much more puzzling 22nd amino acid pyrrolysine, described in *archaea* and bacteria and present in only 1% of sequenced genomes, is universally encoded by the stop codon UAG as well [174].

All recoding strategies provide means for genomic expansion and gene regulation, and it is estimated that as many as one-third of inherited genetic disorders are caused by frameshift or nonsense mutations [154]. In the context of this thesis, recoding mechanisms can be used as functional tools to characterize the ribosomal components involved in maintaining translational fidelity and function.

Scope of Work and Thesis Summary

The progress made over the last 50-60 years in visualizing and understanding the structural constituents of the ribosome is remarkable, as shown in Figure 25. As described in this chapter, the general principles of ribosome function are also very well understood. However, many important questions still remain about ribosomal mechanics, in particular 1) how intersubunit rotation is coordinated, 2) how the different functional centers of the ribosome communicate with one another, 3) the nature of the quality control mechanisms employed to ensure that only functional subunits are allowed to enter the pool of active ribosomes, and 4) the nature and mechanisms of ribosome malfunction in disease.

Studies of the essential ribosomal protein L10 (rpL10) have shed significant light on all of these questions. rpL10 was initially identified in yeast in a screen for mutants that were synthetically lethal with a deletion of subunit 6 of cytochrome bc1 [175]. Subsequent genetic studies showed that *QSR1*, as it was originally named, was essential for protein synthesis and allelic to *RPL10* [176]. This protein plays an essential role in ribosome biogenesis, and its incorporation into the LSU in the cytoplasm is one of the last steps of LSU maturation [177]. In addition, rpL10 is strategically located near functional centers of the ribosome, including the elongation factor and tRNA binding sites. One segment of rpL10 also comes within 13 Å of the PTC. As such, it is the closest protein element approaching the catalytic RNA core of the ribosome, and the protein has consequently been shown to be involved in coordinating aa-tRNA movement near the PTC [178]. The high level of sequence conservation of rpL10 in all organisms and the location close to regulatory and catalytic sites of the ribosome are indicative of its importance in ribosome function, and we have referred to it as the "CPU of the LSU." In additional support of this, recent studies have demonstrated that defects of rpL10 are found in patients suffering from autism and acute T-cell acute lymphoblastic leukemia (T-ALL) [179,180].

The work presented in the following chapters further dissects the role of rpL10 in the ribosome while also addressing important questions regarding translation in general. Chapter 2 describes how a flexible loop of rpL10 near the PTC coordinates ribosomal rotation, that the rotational status is important throughout the ribosomal lifecycle, and offers a model explaining how pre-60S subunits are functionally monitored during ribosome biogenesis. Chapter 3 then demonstrates that malfunction of this loop

influences T-ALL, offers a mechanistic model of the disease, and proposes an explanation for the high incidences of cancer in patients with ribosomopathies. Chapter 4 focuses on the eukaryotic-specific C-terminal "tail" of rpL10, its pivotal role in recruitment of *trans*-acting factors and ribosome biochemistry, and how impairment of this domain can result in autism. Finally, Chapter 5 summarizes all these findings and discusses their significance and future implications.
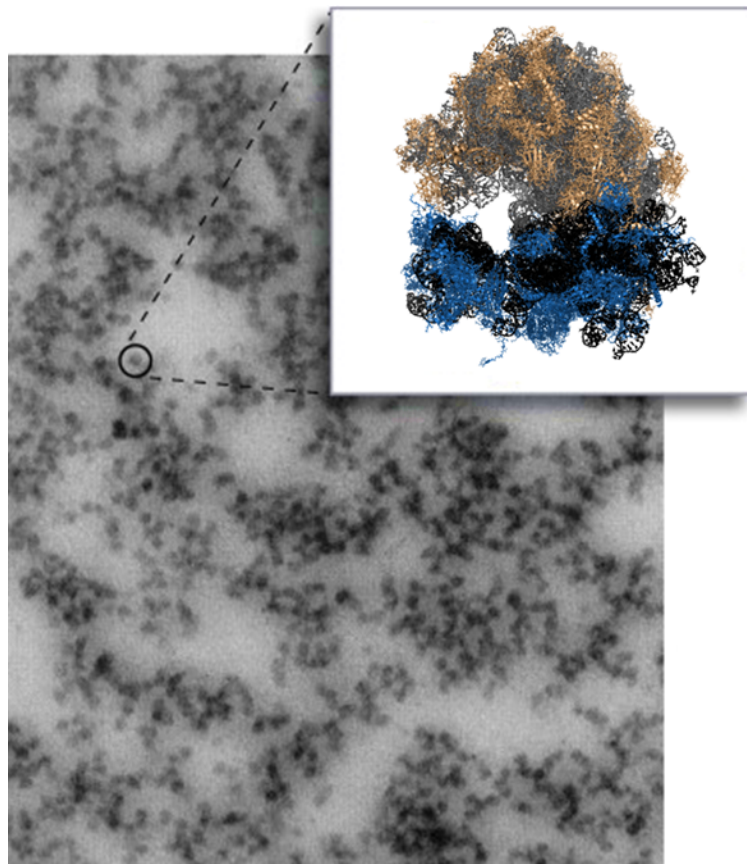
Figure 25. The ribosome over 50 years.
The very first images of "microsomes" and the modern ribosome at atomic resolution. EM image obtained from Kirsch [181], conceptual idea from Dinman [182].

Chapter 2

Eukaryotic rpL10 drives ribosomal rotation

Introduction

The ribosome is an essential and complex nanomachine that provides a model for understanding principles of macromolecular assembly and functional coordination. The eukaryotic yeast ribosome is a 3.6 megadalton RNA-protein complex, consisting of 79 intrinsic ribosomal proteins and 4 ribosomal RNAs (rRNAs) [14]. Different biochemical functions are spatially separated from one another in the two subunits of the ribosome. The small subunit (SSU) contains the mRNA decoding center, while the large subunit (LSU) harbors separate regions with distinct functions: the peptidyltransferase center, PTC (responsible for catalysis), the peptide exit tunnel, three transfer RNA (tRNA) binding pockets, and a single binding site that must distinguish between the two elongation factors and release factor in response to specific circumstances. The subunits must also interact with one another as a holoenzyme to coordinate a complex series of events, particularly allosteric movements that occur throughout the course of the elongation cycle. The two extreme conformational states are termed "rotated" (aka ratcheted or hybrid) and "non-rotated" (aka classical). How information is exchanged over long distances between spatially distinct functional centers, and how these centers then work in concert to ensure timely rotation, proper ligand binding, and ultimately unidirectional and faithful translation remains largely unclear. Additionally, while the roles of the SSU (particularly the head) and tRNAs in ribosome rotation have been investigated, the involvement of the LSU in this process has not been explored.

Ribosomal protein L10 [rpL10, aka L16 [15]] plays essential roles in ribosome biogenesis and translational fidelity. Incorporation of rpL10 into the LSU in the cytoplasm constitutes a late step of LSU assembly [183]. In particular, rpL10 works in conjunction with Shwachman-Diamond protein Sdo1p and the eEF2-like GTPase Efl1p to promote the release of the anti-association factor Tif6p and the nuclear export adapter Nmd3p, the last steps of 60S maturation [47,184,185]. Thus, large subunits lacking rpL10 are unable to join with the SSU. rpL10 is located near the corridor through which aminoacyl-transfer RNAs (aa-tRNAs) move during the process of accommodation and is involved in tRNA movement through this structure [178]. It is also located near several other functional centers of the LSU, including the PTC, the A-site finger (H38), the elongation factor binding site, and the GTPase associated center (see Figure 26). The C-terminus of rpL10 contacts 5S rRNA, which interacts with rpL5 and rpL11 at the head of the central protuberance. Thus, rpL10 is well positioned to act as a sensor of activity near the PTC, and transduce that information to other functional centers to coordinate ribosome function.

An essential internal loop of rpL10 (aa 102-112, previously called the "P-site loop") that makes the closest approach to the PTC (13 Å) of any ribosomal protein is crucial for Tif6p and Nmd3p release [186]. Mutagenesis of the loop revealed two classes of mutants based on their effects on ribosome biogenesis [187]. The current study employs the strongest representative mutants of these two classes: S104D (improper subunit joining and 60S biogenesis defect) and A106R (high 60S/40S ratio).   Here, we present evidence that these mutations promote opposing effects on the natural equilibrium between the two extreme conformational states of the ribosome. Structural and biochemical analyses of

empty ribosomes demonstrate that the S104D mutation drives the ribosome towards the rotated state, favoring binding of eEF2 and disfavoring binding of eEF1A/aa-tRNA/GTP (elongation ternary complex) and inhibiting peptidyltransfer. In contrast, A106R causes empty ribosomes to distribute toward the non-rotated state, favoring elongation ternary complex binding over eEF2, and leaving peptidyltransferase activity unaffected. We also show that the non-rotated conformation favors Sdo1p binding, stimulating binding of tRNAs to the A-site. Further, Sdo1p competes with acetylated-aa-tRNA for binding to the P-site and inhibits peptidyltransfer, suggesting that Sdo1p stabilizes the non-rotated state through binding the P-site. Large scale rRNA chemical modification analyses reveal distinct information transmission pathways originating from rpL10 in the heart of the LSU and emanating throughout the LSU and the SSU.

These observations lead us to propose that the rpL10 loop plays a central role in much of the ribosomal life cycle by helping to set the conformational status of the LSU, coordinate intersubunit rotation, and communicate this information to the decoding center on the SSU. During late LSU biogenesis, the loop senses Sdo1p recruitment to the P-site, initiating a "test drive" to ensure the functionality of pre-60S subunits. After ensuring proper 80S assembly, the loop monitors the tRNA occupancy status of the PTC A-site: in the absence of A-site ligand (aa-tRNA) it can sample this space, while the introduction of ligand displaces it. We suggest that the positioning of the rpL10 loop determines which state the LSU assumes in a process involving cascades of allosteric interactions that link functional centers in the LSU with those in the SSU. The downstream effects of rotational disequilibrium are wide-ranging, impacting translational reading frame maintenance, the ability to discriminate between cognate and near- and non-cognate

codons, and termination codon recognition. Mutants of ribosomal protein L3 that confer opposing effects on ribosome structure and function can suppress the structural, biochemical, and functional defects of the rpL10 loop mutants by re-establishing the normal rotational equilibrium. In sum, we propose that the rpL10 loop is a master controller of ribosome structure and function, influencing critical steps in both ribosome assembly and biogenesis, and the protein-synthetic phase of elongation. We suggest that the unidirectionality of translation is aided by this intrinsic feature of the ribosome, and that the LSU alone has the ability to independently influence intersubunit rotation.
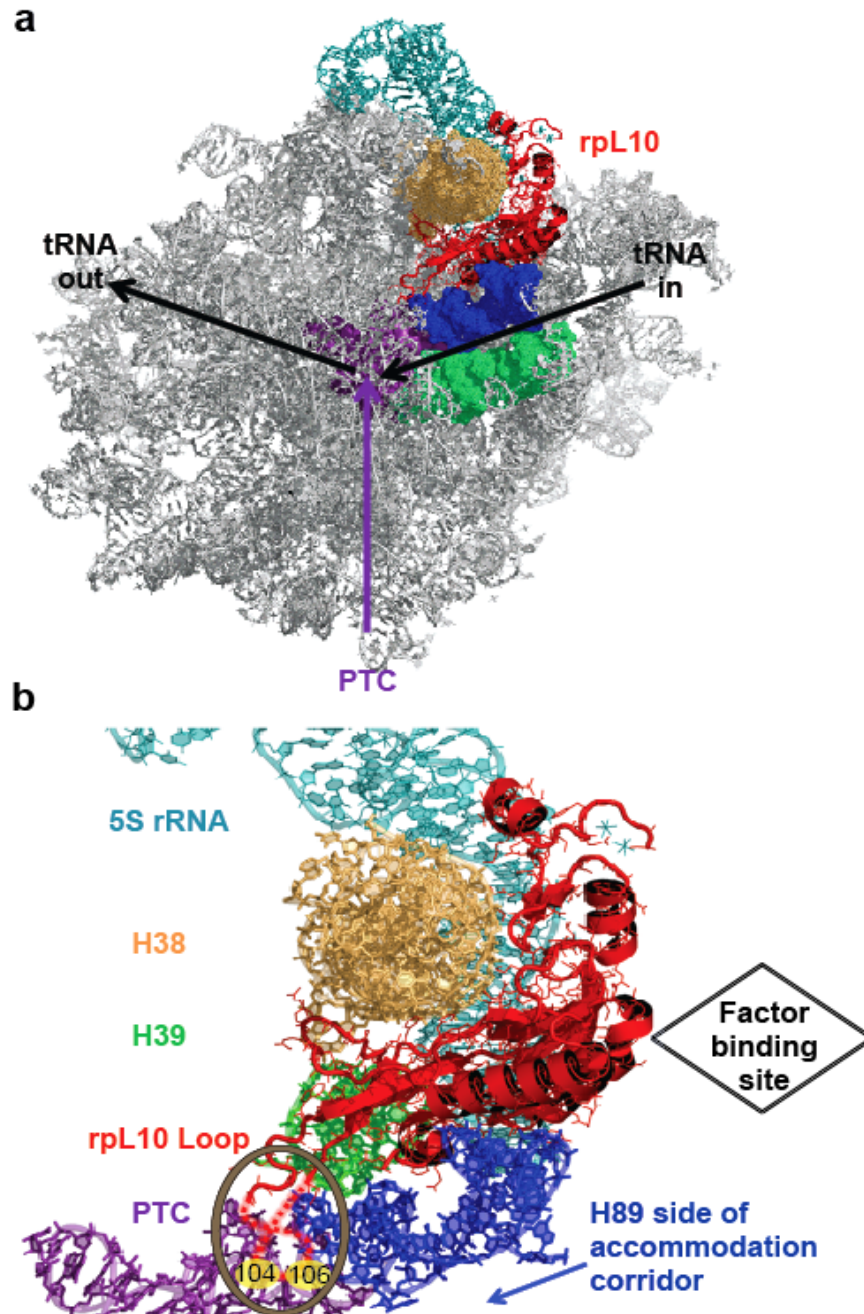
Figure 26. rpL10 is strategically positioned in the core of the LSU.

a. The big picture: rpL10 in the context of the subunit interface of the LSU. **b.** A close-up view of rpL10 and the local environment. The hypothetical loop structure is circled and indicated by dashed red lines and the approximate positions of S104 and A106 are indicated. The protein is situated between Helices 38 and 89, and appears to be an extension of Helix 39. It is located in close proximity to several functional centers of the LSU including the PTC, the aa-tRNA accommodation corridor, and the elongation factor binding site. It is also positioned to communicate with the SSU through Helix 38 and the 5S rRNA.

56

Results

The S104D and A106R mutants promote opposing effects on ligand binding to the ribosomal A- and P-sites. Saturation mutagenesis of the rpL10 loop revealed two classes of mutants based on their ribosome biogenesis defects. Class I mutants, exemplified by rpL10-S104D, displayed halfmer polysomes which are indicative of subunit joining defects on the mRNA. Class II mutants, exemplified by rpL10-A106R, exhibited higher 60S/40S subunit ratios [187]. A summary of additional genetic and functional analyses of loop mutants displaying the strongest defective phenotypes is depicted in Table 1. Of these, rpL10-S104D and rpL10-A106R were chosen for further examination. While the rpL10 loop was not resolved by X-ray crystallography [15], cryo-EM studies suggested that the tip of this loop is in close proximity to the P-site tRNA [188,189]. Thus, it was speculated that P-site ligand binding would be affected by these mutants. However, steady state binding of acetylated-[^{14}C]Phe-tRNA^{Phe} to 80S ribosomes purified from isogenic strains expressing wild-type and mutant forms of rpL10 showed no significant differences in binding of this model P-site ligand to the ribosomal P-site (Figures 27a and 28a). In contrast, the mutants showed significant changes in their ability to bind elongation ternary complex ([^{14}C]Phe-tRNA^{Phe}•eEF1A•GTP) to the ribosomal A-site: specifically the rpL10-S104D mutant promoted a 2-fold increase in K_D for this ligand, while the rpL10-A106R mutant promoted a 2-fold decrease (Figures 27a and 28b). To ascertain whether these differences were due to changes in affinity for the elongation factor or the aa-tRNA itself, the same experiment was performed using [^{14}C]Phe-tRNA^{Phe} alone (i.e. non-enzymatic binding). Under these conditions, the aa-tRNA binding defect of the rpL10-S104D mutant was exacerbated (~6-fold increased K_D

relative to wild-type ribosomes), and this was partially ameliorated by addition of eEF1A and GTP (Figures 27b and 28d). In contrast, the binding of [^{14}C]Phe-tRNA^{Phe} to wild-type or rpL10-A106R ribosomes was not influenced by eEF1A. These data indicate that the tRNA binding defects are intrinsic to the ribosomal A-site and not to binding sites unique to eEF1A.

Eukaryotic elongation factor 2 (eEF2), which drives translocation, is a structural mimic of the elongation ternary complex, and includes a tRNA-like domain (Domain IV) that also interacts with the ribosomal A-site of the decoding center [105]. Steady-state binding assays of purified eEF2 to 80S ribosomes, as monitored by the extent of diphtheria toxin [^{14}C]- ADP ribosylation, also revealed reciprocal changes in K$_D$ values for the two mutants (Figures 27a and 28c). Importantly, while the S104D mutant ribosomes exhibited decreased affinity for aa-tRNA and elongation ternary complex, they displayed increased affinity for eEF2. Conversely, A106R mutant ribosomes displayed increased affinity for aa-tRNA and elongation ternary complex and decreased affinity for eEF2.

Sdo1p is required at a late step in 60S maturation, coupling the GTPase activity of the Efl1p to release of Tif6p [47]. Steady state binding assays using purified [^{32}P]-labeled Sdo1p revealed that mutant ribosomes displayed defects in binding this ligand similar to those observed with elongation ternary complex, i.e. the rpL10-S104D mutant promoted decreased affinity for Sdo1p, while the rpL10-A106R mutant promoted increased affinity for it (Figures 27c and 28e). Sdo1p did not bind mRNA or tRNA alone, and the Sdo1pΔN mutant lacking the N-terminal FYSH domain that is essential for protein function [190] displayed negligible binding to wild-type ribosomes (Figure 28e). Scatchard plot analyses

demonstrated that Sdo1p binds to a single site on the ribosomes (Figure 28f). Competition assays in which wild-type ribosomes were pre-incubated with increasing amounts of Sdo1p revealed that this protein stimulated binding of aa-tRNA to ribosomes in a concentration dependent manner, while inhibiting both binding of Ac-aa-tRNA to the P-site and peptidyltransferase activity (Figure 27d).

	L103S	S104D	C105G	A106R	A106P	A106L
Growth	Slow	Very slow		Very slow		Slow
Temperature sensitivity				Yes		
Tif6 suppression		Yes	Yes		Yes	
Cycloheximide		Hs	S		S	
Anisomycin		Hs	R	R	R	
Polysome profile	↑ 60S	½ mer	½ mer	↑ 60S	½ mer	↓80S

Table 1. Summary of genetic and functional analyses of L10 loop mutants.

Cell growth at various temperatures (30ºC, 15ºC, 37ºC), the ability of Tif6 mutants to suppress growth defects when co-expressed in mutant yeast cells, and the sensitivity to antibiotics were monitored by 10-fold dilution spot plating. S = sensitive, Hs = hypersensitive, R = resistant. Sucrose gradient analyses of mutant cells revealed halfmer defects (1/2 mer), elevated 60S/40S ratios (↑ 60S), or reduced polysomes (↓80S). Blank spaces = wild-type phenotype. The S104D and A106R mutants were chosen for further examination based on these results.
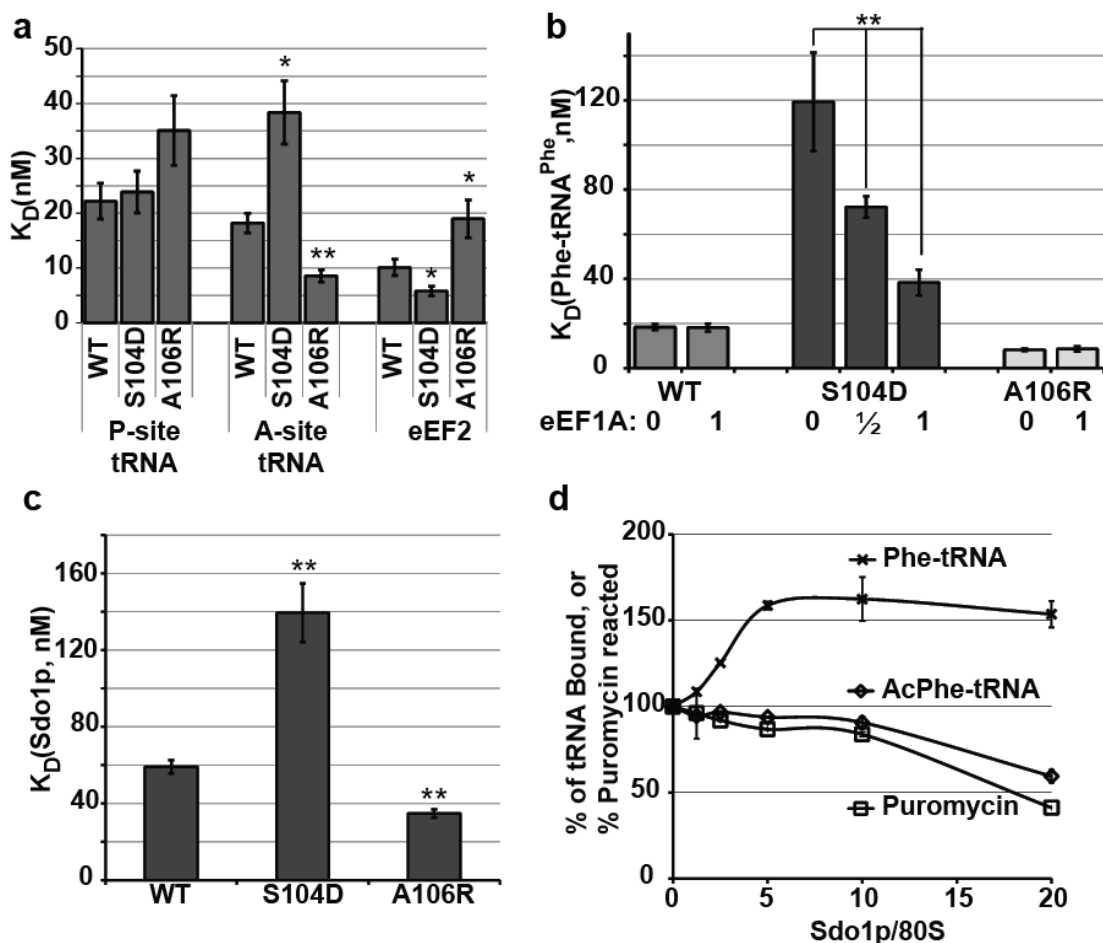
Figure 27. rpL10 loop mutants have opposite effects on ligand binding to the A- and P-sites.

Panels a - c: Steady state binding of indicated ligands to ribosomes isolated from cells expressing wild-type *rpl10* and the *rpl10-S104D* and *rpl10-A106R* mutants. **a.** Dissociation constants obtained from binding assays of Ac-aa-tRNA to the P-site and ternary complex to the A-site as monitored by filter binding, and eEF2 as monitored by extent of ribosylation of unbound protein. **b.** Titration of eEF1A into aa-tRNA binding reactions similar to ternary complex in panel a; 1 = amount for maximum activity. **c.** Dissociation constants obtained from assays of binding of Sdo1p as monitored by levels of radiolabel detection in ribosomes. **d.** Competition assays. Binding of aa-Phe-tRNA[Phe] or Ac-Phe-tRNA[Phe] at half maximal concentrations were monitored in the presence of increasing amounts of Sdo1p. Peptidyltransferase activity was similarly monitored. Bars indicate s.e.m. (n=4 for a-b, n=3 for c), * $P < 0.05$, ** $P < 0.01$ (compared to wild type unless noted).
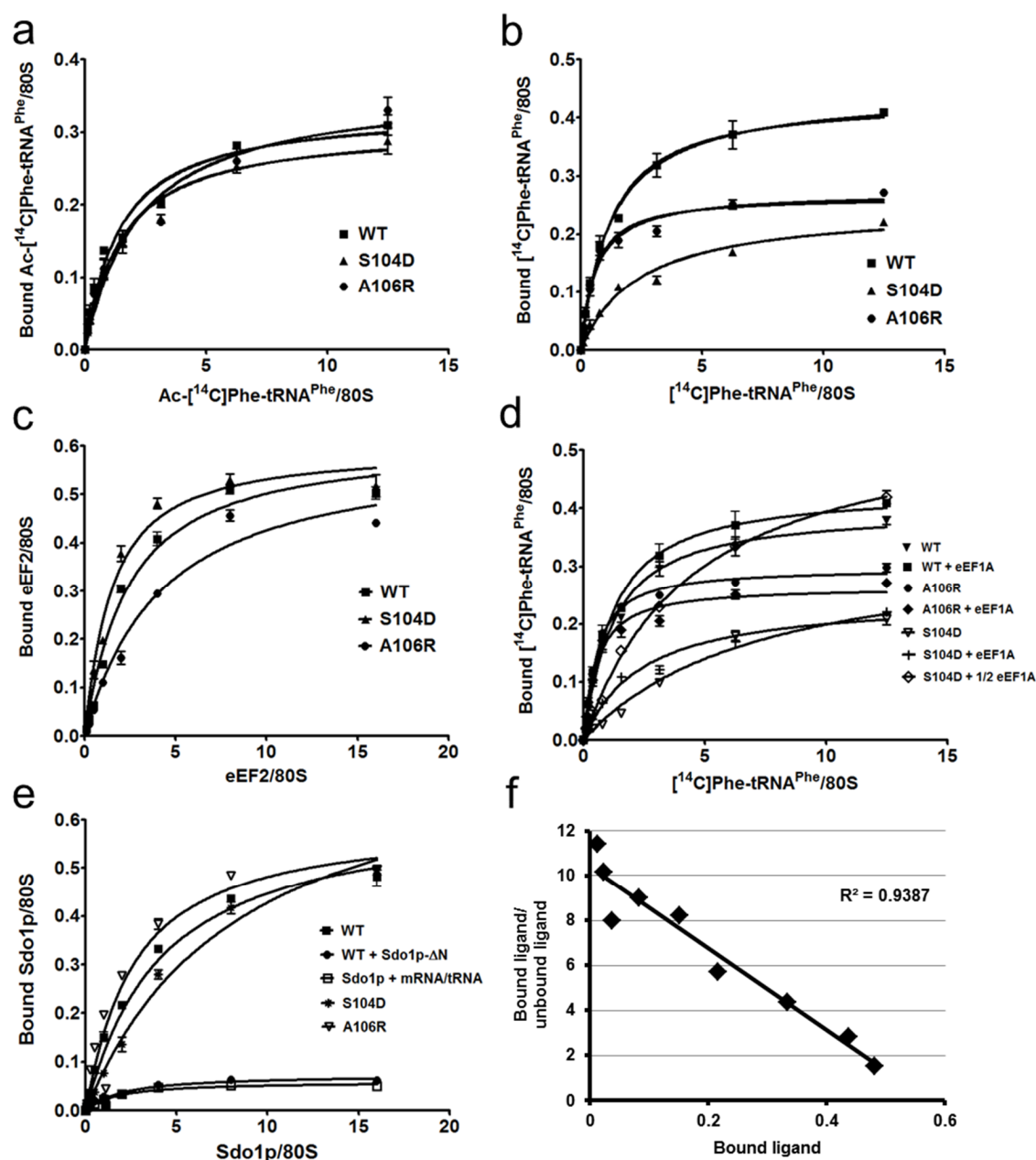
Figure 28. Primary ligand binding data related to Figure 27.

Panels a - c: Single site binding isotherms for ribosomes and various ligands. Binding of Ac-aa-tRNA to the P-sites (panel a), ternary complex to the A-site (panel b), and eEF2 (panel c) to ribosomes isolated from wild-type, *rpl10-S104D* and *rpl10-A106R* cells. **d.** Titration of eEF1A into aa-tRNA binding reactions similar to panel b. **e.** Single site binding isotherms for indicated ribosomes and Sdo1p. Sdo1pΔN is an N-terminal deletion mutant that cannot bind ribosomes. Sdo1p does not bind significantly to mRNA or tRNA alone. **f.** Scatchard plot of Sdo1p binding to wild-type ribosomes indicates single site binding. 5 pmoles of ribosomes in 120 μl total volume were used at each dilution throughout. Bars indicate standard error of the mean.

The A106R and S104D mutants have opposing effects on the rotational equilibrium of the ribosome. During the elongation cycle, the ribosome transits through a large number of conformations, characterized at the extremes by states described as non-rotated and rotated [15,101,104,109,110,112]. Recent single molecule experiments using *E. coli* ribosomes have shown that the aa-tRNA•EF-Tu•GTP elongation ternary complex has higher affinity for non-rotated ribosomes than rotated ribosomes, and that the converse is true for EF-G [191]. Thus, the ligand binding data described above suggested that the A106R and S104D mutants drive the structural equlibria of ribosomes toward either the non-rotated (substrate for binding elongation ternary complex) or rotated (substrate for eEF2) states respectively. While chemical modification profiles and atomic resolution structures are well-defined for non-rotated and rotated *E. coli* ribosomes [110,192–196], no equivalent information exists regarding yeast ribosomes. Thus, in order to examine the rotational status of yeast ribosomes, it was first necessary to demonstrate that chemical protection patterns of well-defined *E. coli* and yeast ribosome complexes are similar. For *E. coli*, the standard for non-rotated ribosomes are those which are primed with polyU and contain N-Ac-PhetRNA[Phe] in the P-site, while rotated ribosomes are primed with polyU and contain deacylated tRNA in the P/E site and EF-G-GDPNP [195]. Similar complexes were prepared using yeast ribosomes (rotated yeast ribosomes contained eEF-2-GDPNP instead of EF-G-GDPNP). These two complexes, plus empty wild-type control ribosomes were chemically probed with 1M7 (or DMSO only controls), and base reactivities were assessed by hSHAPE and quantified using ShapeFinder [197,198]. Representative complete electropherograms for these three samples are shown in Figure 29.
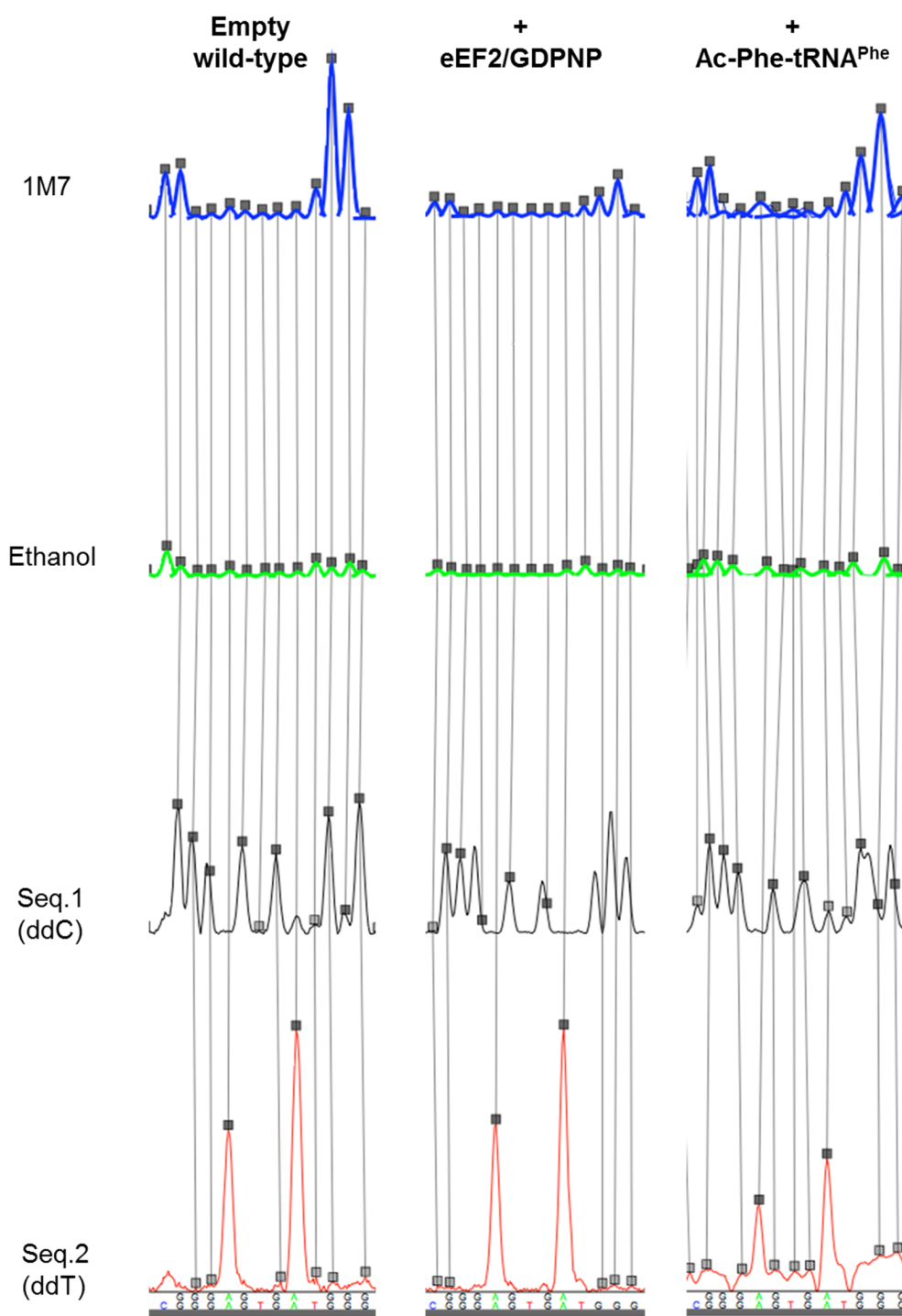
Figure 29. Visualization of chemical probing data by hSHAPE.

A representative electropherogram segment from chemical probing in H63 of the LSU for the indicated complexes showing differences in chemical reactivities (peak areas). The areas under the 1M7 reactivity peaks are integrated to generate quantitative data and enable statistical analyses (see Table 2). Ethanol is the negative control.

Table 2 shows that the chemical modification profiles of landmark *E. coli* rRNA bases are very closely matched by their yeast counterparts in the non-rotated and rotated states (compare columns 3 and 4, with columns 6 and 7). Columns 8 - 10 of Table 2 also depict conversion of the statistically normalized reactivity data to a scale from 0 – 4, with 4 being most reactive [197,199]. Occupation of the P-site by Ac-aa-tRNA (non-rotated ribosomes) resulted in nearly identical chemical modification patterns at equivalent rRNA bases in the P-sites of the small and large subunits, and in the large subunit E-sites (indicated by color coded boxes in Table 2). Similarly, the chemical modification patterns in the large subunit P- and E-sites of rotated yeast ribosomes closely matched published data for rotated *E. coli* ribosomes. Additionally, the non-rotated control was verified biochemically by comparing the ternary complex and eEF2 steady state binding profiles (Figure 30). Note that the rotated control could not be biochemically assessed as the factor binding site was already occupied by eEF2-GDPNP. Collectively, these data demonstrate that these two complexes represent non-rotated and rotated yeast ribosomes.

E. coli nucleotide[1]	Yeast nucleotide[2]	E. coli P site occupied compared to empty 70S[3]	E. coli EF-G-GDPNP compared to empty 70S[4]	80S empty[5]	80S P site occupied[6]	80S eEF2-GDPNP[7]	80S empty reactivity[8]	80S P site occupied reactivity[9]	80S eEF2-GDPNP reactivity[10]
SSU P-site									
A532	A579	Weakly protected		29.209533	19.3633623	23.26285	3	2	2
G693	G904	Protected		21.486294	2.30601785	5.4394358	3	1	1
A794	A1005	Protected		5.0085212	0.63071889	2.8545354	1	0	0
C795	C1006	Protected		0.3092358	0.22039727	0.0685841	1	0	0
G926	G1150	Protected		NI	NI	NI			
G966	U1191	Weakly protected		NI	NI	NI			
G1338	G1575	Weakly protected		52.590355	37.046344	10.990177	3	2	2
LSU P-Site									
A1916	A2259	Weakly protected		NI	1.46208226	0.7667143	NI	0	0
A1918	G2261	Weakly protected		16.591722	12.9900386	6.2834256	2	1	2
U1926	U2268	Weakly protected		237.04377	0.40327763	18.495792	4	0	2
G2252	G2620	Protected	Protected	7.3710908	2.34212702	3.3526858	2	1	1
G2253	G2621	Protected	Reactive / unchanged	5.7993268	2.77326129	5.8762237	2	1	2
A2439	A2808	Protected	Protected	NI	NI	1.1447785	0	0	1
A2451	A2820	Protected	Protected	70.682962	0.27775391	11.154668	4	0	2
G2505	G2874	Weakly protected		1.3841216	1.58462719	1466.4545	1	1	4
U2506	U2875	Protected		8.4806306	4.65375882	0	2	1	0
U2584	U2953	Protected		1.8857207	0.57815281	0.9600475	1	0	0
U2585	U2954	Protected		80.722973	NI	11.056566	4	NI	2
LSU E-site									
G2112	A2456	Reactive / unchanged	Protected	1.2368216	2.1285347	0.1310783	1	2	0
G2116	U2460	Reactive / unchanged	Protected	2.7718079	3.18348329	1.6371288	1	2	1
C2394	C2764	Reactive / unchanged	Protected	0.4569259	0.29872902	0.0868647	0	0	0

Weakly protected
Protected
Reactive / unchanged
NI=Not Interpretable

Table 2. Comparison of yeast rRNA chemical modification profiles with non-rotated and rotated *E. coli* standards.

1. *E. coli* rRNA base number. **2.** Corresponding *S. cerevisiae* rRNA base number. **3.** Chemical modification profile comparing polyU primed *E. coli* ribosomes containing Ac-aa-tRNA in the P-site to empty ribosomes using nomenclature as described [195]. **4.** Chemical modification profile comparing polyU primed *E. coli* ribosomes containing deacylated tRNA in the P-site plus EF-G-GDPNP to empty ribosomes using nomenclature as described [195]. **5.** Intensity of normalized hSHAPE signals in empty wild-type yeast ribosomes obtained from integrated areas under electropherogram peaks in arbitrary units as described [197]. **6.** Intensity of normalized hSHAPE signals in polyU primed wild-type yeast ribosomes containing Ac-aa-tRNA in the P-site. **7.** Intensity of normalized hSHAPE signals in polyU primed wild-type yeast ribosomes containing deacylated tRNA in the P-site plus eEF2-GDPNP. **8-10.** Arbitrary units from columns 5-7 converted to statistically determined reactivity values as described [199]. Boxes are colored to highlight congruent results where the extent of base reactivity/protection is determined relative to empty wild-type ribosomes.
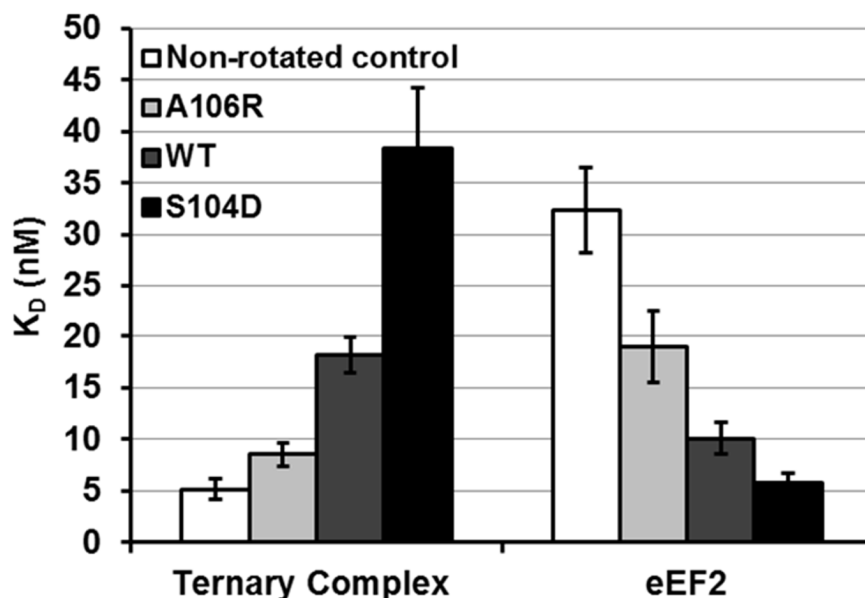
Figure 30. Biochemical verification of the rotational controls.
Dissociation constants of ternary complex and eEF2 for empty wild-type and control non-rotated (+Ac-Phe-tRNA^{Phe}) ribosomes. Bars indicate s.e.m. (n=4**).**

Having established standards defining the chemical reactivity profiles of non-rotated and rotated yeast ribosomes, these were used to determine the rotational statuses of mutant ribosomes. To this end, the chemical protection profiles of "landmark" basepair interactions located in several universally conserved intersubunit bridges [15,85,111,112] were examined using vacant ribosomes. Although FRET experiments showed that vacant bacterial ribosomes are not as structurally dynamic as pre-translocation ribosomes (i.e. containing deacylated tRNA in the P site) [108], we nonetheless chose to make comparisons using vacant ribosomes for two reasons: 1) to monitor the intrinsic influence of the L10 internal loop on ribosome conformational states, i.e. in the absence of *trans*-acting factors (e.g. tRNAs), and 2) because ribosomes harboring deacylated tRNAs in the P-sites alone do not occur in physiological conditions.

The B7a intersubunit bridge undergoes dramatic rearrangements during ribosome rotation [111]. Specifically, when the ribosome is in the non-rotated state, *E. coli* A702 (yeast G913) of the small subunit rRNA interacts with *E. coli* A1847 (yeast A2207) of the large subunit rRNA, protecting both bases from chemical attack. This interaction is disrupted when the ribosome assumes the rotated state, rendering both bases susceptible to chemical modification (Figures 31 and 32a). Kethoxal was used to probe G913, and 1M7 was used to probe A2207, and the extent to which these bases were modified in purified empty isogenic wild-type and mutant ribosomes, and with control rotated and non-rotated ribosomes was quantitatively assessed and normalized using hSHAPE [199]. Figure 32b and 32c show that both of these bases were reactive along a continuum, beginning with non-rotated wild-type control (least reactive) to rpL10-A106R, empty wild-type, rpL10-S104D, and finally rotated wild-type control (most reactive). The intermediate peak heights observed with empty wild-type ribosomes are consistent with the view that the 80S ribosome is free to transit between the two states in the absence of ligands [101].
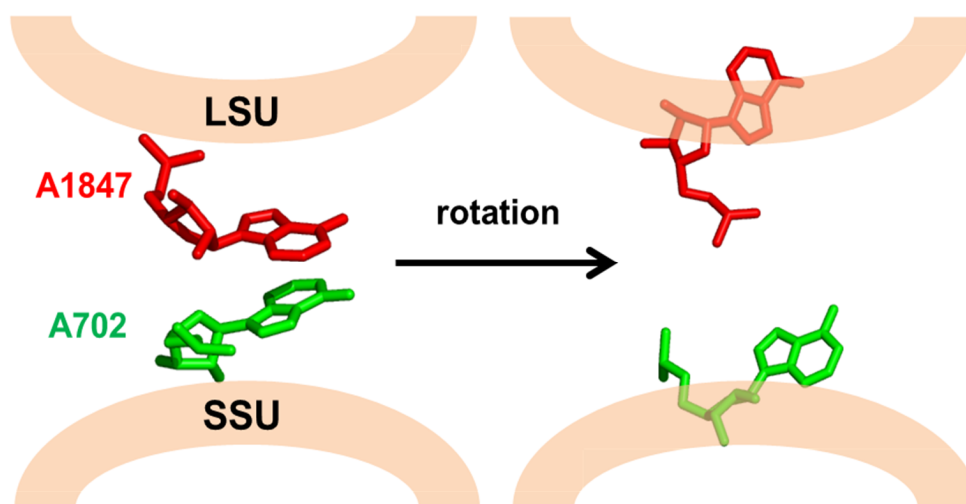
Figure 31. Structure of the B7a intersubunit bridge in the non-rotated and rotated states in *E. coli* ribosomes.

The interaction between A1847 in the LSU and A702 in the SSU is disrupted upon rotation, rendering both bases susceptible to chemical modification. Structures were generated in PyMOL using the most recent high resolution structures of bacterial ribosomes [109].
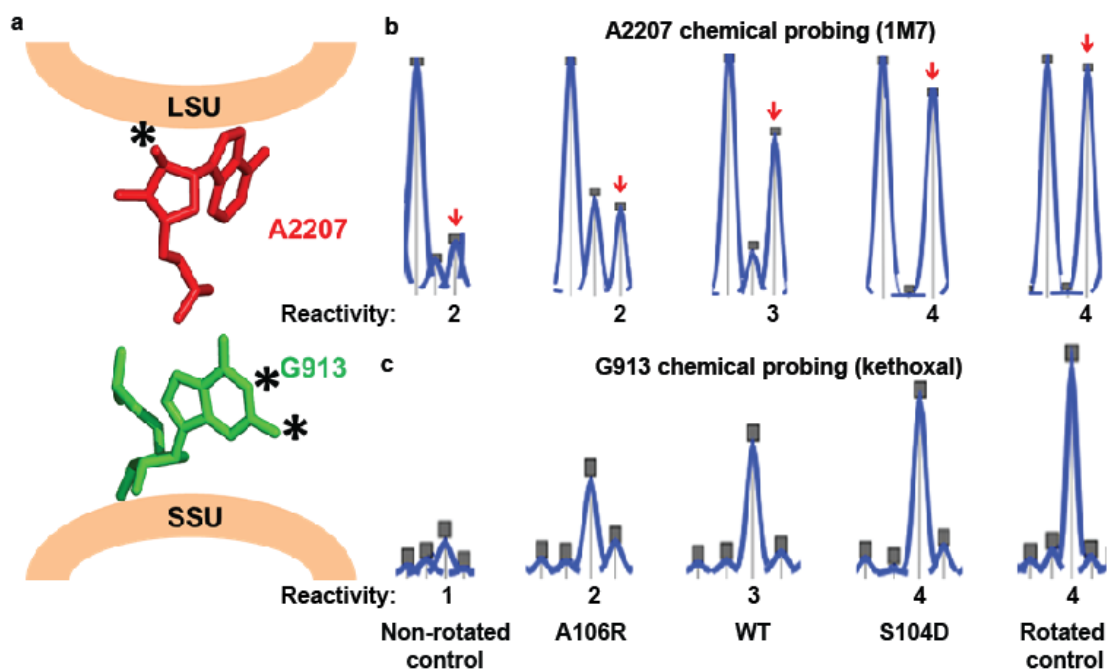
Figure 32. rpL10 loop mutants alter the rotational equilibrium of the ribosome.

a. The yeast B7a intersubunit bridge. In the non-rotated state, A2207 (25S rRNA) forms an interaction with G913 (18S rRNA). In the rotated state, that interaction is disrupted, and the marked 2' OH-group on A2207 becomes accessible to modification by 1M7. Similarly, marked atoms on G913 become accessible to modification by kethoxal upon rotation. **b.** Reactivity peaks obtained by hSHAPE after probing of the landmark base A2207 (arrows) at the LSU side of the B7a intersubunit bridge with 1M7. **c.** Reactivity peaks obtained by hSHAPE after chemical probing of the landmark base G913 at the SSU side of the B7a intersubunit bridge with kethoxal. Data were assigned five levels of reactivity: 0 (for less than a trace's median value), 1 (for a value between the median and the mean), 2 (for a value between the mean and the 1st standard deviation), 3, (for a value between the 1st and the 2nd standard deviation) and 4 (for values above the 2nd standard deviation). Mean, median and standard deviation were calculated on a per trace basis.

Additional key rRNA bases known to undergo structural changes during intersubunit rotation were also probed. For example, the B2a intersubunit bridge, formed between the distal loop of H69 of the LSU and h44 of the SSU is important for substrate selection on the ribosome [200], and bases comprising this bridge undergo significant rearrangement during subunit rotation, albeit not as dramatic as the B7a bridge [112]. Table 3 shows that bases involved in the B2 bridge are less reactive in non-rotated control and rpL10-A106R mutant ribosomes than their rotated control and rpL10-S104D counterparts. The B3 bridge was utilized as an internal control because it is not disrupted during intersubunit rotation, and is thought to be the pivot around which the subunits rotate. Consistent with this, no significant changes in B3 base reactivities were observed. The aa-tRNA accommodation corridor (AC) closes upon ribosome rotation, rendering the "gate bases" less reactive [200–202]. This is reflected as increased chemical reactivities of these bases (U2860, U2924 and U2926) in non-rotated control and A106R mutant ribosomes as compared to S104D and rotated controls. Additionally, specific bases in the Sarcin/Ricin loop are reactive in non-rotated *E. coli* ribosomes [195]. The same protection patterns are observed at the analogous yeast rRNA bases (U3023 and A3027). Collectively, the analyses shown in Table 3 support the hypothesis that the S104D mutant shifts the structural equilibrium of 80S ribosomes toward the rotated state and that the A106R mutant shifts it toward the non-rotated state.

Region	rRNA base	Non-rotated	A106R	S104D	Rotated
B7a	A2207	2	2	4	4
	G913 (SSU)	1	2	4	4
B2a	U2258	2	2	3	4
	A2262	0	0	1	2
	C1644 (SSU)	1	1	2	2
	G1645 (SSU)	0	0	2	1
B3	U2301	0	0	1	1
	G2302	0	0	0	0
	A1655 (SSU)	1	2	2	2
	U1656 (SSU)	2	2	2	2
AC	U2860	1	2	0	0
	U2924	4	2	0	1
	A2926	4	2	1	1
SRL	U3023	1	1	0	0
	A3027	2	3	0	0

Table 3. Establishing the rotational status of mutant ribosomes.

Non-rotated control yeast ribosomes were primed with polyU and contained Ac-Phe-tRNA[Phe] in the P-site. Rotated control ribosomes were primed with polyU, loaded with deacylated Phe-tRNA, and incubated with eEF2-GDPNP. These complexes, along with salt-washed empty rpL10-A106R and rpL10-S104D ribosomes were chemically probed with 1M7 or kethoxal and analyzed by hSHAPE. B7, B2a and B3 denote the probed intersubunit bridges. AC: Accommodation Corridor. SRL: Sarcin/Ricin Loop. Numerical values reflect statistically normalized reactivities on a scale of 0 - 4, with 4 being most reactive [197,199].

The S104D and A106R mutants define local and long distance changes in rRNA structure corresponding to ribosome rotational status. Having established the rotational status of the mutant ribosomes, 1M7 and hSHAPE were used to quantitatively assess the chemical reactivities of approximately half (~2000 nt) of the rRNA content of salt-washed empty 80S ribosomes purified from isogenic cells expressing wild-type and the mutant forms of rpL10. The highly reproducible quantitative data enabled subtraction analyses for each base probed. Figures 33-37 employ a heat map based approach in which the reactivity data obtained from A106R mutant ribosomes was subtracted from data obtained from S104D mutant ribosomes. This analysis yields maps highlighting the differences in rRNA base reactivities between the conformational states of the two mutants. In these maps, warmer colors signify higher reactivity, and implicit higher flexibility of rRNA bases in S104D relative to A106R, while cooler colors correspond to lower reactivity, and implicit higher structure and constraint. Reactivity scale numbers denote the extent of the differences with each step in color as statistically determined [199]. These are mapped onto 2-dimensional flat rRNA maps in Figures 33-35, onto 3-dimensional atomic resolution structures in Figures 36-37, and are summarized in Figure 43c.

Significant differences between the two mutants were observed in the core of the PTC, the rRNA structure most proximal to the rpL10 loop (Figure 33). Three of the four bases proposed to play central roles in the induced fit model of peptidyltransfer [203], i.e. G2922 (*E. coli* G2553), U2924 (*E. coli* U2555), and U2954 (*E. coli* U2584) were less reactive in the rpL10-S104D mutant as compared to rpL10-A106R suggesting a role for yeast rpL10 in this process. The universally conserved A2819 (*E. coli* A2450), G2874 (*E.*

coli G2505), and U2875 (*E. coli* U2506) that constitute the "entrance" to the PTC [202] also showed dramatic differences in chemical reactivities (Figures 33 and 36).

Moving outward from the loop, rpL10 is framed by Helices 38 (the A-site finger), 39, 43 and 89. Significant differences in chemical reactivities between the two mutants are seen in all of these structures (Figures 33 and 34), suggesting that structural rearrangements involving the flexible loop may be transduced through the body of rpL10 to neighboring rRNA structural elements. Focusing on these elements in more detail, Helices 89 and 90 - 92 (Figure 33) form the "accommodation corridor" through which 3' ends of aa-tRNAs transit as they enter the PTC [202]. In this structure, U2860 in H89 (*E. coli* U2491) and U2924 in H92 (*E. coli* U2555) interact to "close" the accommodation corridor in the rotated state. Conversely, they do not interact in the non-rotated state and should be more extensively chemically modified when the accommodation corridor is open. In support of our model, the difference map shown in Figure 33 and summarized in Table 2 demonstrates that these bases are more protected from chemical attack in S104D mutant ribosomes as compared to A106R mutants.

rpL10 also interacts directly with Helix 39. Examination of Figure 34 reveals large scale structural differences between the two mutant ribosomes extending from this helix to Helix 44 (PTC-distal). Importantly, these include the GTPase activating center (GAC) and the H43-44 structure, upon which the P0/P1/P2 (*E. coli* L7/L12) stalk is assembled [204]. This region of the LSU interacts with both the elongation ternary complex and eEF2 at different stages during the elongation cycle. As discussed below, we suggest that the structural differences identified here trace an information transmission pathway that helps the ribosome distinguish between different *trans*-acting factors at different

points in its lifecycle. One such transmission pathway is shown in Figure 37: here, the reactivity data from Figure 34 is plotted onto the yeast ribosome high resolution 3D structure to illustrate a network of rRNA helices connecting the PTC-proximal and PTC-distal portions of rpL10.

The three site allosteric model posits that structural changes in the ribosomal A and E sites are linked [205], and studies from our laboratory have identified an extensive network of rRNA structural changes extending along the entire path taken by tRNAs as they transit the ribosome [178,201,206,207]. Examination of the chemical modification patterns in Helices 82 – 88 (Figure 33), which trace the path of tRNAs from the A- to the E-sites in the LSU, reveals extensive differences in rRNA base reactivities between the two mutants consistent with linkage between the A-and E-sites.
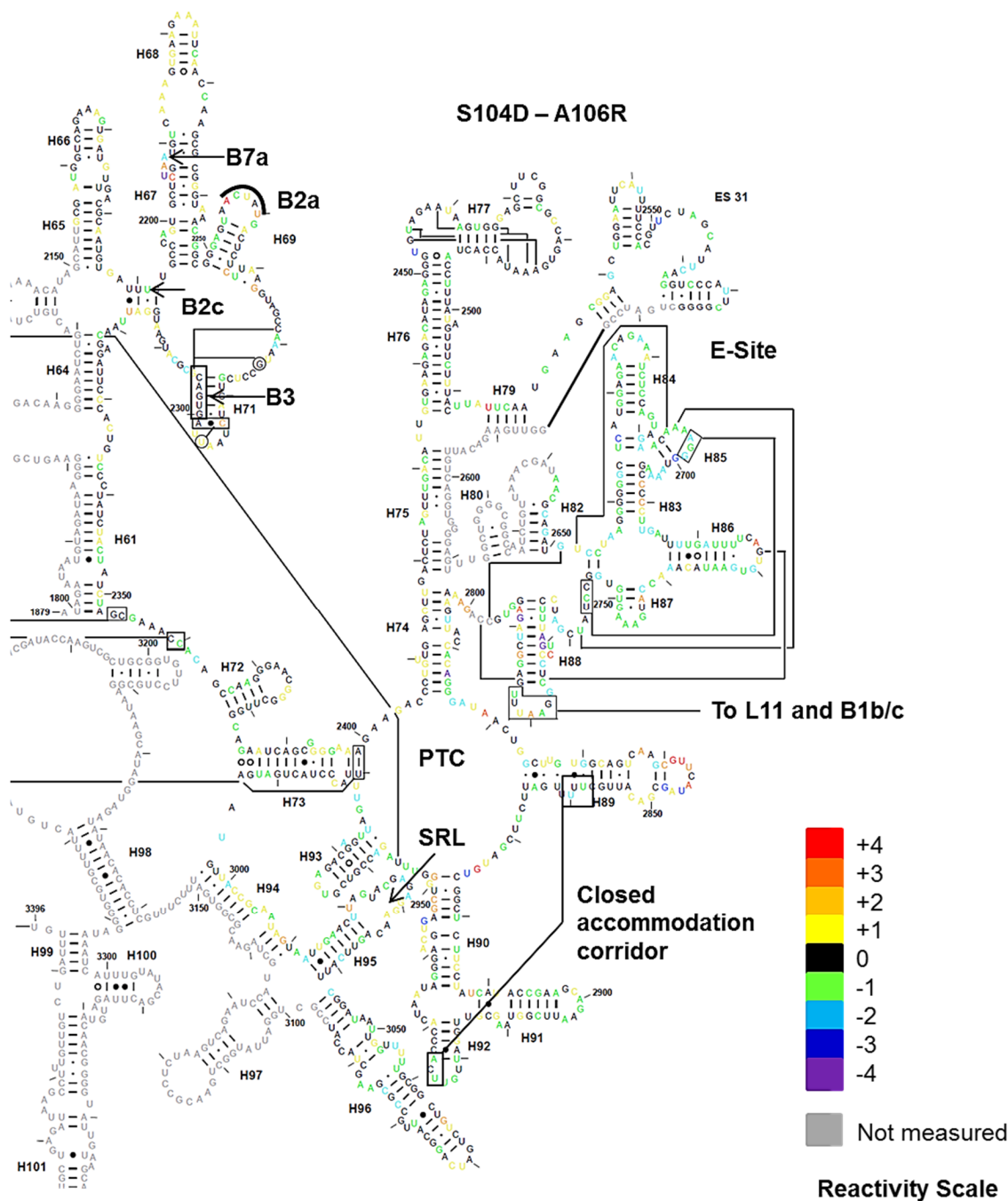
Figure 33. Structural probing analysis of 3' of the LSU.

Chemical probing analysis using 1M7 and hSHAPE, showing S104D – A106R difference map spanning Helices 61 to the 3' end of 25S rRNA. PTC: peptidyltransferase center. SRL: sarcin ricin loop. The scale at right indicates the extent of differences in reactivities with each number corresponding to one standard deviation from the mean reactivity as previously described [199].
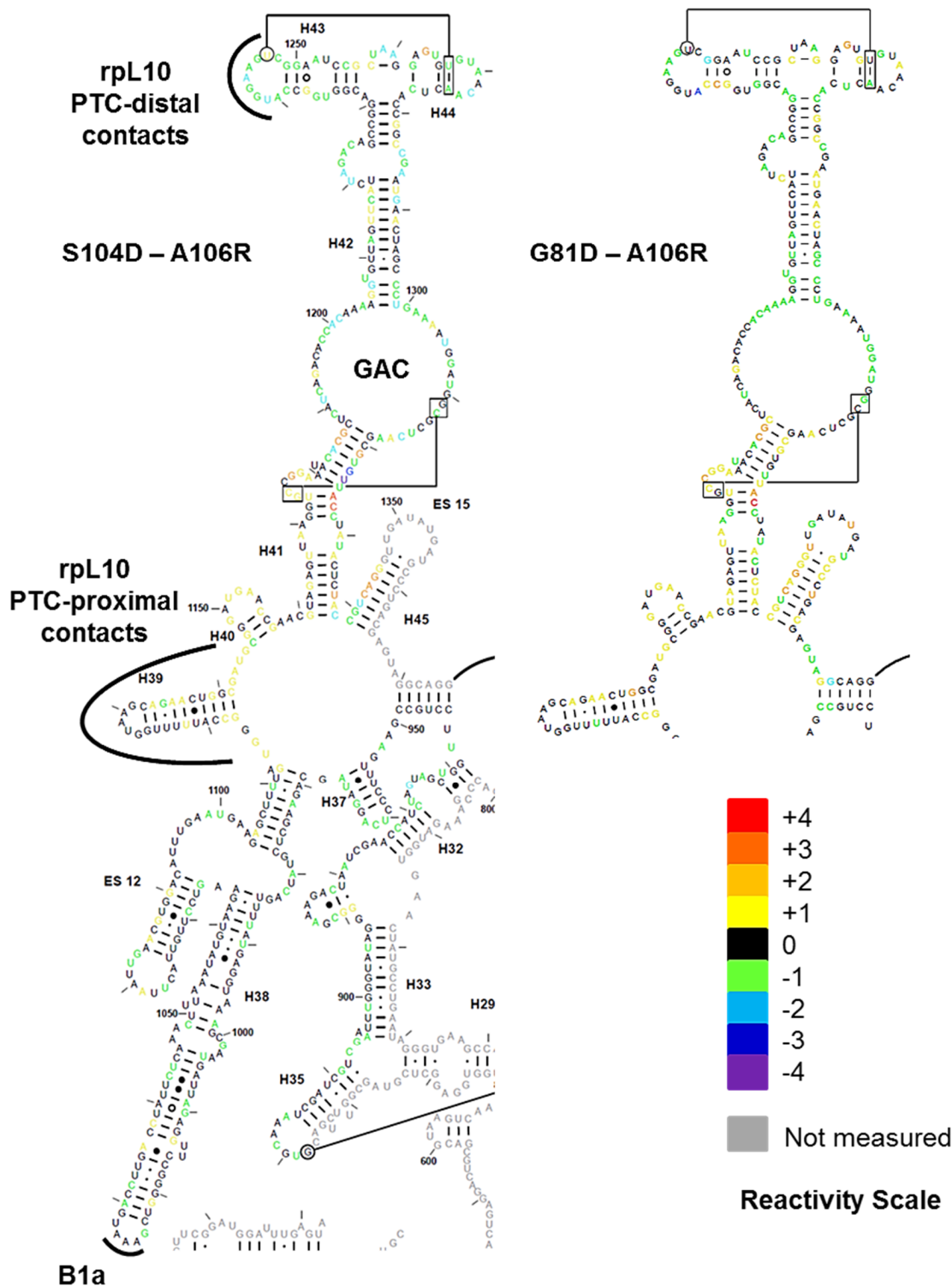
Figure 34. Structural probing analysis of 5' of the LSU.

Heat maps showing differences in 1M7 reactivities between S104D and A106R (left) and G81D and A106R (right) spanning Helices 38 – 44. GAC: GTPase-associated center.

The distal tip of H38 forms the LSU partner of the B1a intersubunit bridge. Although no differences in base reactivities were observed in this structure (Figure 34), presumably because it is intrinsically highly mobile [15,193,208], changes were observed in its SSU partner in the distal loop of h33, part of the 3' major or "head domain" of the SSU (Figure 35). A block of changes in rRNA base reactivities were also observed along the universally conserved helices 32 – 35 in the 3' major domain of the 18S rRNA. These map to the mRNA entrance tunnel on the SSU opposite the decoding center (see Figure 43c). In the 3' minor domain, A1755 (*E. coli* A1492), which plays a central role in stabilizing cognate codon:anticodon interactions in the decoding center [84], is much more protected from chemical modification in rpL10-S104D compared to rpL10-A106R ribosomes (Figure 35). The head of the SSU undergoes a dramatic series of rearrangements during intersubunit rotation [109,209]. Multiple differences in rRNA base reactivities were also noted throughout the head domain (h38 – h43), providing evidence that the rpL10 loop may influence intersubunit rotation through the B1b/c bridge in a pathway involving 5S rRNA and rpL11. This is supported by pronounced differences in rRNA chemical protection patterns at the tip of H88 (Figure 33), which interacts with rpL11 as a monitor of P-site tRNA occupancy [206]. This pathway is shown in Figure 43c.
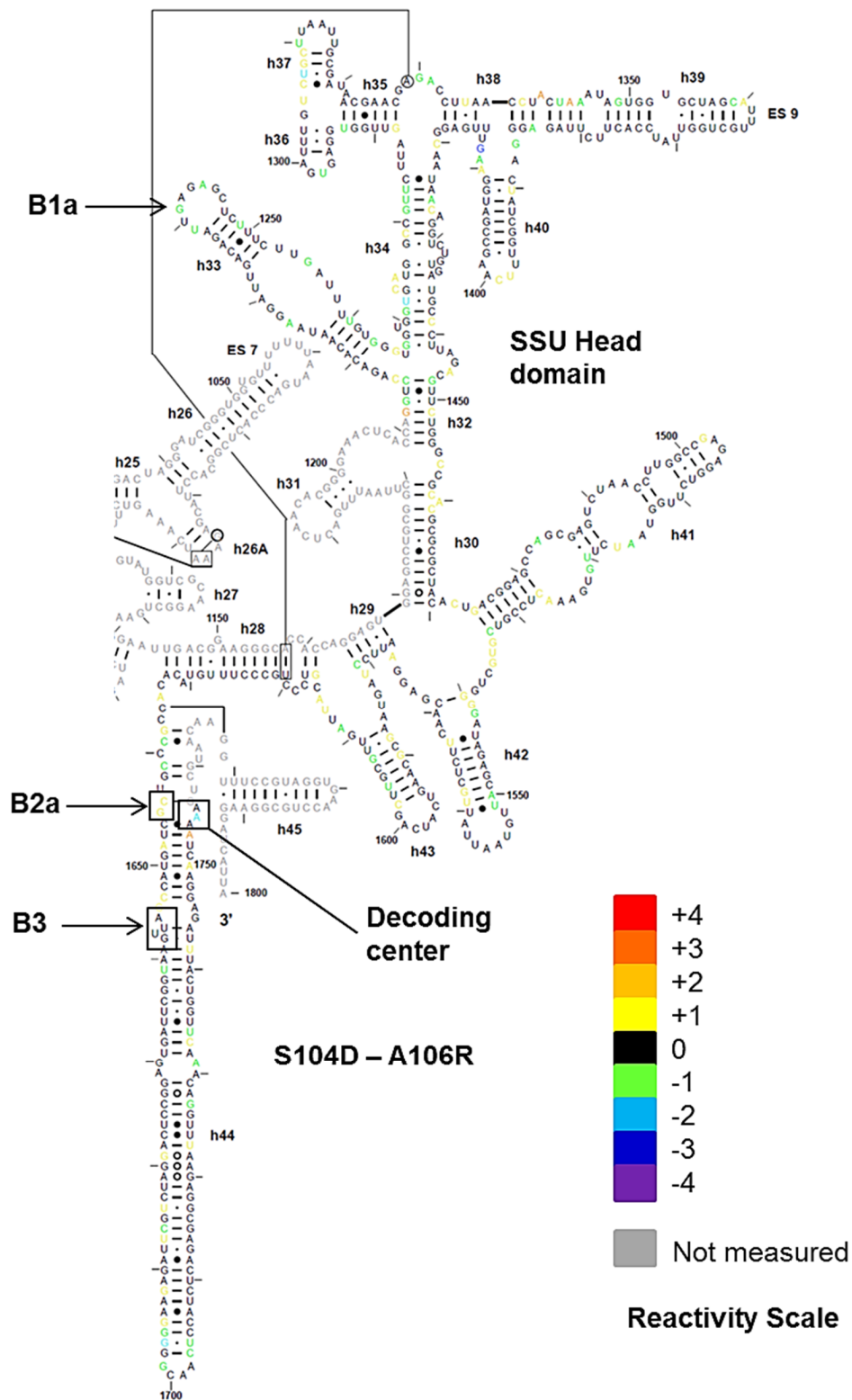
Figure 35. Structural probing analysis of the SSU.

S104D – A106R difference map of SSU rRNA encompassing the 3′-major, and 3′-minor domains.
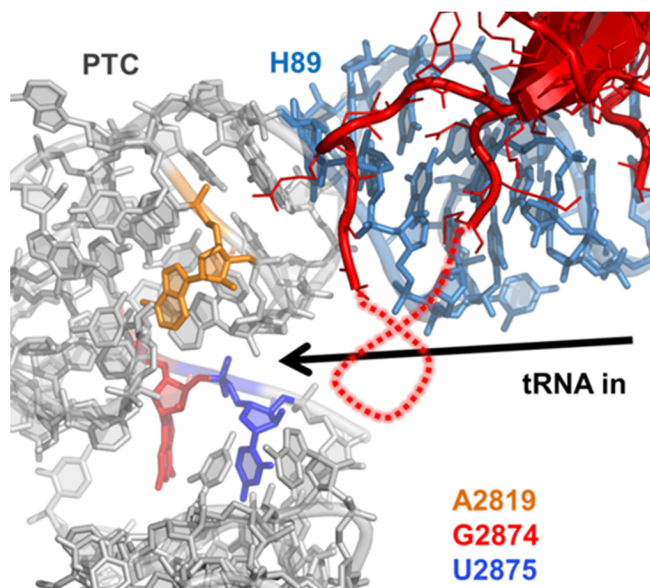
Figure 36. 3D reactivity data of the PTC.
Reactivity data from Figure 33 plotted onto 3D structures, showing the critical bases A2819, G2874 and U2875 forming a triangle in the core of the PTC.
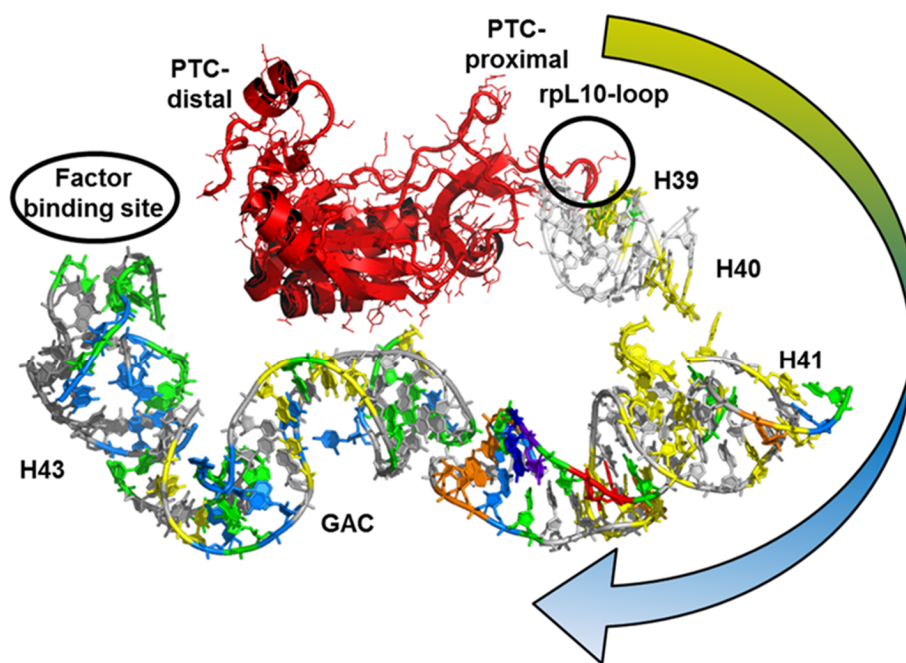
Figure 37. 3D reactivity data of the factor binding site.
Superimposition of data from Figure 33 onto the yeast ribosome high resolution structure.

Identification of important points of contact through which structural changes in rpL10 are communicated to the surrounding rRNA. For structural changes in the loop of rpL10 to be broadly communicated to both subunits, information needs to be transduced through points of contact between rpL10 and local rRNA structural elements. For example, structural changes at amino acid R7, located in the N-terminal "hook" of rpL10, are involved in opening and closing the accommodation corridor [178]. Examination of mutants identified in a previous genetic screen of *rpl10* mutants suggested two additional candidates: F94 and G81 (Figure 38). F94 interacts with H38, and the F94I mutant was chosen for deeper analyses because of its strong resistance to anisomycin (not shown), a competitive inhibitor of aa-tRNA binding to the A-site. Replacement of the aromatic phenylalanine with isoleucine (F94I) produced ribosomes with higher affinity for elongation ternary complex and decreased affinity for eEF2, i.e. distributed toward the non-rotated state similar to the A106R mutant (Figure 39a). hSHAPE analysis revealed that rRNA bases proximal to F94 (Figure 39d, circled) were deprotected in the F94I mutant, presumably due to loss of interactions involving the aromatic ring of phenylalanine. Interestingly, bases further down the H38 structure (Figure 39d, boxed) that interact with the aa-tRNA D-loop showed decreased reactivities similar to an rRNA mutant of these bases that also displayed increased affinity for elongation ternary complex [210]. G81 is located at the opposite end of the body of rpL10, closer to the solvent exposed (PTC-distal) side of the protein, and is one of the amino acid residues closest to the elongation factor binding site (H43). The G81D mutant was chosen because of its anisomycin hypersensitivity (not shown), and it promoted the opposite effects, i.e. decreased affinity for elongation ternary complex and increased affinity for

eEF2 (Figure 39a-c). hSHAPE analysis also revealed that rRNA bases comprising the eEF2 binding site and the GTPase-associated center in G81D underwent changes in reactivity similar to those observed with S104D (Figure 34). These findings suggest that, like S104D, G81D distributes ribosomes toward the rotated state.
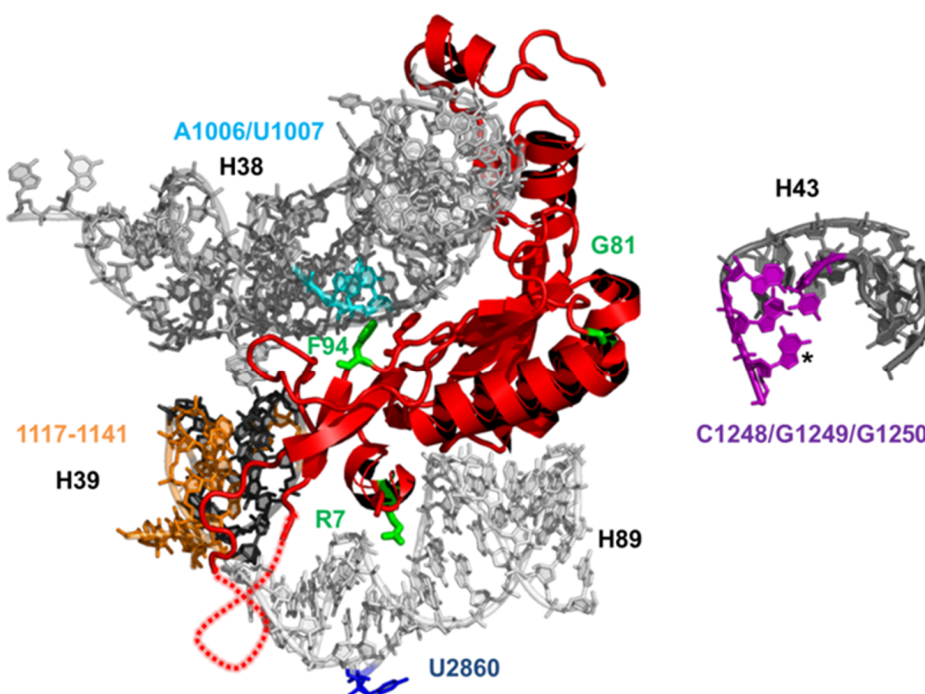
Figure 38. Points of rpL10 important for intersubunit rotation.

Important bridges between L10 and the surrounding rRNA found to be involved in inter-subunit rotation are shown in green. U2860, the H89-side of a closed accommodation corridor, is shown in blue. Bases with increased reactivities in H39 are shown in orange. Bases with decreased reactivities in H43 are shown in purple, with the base proposed to contact G81 starred. The bases in H38 that interact with the phenyl rings of F94 are shown in cyan.
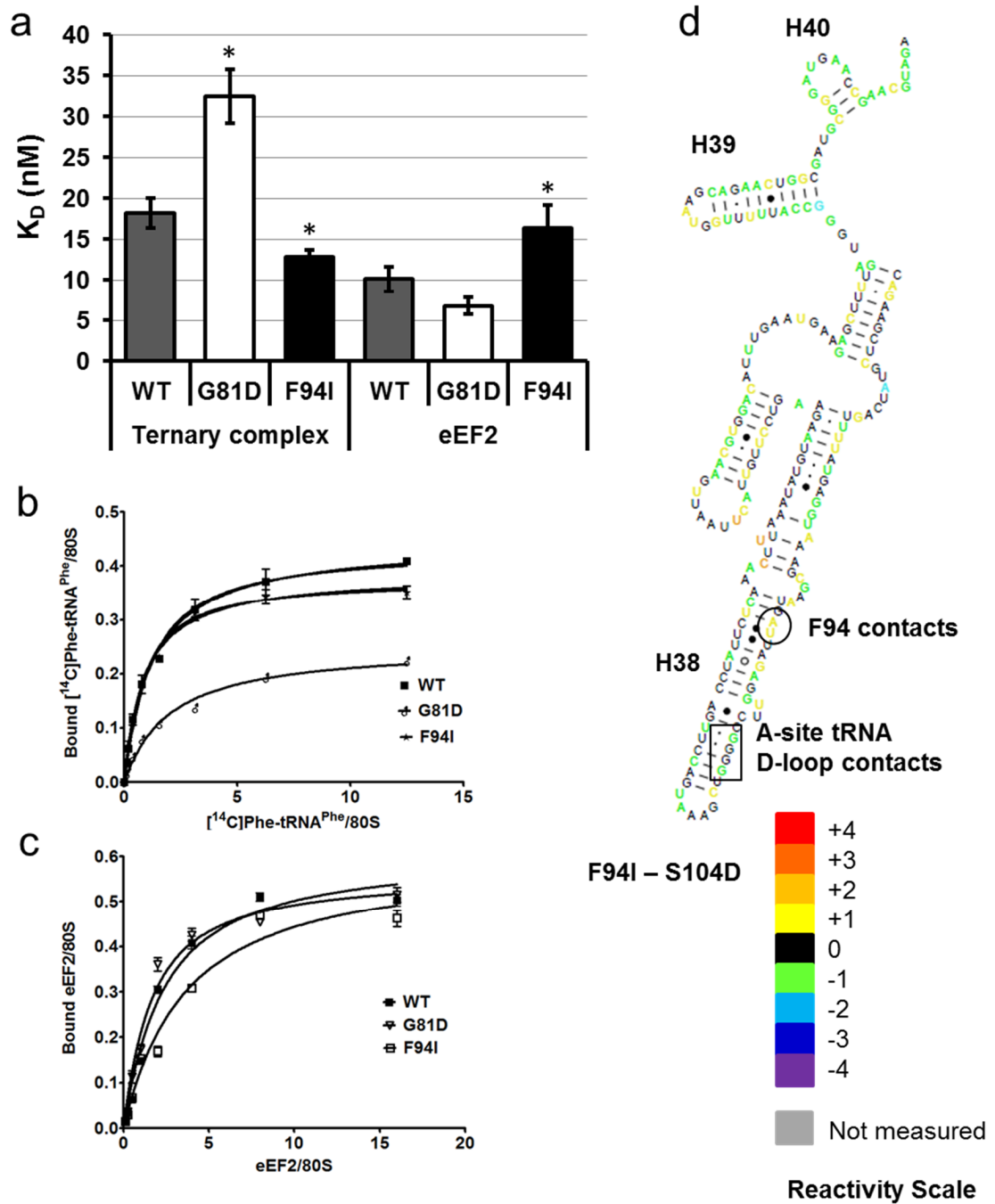
Figure 39. Primary data related to rotational mutants from Figure 38.

a. Dissociation constants of *RPL10, rpl10-F94I and rpl10-G81D* ribosomes with ternary complex and eEF2. Bars indicate s.e.m. (n=4, * *P* < 0.05). **b and c.** Single site binding isotherms for data shown in panel a. **d.** hSHAPE difference map of F94I minus S104D spanning Helix 38 – Helix 40.

Effects of rpL10 loop mutants on peptidyltransferase activity and translational fidelity. A single round, puromycin-based assay of peptidyltransferase activity [211] revealed that S104D mutant ribosomes promoted approximately 60% of peptidyltransferase activity relative to wild-type and A106R mutant ribosomes (Figures 40a-b). As peptidyltransfer occurs in the context of the non-rotated state, this further supports the hypothesis that the rpL10-S104D mutant drives the equilibrium of ribosomes toward the rotated state. Programmed -1 ribosomal frameshifting (-1 PRF) directed by L-A virus-derived sequence requires slippage of both A- and P-site tRNAs [154], while Ty*1* directed +1 PRF only requires slippage of P-site tRNA [166]. Both mutants promoted enhanced -1 PRF but had no effects on +1 PRF (Figure 40c). To more completely understand how the structural changes induced by the S104D and A106R mutations impact the ability of the ribosome to accurately decode mRNAs, we employed dual-luciferase translational fidelity assays designed to measure rates of misreading of near- and non-cognate tRNAs [212], and misreading of a UAA termination codon [213]. The S104D mutant was generally more inaccurate than wild-type, the magnitude of which became greater as the extent of codon/anticodon mismatches increased (Figure 40d). In contrast, decoding was largely unaffected in cells expressing the A106R mutant, although decoding of near-cognate tRNAs was slightly more accurate.
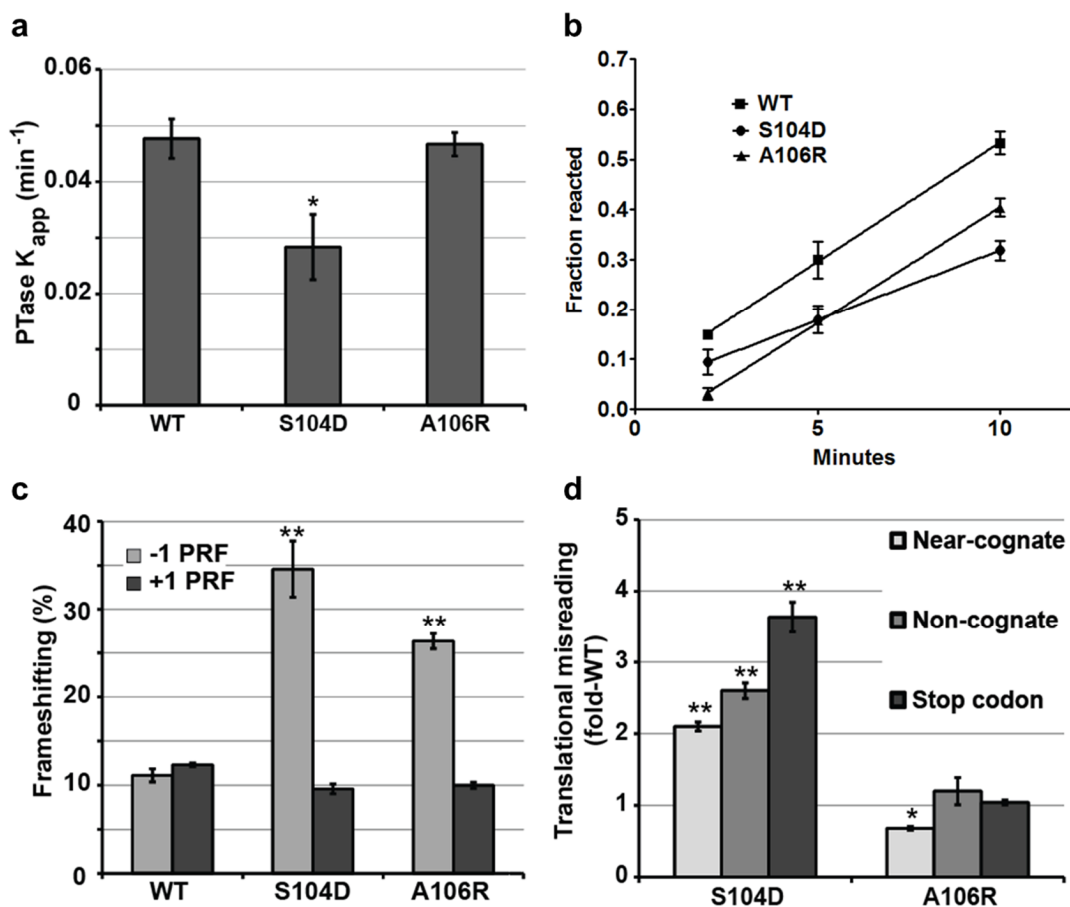
Figure 40. rpL10 loop mutants affect peptidyltransferase activity and translational fidelity.

a. Apparent rates of peptidyltransfer from single turnover peptidylpuromycin reactions for indicated ribosomes. **b.** Single round peptidyltransferase reaction data for wild-type and *the rpl10-S104D and rpl10-A106R* mutants. **c.** Programmed -1 and +1 ribosomal frameshifting values obtained using dual-luciferase reporters. **d.** Misincorporation of a stop codon, and near- and-noncognate amino acids in mutants compared to wild-type levels as monitored using dual-luciferase reporters. Bars indicate s.e.m. (n=4), * $P < 0.05$, ** $P < 0.01$.

An intra-ribosomal suppressor of the S104D mutant reveals the importance of LSU allostery in function of the mature ribosome. If the rpL10 mutants affect the distribution of ribosomes between the non-rotated and rotated states by altering the distribution of allosteric structures intrinsic to the ribosome, then mutants of other ribosomal components that promote opposing effects may be able to suppress the defects exhibited by the *rpl10* mutants. The L3-W255C mutant, which lies in a flexible loop (the W-finger) on the opposite side of the aa-tRNA accommodation corridor from rpL10 (Fig. 43c) promotes increased affinity of ternary complex to the A-site and decreased affinity for eEF2 [211]. A high copy plasmid expressing L3-W255C was able to almost completely suppress the biochemical (binding of ternary complex and Sdo1p to the A-site), and translational fidelity (-1 PRF) defects of the rpL10-S104D mutant (Figure 41a-c and Figure 42a-b). The ability of this mutant to correct the changes in rRNA structure at the B7a bridge promoted by the rpL10-S104D mutant (Figure 41d) demonstrates that the proper rotational equilibrium was re-established. The control experiment, co-expression of L3-W255C with the wild-type *RPL3*, did not affect any of these parameters. Interestingly, this mutant did not suppress the rpL10-S104D slow growth defect (data not shown) or the ribosome biogenesis defect of rpl10-S104D, as assessed by polysome profiling (Figure 42c). No mutants of L3 able to suppress the rpL10-A106R mutant were identified.
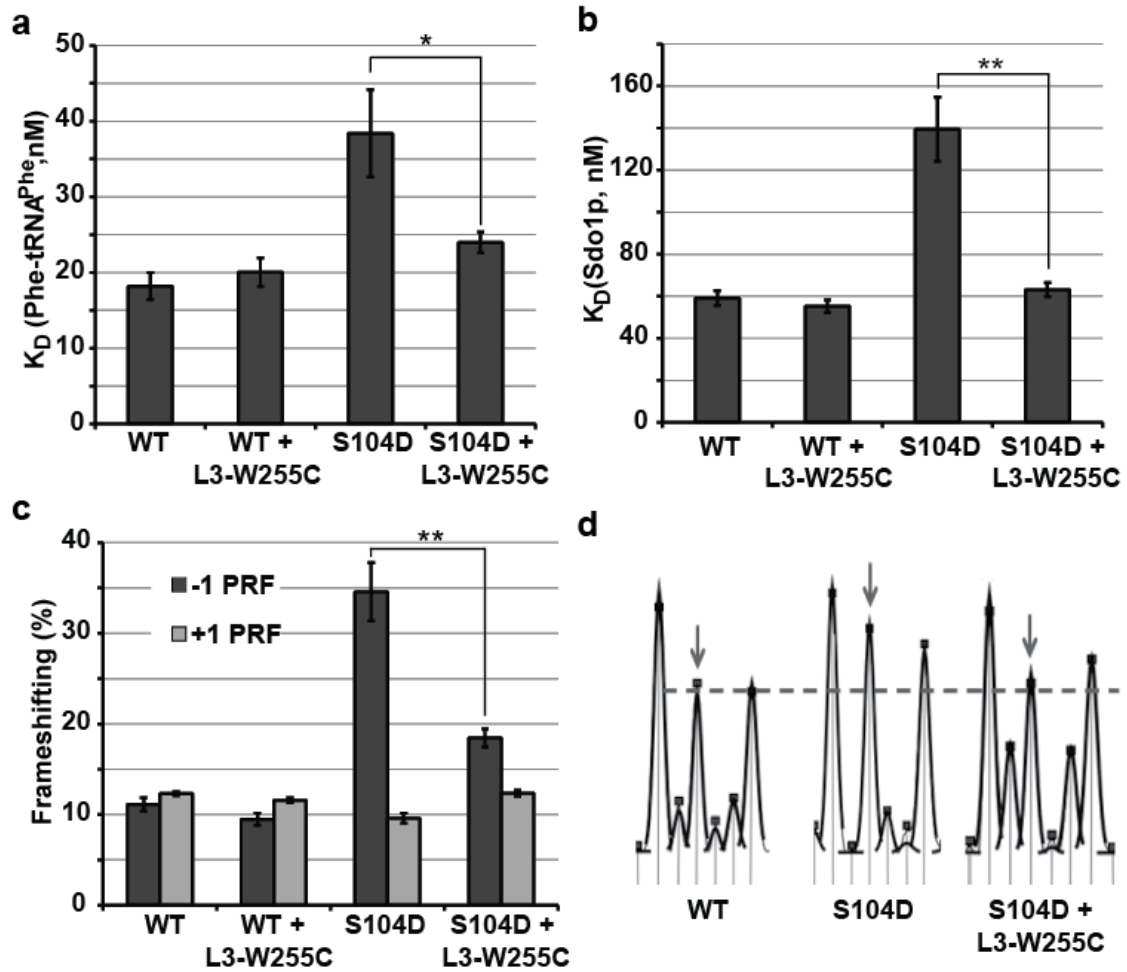
Figure 41. A mutant of rpL10 can be intrinsically suppressed with an rpL3 mutant.

Panels a-b. Binding ternary complex and Sdo1p to indicated ribosomes. **c.** Frameshifting analyses. **d.** Structural probing of the landmark base A2207 (arrows) at the LSU side of the B7a intersubunit bridge with 1M7. Bars indicate s.e.m. (n=4 for a and c, n=3 for b), * $P < 0.05$, ** $P < 0.01$.
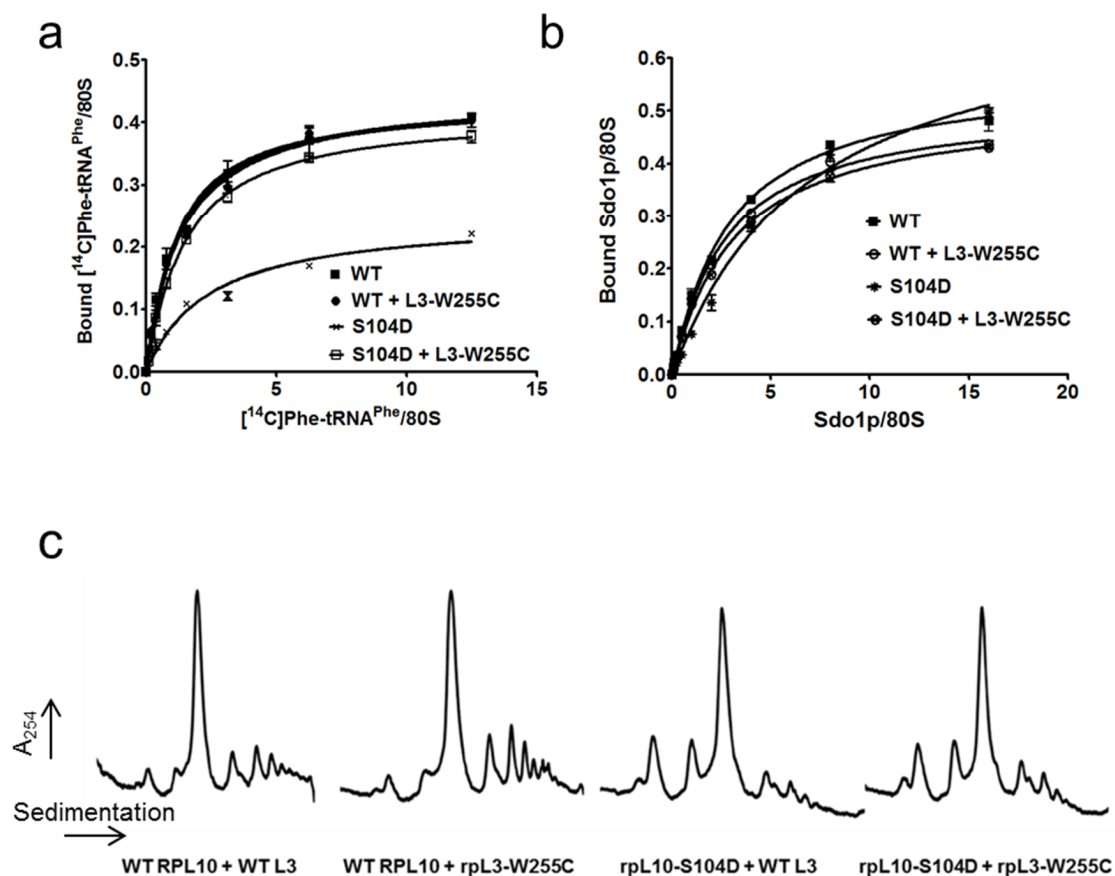
Figure 42. Primary data related to Figure 41.

Single site binding isotherms for wild-type and rpL10-S104D ribosomes isolated from cells expressing the *rpl3-W255C* mutant or empty vector. **a.** Binding of ternary complex to the A-site. **b.** Binding of Sdo1p. 5 pmoles of ribosomes in 120 µl total volume were used at each dilution. Bars indicate standard error of the mean. **c**. Sucrose density gradient analysis. Cultures of AJY2104 (*GAL1:RPL10*) expressing *RPL10* or *rpl10-S104D* and *L3* or *L3-W255C* were grown in glucose to repress genomic *RPL10* for 6 hrs before cells were harvested. Extracts were prepared and 9 A_{260} units were sedimented through 7–47% sucrose gradients.

Discussion

Eukaryotic rpL10 and its prokaryotic homologs L16 in bacteria and L10e in *archaea* contain a conserved internal loop that approaches the catalytic center of the large subunit. This loop is not resolved in atomic resolution structures of vacant yeast [15] or prokaryotic ribosomes [214], suggesting that this structure is dynamic. However, the internal loop is resolved in high-resolution crystal structures of bacterial ribosomes containing P-site tRNA [189,215] and in cryo-EM imaging of translating yeast ribosomes [188], suggesting that it is stabilized by tRNA binding. While the loop is shorter in the bacterial and archaeal homologs, the N-terminus of the L27 proteins from these kingdoms appear to provide the structural mimic for the tip of this loop [216]. Here, we have shown that mutations of this loop affect the rotational status of the ribosome, altering the ribosome's affinity for Sdo1p at the P-site, for aa-tRNAs and eEF2 at the A-site, and globally affecting ribosome function from biogenesis through translational fidelity.

Current models posit that ribosomal rotational status is solely determined by binding of different tRNA species and *trans*-acting GTPases [96,106,217]. However, the findings presented here suggest that control of rotation is an intrinsic property of the ribosome. We suggest that when the A-site is unoccupied by ligand, the flexible rpL10 loop can sample this space: we call this the "flipped in" conformation. In contrast, occupation of the A-site by tRNAs displaces, or "flips out" this loop (Figure 43a-b). The effects of the two rpL10 mutants on A-site associated functions and on ribosome structure in the absence of ligands suggest that this loop has an intrinsic, central role in establishing the rotational status of the ribosome. The finding that non-enzymatic binding of aa-tRNA to the A-site exacerbates the low affinity defect and that

peptidyltransferase activity is diminished in rpL10-S104D provide additional support for this idea. Addition of the positively charged arginine residue may create new charge-charge interactions with the A-site to stabilize the "flipped in" state making it more difficult to displace by aa-tRNA (Figure 43a). Conversely, addition of a negatively charged residue in the S104D mutation may interfere with the ability of the loop to stably occupy the A-site due to charge repulsion effects with this rRNA-rich environment, thus stabilizing the "flipped out" conformation (Figure 43b).

Multiple lines of evidence (visualized in Figure 38) support the rpL10 lateral displacement model shown in Figure 43a-b. Chemical probing with 1M7 revealed increased reactivity of the tip of H39 near the PTC-proximal end of rpL10 in the S104D and G81D mutants (Figure 36), suggesting that rpL10 loses contact with this element in the rotated state. This is accompanied by increased protection of bases in H43 (elongation factor binding site) on the opposite (PTC-distal) end of the body of rpL10, suggesting that this side of the protein moves closer to H43 (the eEF binding site in Figure 43). Notably, 25S rRNA G1249 is even more protected from chemical modification in rpL10-G81D relative to rpL10-S104D mutant ribosomes, suggesting that the longer sidechain at this residue increases the extent to which it interacts with the nucleobase. The converse rRNA chemical reactivity patterns are observed with the A106R and F94I mutants, which favor the non-rotated state. Along the "top" of rpL10, the F94I mutant promoted increased reactivity of bases in H38 that normally interact with this amino acid residue, indicating that this contact was broken by loss of the aromatic sidechain. These findings suggest that the phenylalanine sidechain intercalates into H38, pulling this structure along with it as rpL10 is laterally displaced, as evidenced by

changes in the reactivity of the small subunit side of the B1a intersubunit bridge (Figure 35). The observation that there are no differences in the reactivities of these bases (A1006 and U1007) in rpL10-S104D compared to rpL10-A106R ribosomes (Figure 34) indicates that F94 remains associated with this region of H38 throughout this proposed lateral movement. On the "bottom" side of rpL10, decreased reactivity of bases in the accommodation corridor in rotated control ribosomes and the S104D mutant (Table 2) is consistent with prior observations that another feature of rpL10 called the N-terminal "hook" releases H89 to close the corridor in the rotated state [178].

How can a change in the position of a small peptide loop affect the conformation of a large and complex macromolecule like the ribosome? We suggest that this small conformational change is amplified through a complex series of allosteric networks. Like the gas pedal in an automobile, the rpL10 loop is physically linked to multiple functional centers of the machine. The chemical structural probing studies reveal allosteric information exchange networks propagating out from rpL10 to all of the functional centers of the ribosome (diagrammed in Figure 43c). These pathways completely frame the path through which tRNA moves through the ribosome during translation, including the accommodation corridor and decoding center, the PTC, and the E-site. They also encompass the critical intersubunit bridges involved in rotation through the elongation cycle and the elongation factor binding site. Previous studies provide evidence that flexible peptide elements provide mobile platforms upon which allosteric switches can be built and are widely used by the ribosome as transducers of information, supporting the notion that structural elements intrinsic to the ribosome play important roles in coordinating ribosomal conformations. These include the N-terminal hook of rpL10 [178],

the W-finger, N-terminal extension, and Basic Thumb elements of rpL3 [211,218,219], an internal loop located in rpL5 [220], and the P-site loop of rpL11 [206]. Importantly, there is a considerable degree of overlap between the allosteric networks identified in these and other studies [200,201,207,210,221], indicating that they are all components a single network of "switches" and "wires" that coordinate ribosome structure with function. This is further supported by the observation that a mutant in one switch, rpL3-W255C, can suppress the biochemical and translational fidelity defects of a second, i.e. the rpL10-S104D loop mutant. What distinguishes the rpL10 loop from other elements are the broad effects of loop mutants on ribosome biogenesis, elongation and termination. These effects argue that the rpL10 loop is the central control element in this complex wiring scheme. It should be noted that while we interpret our results as evidence for the influence of rpL10 on ribosome equilibria, alternative explanations are also possible. For example, these results could be interpreted as evidence for changes in rRNA folding and the structure of the large subunit. However, incorporation of L10 occurs very late in the process of eukaryotic ribosome biogenesis after the pre-60S subunit has been exported to the cytoplasm, well after the core of the large subunit has been folded. Thus, the effects of these single amino acid mutants of rpL10 on rRNA folding are likely to be minimal.
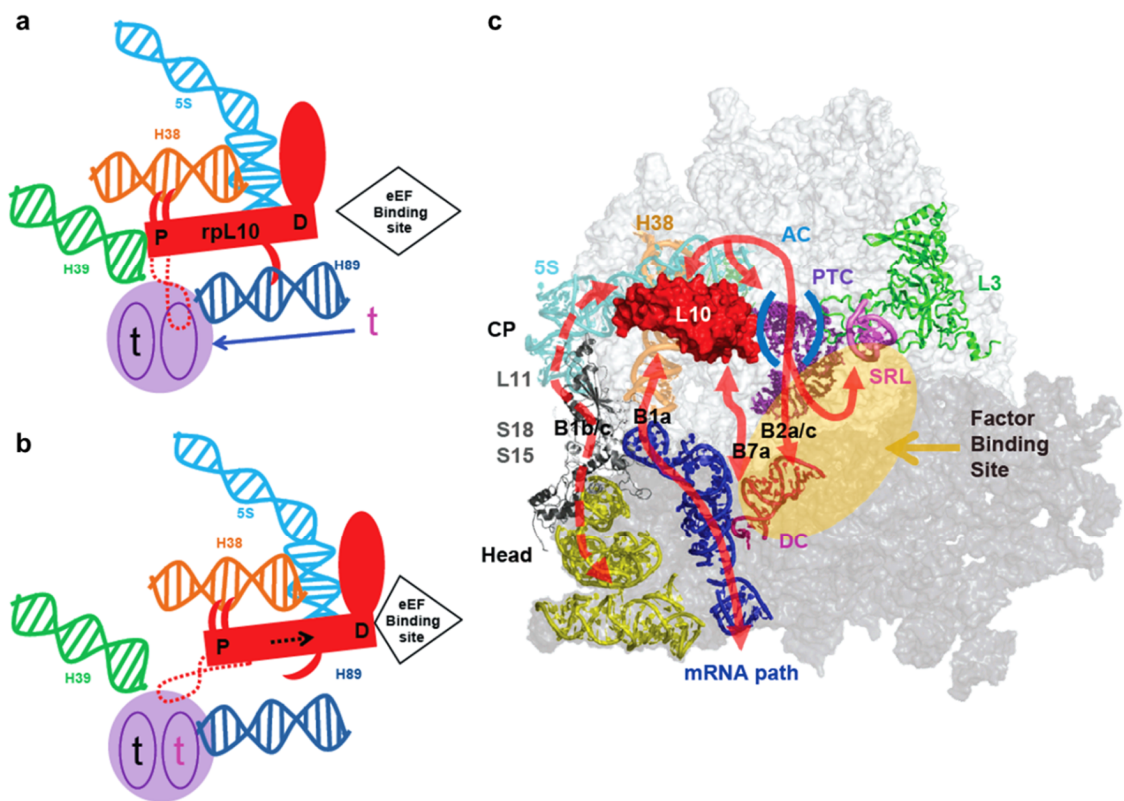
Figure 43. Models of rpL10 function: rpL10 is at the center of a cascade of allosteric communication pathways throughout the ribosome.

a. The rpL10 loop "flipped in" conformation is the substrate for ternary complex and Sdo1p. P: PTC-proximal, D: PTC-distal. **b.** The "flipped out" loop conformation, substrate for eEF2. Binding of an aa-tRNA (indicated by the red "t") causes displacement of the loop from the A-site, precipitating structural rearrangements in rpL10. These include lateral displacement of the main body of the protein (dashed black arrow) and H38 toward the elongation factor binding site, creating the binding platform for eEF2. Release of the N-terminal hook of rpL10 from H89 enables closing of the aa-tRNA accommodation corridor. These movements also initiate allosteric transmission of information through the communication pathways shown in panel c to distantly located functional centers of the ribosome to set the stage for the next phase of elongation. These include rearrangements in the E-site in preparation for release of deacylated tRNA, and interactions with the decoding center and small subunit to initiate subunit rotation.

c. Summary of chemical probing experiments mapping the allosteric information exchange pathways emanating from rpL10 to all the functional centers of the ribosome to influence intersubunit rotation. Intersubunit bridges B1a, B1b/c B2a/c, and B7a and ribosomal proteins L3, L10, L11, S15 and L18 are labeled. CP: Central Protuberance of the LSU. AC: Accommodation Corridor. PTC: Peptidyltransferase Center. SRL: Sarcin/Ricin Loop. DC: Decoding Center.

The rotational status of the 80S ribosome is an important determinant for binding of *trans*-acting factors, optimizing PTC activity and translational fidelity. Both mutants promoted increased rates of -1 PRF (Figure 40c), which requires slippage of both A- and P-site tRNAs [222], but did not affect +1 PRF, which only requires slippage of P-site tRNA [166]. This is consistent with the observation that the rpL10 loop mutants only affected A-site tRNA binding. Increased utilization of near- and non-cognate tRNAs, and termination codon readthrough by the rpL10-S104D mutant (Figure 40d) may be explained by the observation that A1755 (*E. coli* A1492) in h44 was hyperprotected from chemical modification (Figure 35). Flexibility of this base is critical for accurate decoding by stabilizing a mini-helix between cognate codon:anticodon interactions [84,223]. Concurrently, LSU A2256 (*E. coli* A1913) in H69 was hyper-reactive in rpL10-S104D ribosomes (Figure 33). This base also plays a central role in mRNA decoding where it is paired with A1492 in the non-rotated state, but is unpaired and flexible in the rotated state [92]. We suggest that the propensity of rpL10-S104D ribosomes to assume the rotated stated limits the ability of these bases to participate in mini-helix formation, leading to increased utilization of non-cognate ligands.

Considering the mechanisms in place to ensure fidelity of gene expression we expect that safeguards have evolved to ensure that only correctly functioning ribosomes are utilized in translation. Ribosome assembly culminates in cytoplasmic maturation where essential ribosomal proteins are added and *trans*-acting factors are released [40]. A critical step in this pathway is the release of the anti-association factor Tif6p by the concerted action of Sdo1p and the eEF2 paralog Efl1p. The observation that suppressing mutations in Efl1p appear to facilitate a conformational change in the protein akin to the

conformational change observed in eEF2 engendered the proposal that the LSU undergoes a "test drive" in which the integrity of the P-site is assessed through activation of the GTPase of Efl1p [187]. Notably, similar functional checkpoints governing pre-40S maturation have recently been proposed [224,42]. The findings presented in the current study add further support and detail to this model. Specifically, the ability of Sdo1p to compete for Ac-aa-tRNA binding in the P-site, inhibit peptidyltransferase activity, and stimulate aa-tRNA binding to the A-site [similar to the stimulatory effect of P-site bound Ac-aa-tRNA on aa-tRNA binding to the A-site [225]] all suggest that Sdo1p interacts with the P-site, stabilizing a pseudo-non-rotated state of the LSU alone.

The structure of Sdo1p has been likened to tRNA (Figure 44) [226], and we propose that Sdo1p is a mimic for a P-site ligand that couples the GTPase activity of the elongation factor mimic Efl1p [47] to drive a pseudo-translocation event on the LSU (Figure 45). Because Efl1p and Sdo1p appear to act on 60S independent of 40S, we suggest that the rpL10-S104D and –A106R mutants promote conformational changes within the 60S subunit alone that are analogous to those in the 60S subunit in the context of rotated and non-rotated 80S ribosomes. The 60S subunit "test drive" appears to provide the primary quality control check on assembly and function of the LSU before it is released into the pool of actively translating ribosomes. In particular, the ability to bind biogenesis ligands that structurally mimic elongation factors as well as the ability to undergo GTP hydrolysis is being functionally tested during this quality control point. Failure at any of these steps leads to the inability of Tif6p and Nmd3p to dissociate, and the subsequent degradation of such improperly assembled subunits through the non-functional ribosomal decay pathway [227]. Sdo1p binding defects in the "pseudo-rotated"

S104D mutant can be intrinsically suppressed with the rpL3-W255C mutant, likely due to its ability to re-establish the correct pre-LSU conformation. However, the failure of this mutant to rescue the ribosome biogenesis defect suggests that quality control involves more than mere monitoring of ligand binding.
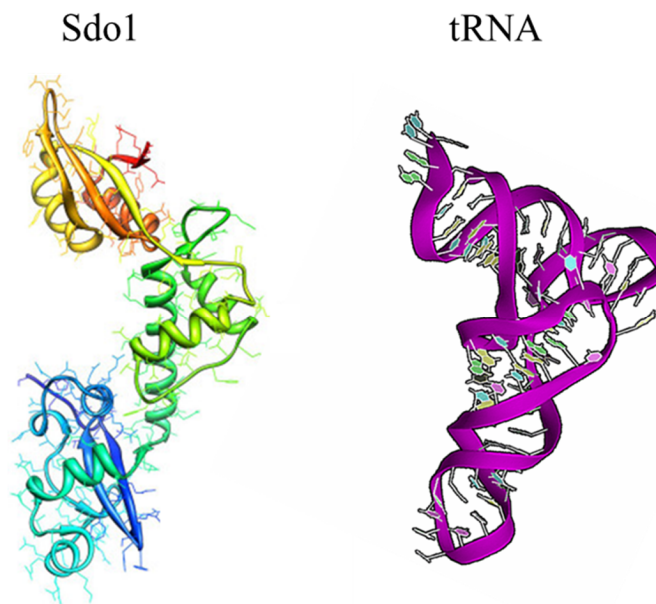
Figure 44. Sdo1 structurally resembles tRNA.

Sdo1 and tRNA appear to be structural mimics that function at distinct time points during the ribosomal life cycle. Image modified from Ng [226].
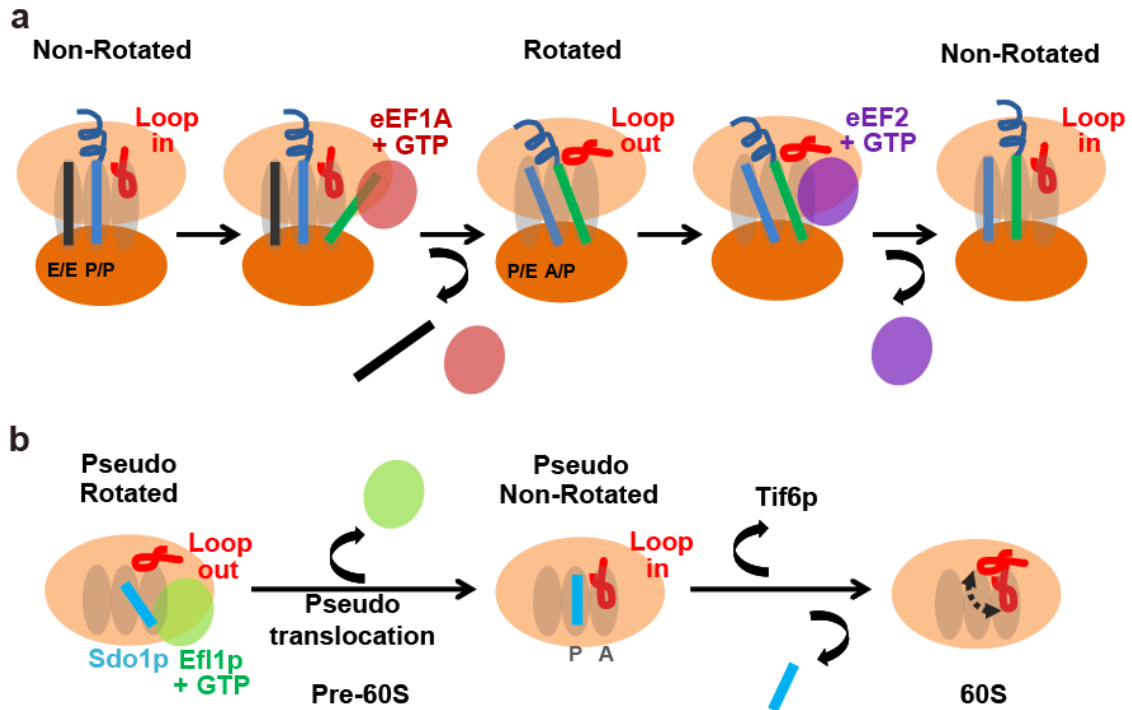
Figure 45. Involvement of the rpL10 loop in ribosome rotation throughout the ribosomal life cycle.

a. The elongation cycle of translation: rpL10 loop positioning and ligand binding. The elongation cycle begins at left with the ribosome in the non-rotated state where the E-site contains a deacylated tRNA, the P-site is occupied by peptidyl tRNA, and the un-occupied A-site can be sampled by the rpL10 loop, i.e. the "flipped in" conformation. Following elongation ternary complex binding, aa-tRNA accommodation and peptidyltransfer, tRNAs assume the hybrid states and the loop assumes the "flipped out" conformation, signaling the ribosome to assume the rotated state. eEF2 binds to rotated ribosomes, resulting in translocation, and the elongation cycle begins anew.

b. The "test drive." Sdo1p and Efl1p interact with the pre-60S subunit in the pseudo-rotated state. Efl1p-mediated pseudo-translocation drives Sdo1p into the P-site, stabilizing the pseudo-non-rotated state with the rpL10 loop in the "flipped in" conformation. This is followed by release of the anti-association factor Tif6p and Sdo1p, promoting the final steps of 60S maturation.

The biomedical importance of the rpL10 loop was recently highlighted by the discovery that a significant fraction of T-cell acute lymphoblastic leukemia patients harbor mutations of R98, and in one patient at Q123, both of which lie at the base of the loop [179]. Remarkably, these mutations prevent the release of Tif6p and Nmd3p, but can be suppressed by mutations in Nmd3p, indicating that like the S104D mutation, R98 and Q123 mutations in human *Rpl10* cause a failure during the "test drive" of the 60S subunit. These findings suggest that defects in ribosome biogenesis and/or in translational fidelity may be drivers of this neoplastic disease. Investigations are currently underway to address these questions, and some of these findings are presented in the following chapter.

Chapter 3

Ribosomopathies: a new model for cancer biogenesis

Introduction

It has become clear that deregulation of a process as essential as cellular protein translation may play a central role in cancer development. Key cancer oncogenes and tumor suppressors act as master regulators of the translational apparatus. For instance, MYC expression in cancer cells causes elevated expression of several ribosomal proteins and translation factors and PTEN inactivation results in mTOR activation and phosphorylation of ribosomal protein S6, eventually leading to increased translation of ribosomal proteins, elongation factors and ribosome biogenesis factors [228]. Over the last decade several congenital disease syndromes have become linked to genetic defects in ribosomal proteins or ribosome biogenesis factors. These syndromes, collectively called 'ribosomopathies', are characterized by pleiotropic abnormalities including birth defects, heart and lung diseases, connective tissue disorders, anemia and ataxia, and mental retardation [43]. A common feature is that patients suffering from these diseases have a significantly elevated risk of developing cancer [229]. Thus, ribosomopathies present an intriguing paradox: while patients initially present with hypo-proliferative disorders such as anemias, those who survive to middle age often develop hyper-proliferative diseases, i.e. cancers. This appears to be a general phenomenon: loss of function mutations in several ribosomal proteins have been shown to cause tumor development in zebrafish [230]. Although there is thus clear indication for a role for deregulated translation in cancer

cells, it is currently unclear how alterations that affect a vital cellular function as protein translation may promote the hypo-to-hyper-proliferation switch and carcinogenesis.

Acute T-cell lymphoblastic leukemia (T-ALL) is a hematopoietic malignancy caused by accumulation of genetic lesions in developing T-cells that has recently been linked to ribosome dysfunction. T-ALL accounts for 15% of all pediatric leukemias and 20-30% of pediatric patients do not achieve long-term remission [231]. Exome sequencing on 67 T-ALL patients revealed that 9.8% of pediatric and 7.2% of adult T-ALL patients had somatically acquired mutations in the large ribosomal subunit protein genes *RPL10*, *RPL5* and *RPL22* [179]. Mutations in *RPL10* were the most frequent ribosome mutations identified in this study and were almost exclusively in residue arginine 98 (R98) with the exception of one patient harboring the Q123P mutation which lies adjacent to R98 within the rpL10 3D structure. Both residues are at the base of a flexible loop in rpL10 that closely approaches the peptidyltransferase center in the catalytic core in the ribosome (Figure 46). The rpL10 protein is highly conserved across species: the yeast and human proteins are interchangeable and residue 98 is invariantly an arginine [180]. As described in the previous chapter, rpL10 plays an important role in the late stages of 60S ribosomal subunit biogenesis. Both immature subunits are functionally inactive as they enter the cytoplasm and require additional maturation events and association with each other before they can engage in protein synthesis [40]. A critical step in 60S maturation is the release of the anti-association factor Tif6, followed by release of Nmd3, the primary export adaptor for the pre-60S subunit in yeast and in humans [232,231]. Tif6 release requires Sdo1 and the GTPase Efl1, a paralog of translation elongation factor 2. As detailed in the previous chapter, we have proposed that an essential internal loop of rpL10 initiates a

"test-drive" of the 60S subunit involving these factors as a quality control checkpoint in ribosome assembly, ensuring that only properly functioning subunits are allowed to progress into the translationally active pool of ribosomes. Defective ribosomes carrying mutations in rpL10 specifically fail in this "test drive" leading to their degradation through the non-functional ribosomal decay pathway [227].

To test the impact of the T-ALL-associated mutations, the *rpl10-R98S* and *rpl10-R98C* mutants were expressed in yeast cells as the sole forms of *RPL10*. These mutations impaired cellular proliferation and polysome profiling revealed modest changes in the ratios of free 60S vs. 40S subunits, markedly reduced polysomes, and the presence of halfmers (initiation complexes waiting to join with 60S subunits), suggesting defects in both ribosome biogenesis and subunit joining. Examination of Tif6 and Nmd3 recycling in these strains revealed that both proteins accumulated in the cytoplasm, indicating a defect in their release [179]. Thus, the *rpl10-R98S* and *rpl10-R98C* mutations appeared to arrest 60S biogenesis in the Efl1-dependent quality control step. Consistent with the yeast-based observations, mouse lymphoid cells expressing *rpl10-R98S* had lower proliferation rates than cells expressing wild type *RPL10* and showed defective polysome profiles [179].

In the studies presented here, the *rpl10-R98S* mutant was used to elucidate the molecular mechanisms underlying the translational defects that may lead to carcinogenesis. *Trans*-acting factors were identified that suppress the biogenesis defect of the *rpl10-R98S* mutant, thereby re-establishing ribosome production and cell proliferation. However, we show that suppression of the biogenesis and growth impairment defects fail to suppress the profound molecular and functional defects of

rpL10-R98S ribosomes. These ribosomes display rotational disequilibrium and resulting ligand binding defects. Such defects in turn promote elevated rates of programmed ribosomal frameshifting and destabilization of - 1 PRF signal containing messages. One class of -1 PRF mRNAs plays a critical role in yeast telomere maintenance [161]. In *rpl10-R98S* cells, the steady-state abundance of these mRNAs is decreased, resulting in short telomeres. These results suggest that suppression of the growth defect results from bypassing the "test drive" and the non-functional ribosome decay (NRD) apparatus, a quality control system that enables cells to identify and eliminate sub-optimal ribosomes [227]. The suppressed cells then continue to actively produce and use mutant ribosomes that have specific biochemical and translational fidelity defects. These findings lead us to propose two different but not mutually exclusive models for ribosome mutations promoting cancer: 1) mutant ribosomes drive an altered gene expression program, promoting T-ALL; 2) the suppressing mutations these cells acquire to overcome the growth defects are, themselves, drivers of T-ALL. This work defines novel mechanisms by which acquired mutations in a ribosomal protein can promote dysregulation of gene expression and cancer.
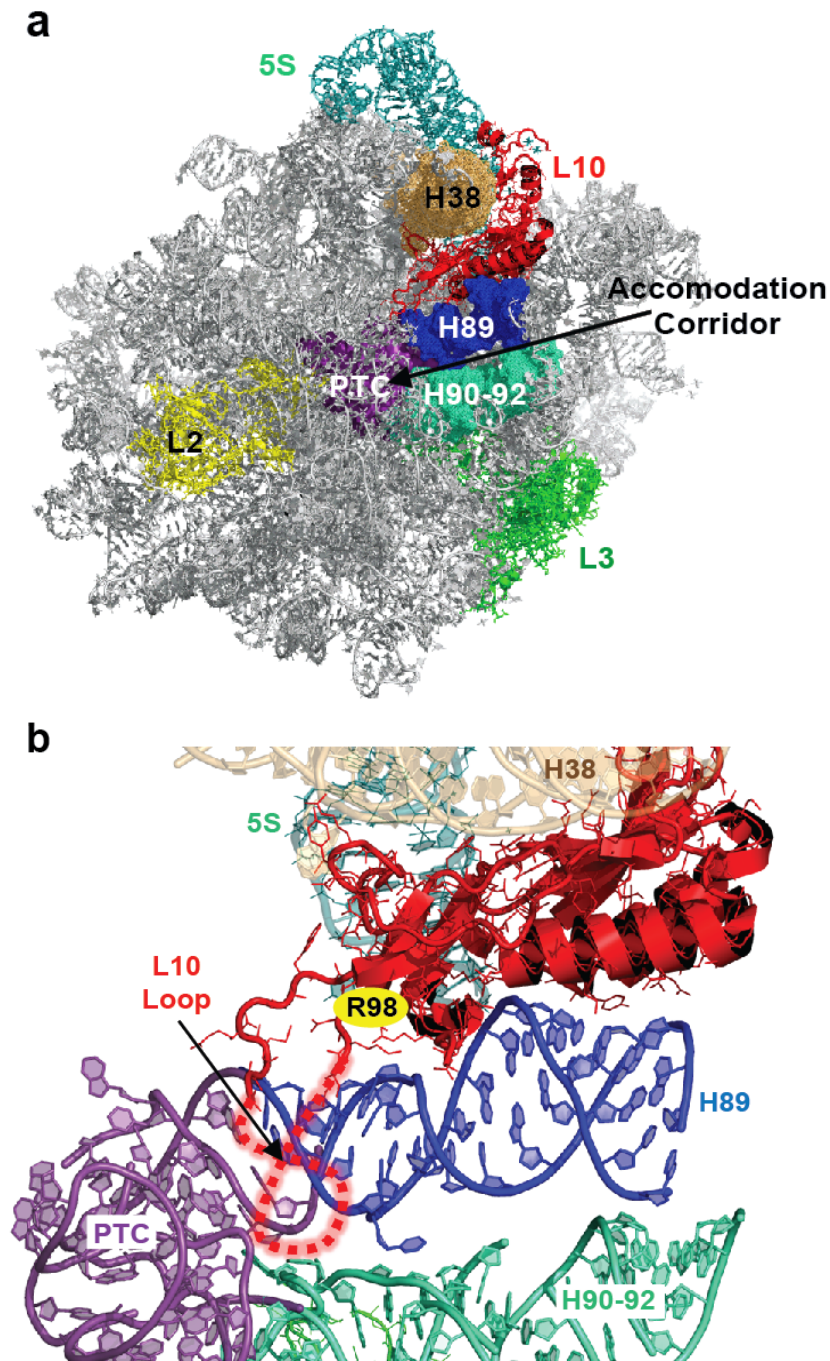
Figure 46. Localization of rpL10 and the loop in the large ribosomal subunit.

a. rpL10 in the context of the crown view of the LSU. **b.** Close-up of rpL10 and the local environment. The hypothetical loop structure is indicated by dashed red lines and the position of R98 is indicated. rpL10 is situated between Helices 38 and 89 and located in close proximity to several functional centers of the LSU including the PTC, the aa-tRNA accommodation corridor, and the elongation factor binding site. PTC: peptidyltransferase center. Images were generated using PyMOL.

102

Results

The *rpl10-R98S* growth and biogenesis defects are suppressed by the *NMD3-Y379D*

mutant. Despite the proliferation impairment in *in vitro* lymphoid cell cultures

expressing *rpl10-R98S*, the mutations in the patients were somatically acquired, were

present in 100% of tumor cells in most patients, and were recurrent in 6.5% of pediatric

patients [179]. These observations strongly suggest that these mutations must have been

selected for in pre-cancerous cells because they imparted some particular advantage. We

have noted that yeast carrying the *rpl10-R98S* mutation readily acquire suppressing

mutations that compensate for the growth defect. Sequencing of candidate suppressing

genes identified a mutation in the export adapter *NMD3, NMD3-Y379D*, which

suppresses the growth defect (Figure 47) and the ribosome biogenesis defect (Figure 48)

of *rpl10-R98S* cells. Whole genome sequencing of an additional mutant identified

aneuploidy for chromosome VIII bearing *NMD3* (data not shown). Indeed, increased

gene dosage of *NMD3* also suppresses the *rpl10-R98S* defects (Figures 47 and 48).
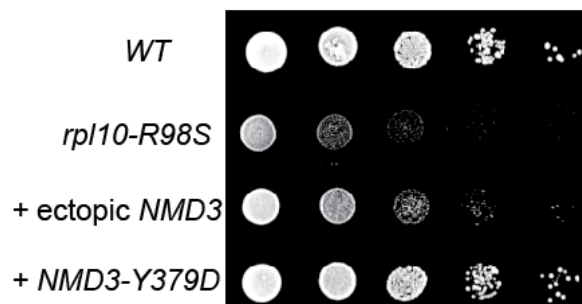
Figure 47. Overexpression of *NMD3* or co-expression of *NMD3-Y379D* suppresses the *rpl10-R98S* growth defect.
Ten-fold dilution spot assay of isogenic strains demonstrating that the *rpl10-R98S* growth defect is suppressed by ectopic expression of *NMD3* and by the *NMD3-Y379D* mutation.
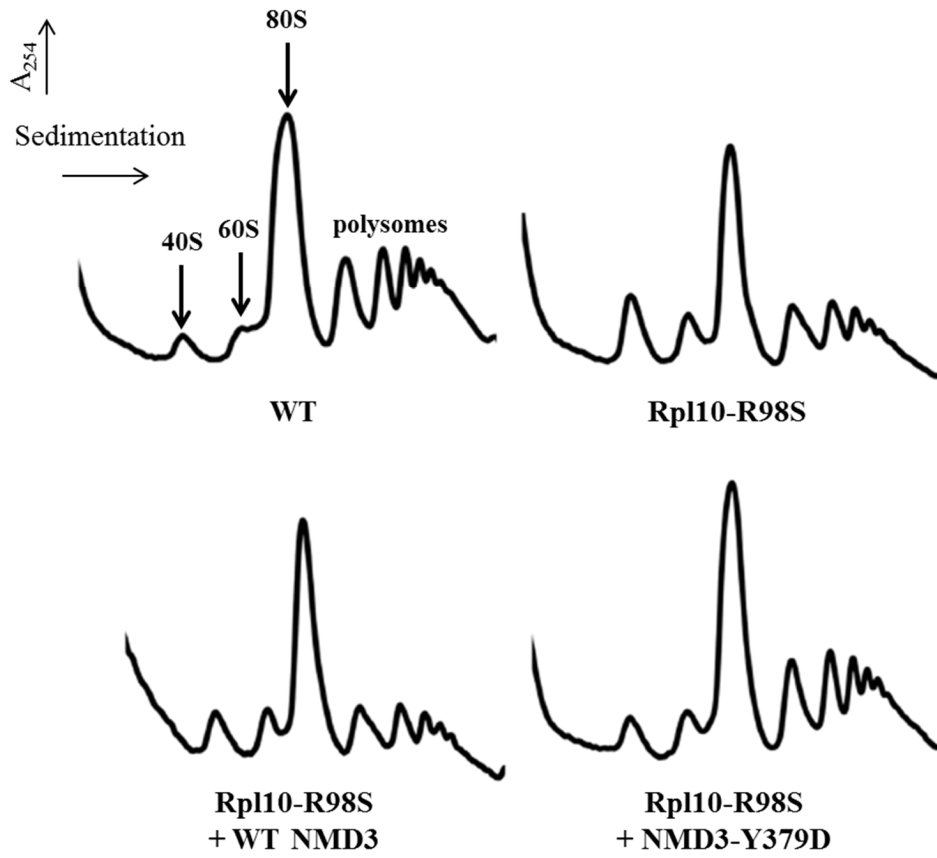
Figure 48. Overexpression of *NMD3* or co-expression of *NMD3-Y379D* suppresses the *rpl10-R98S* biogenesis defect.

Sucrose density gradient analysis. Indicated strains were grown in glucose to repress genomic *RPL10* for 6 hrs before cells were harvested. Extracts were prepared and 9 A_{260} units were sedimented through 7–47% sucrose gradients.

The *rpl10-R98S* mutation alters ribosome rotational status, and this defect is not suppressed by co-expression of *NMD3-Y379D.* As shown in the previous chapter, the internal loop of rpL10 is a central driver of ribosomal rotation. Thus, we examined the previously established landmark of ribosomal rotation (the B7a intersubunit bridge, see Chapter 2) to assess the rotational status of the mutant ribosomes. 1M7 was used to probe A2207 of the LSU-side of the B7a intersubunit bridge, and the extent to which these bases were modified in purified empty isogenic wild-type, mutant, and control ribosomes was quantitatively assessed and normalized using hSHAPE. Reactivity profiles in Figure 49 show that rpL10-R98S ribosomes are in a structural disequilibrium favoring the rotated state. Importantly, this defect is not suppressed by co-expression of *NMD3-Y379.*
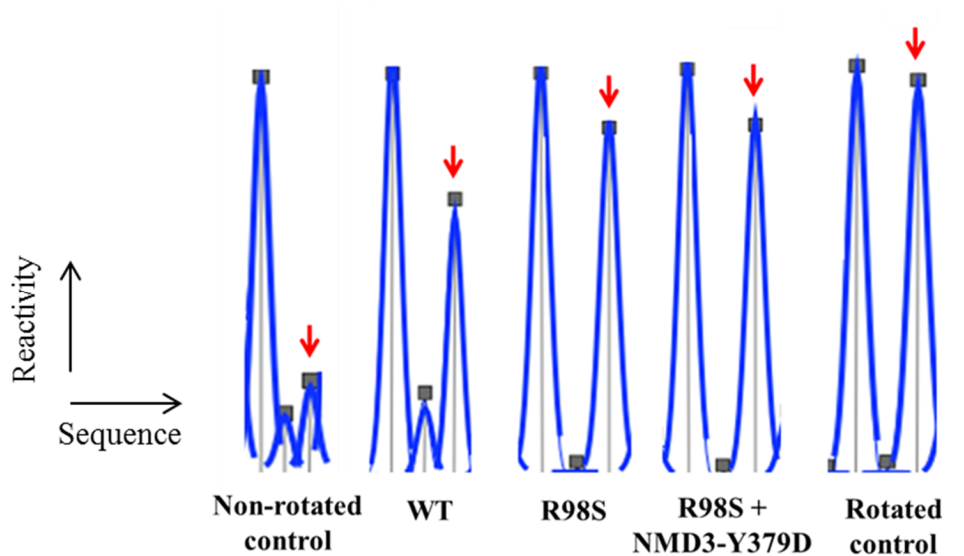
Figure 49. Co-expression of *NMD3-Y379D* does not suppress the *rpl10-R98S* rotational defect.
Reactivity peaks obtained by hSHAPE after probing of the landmark base A2207 (arrows) at the LSU side of the B7a intersubunit bridge with 1M7. This demonstrates that the R98S mutant pushes ribosomes towards the rotated state, and this defect is not suppressed by *NMD3-Y379.*

The *rpl10-R98S* mutation alters ribosomal affinity for specific ligands, and this defect is not suppressed by co-expression of *NMD3-Y379D*. Characterization of other yeast *rpl10* mutants has revealed the role of this protein in recruitment of *trans*-acting factors to the ribosome, which depend on the correct rotational state (see Chapter 2). Given the rotational defect of rpL10-R98S ribosomes, their ability to bind several ligands was assayed. Steady-state binding experiments using ribosomes purified from isogenic yeast strains revealed that rpL10-R98S ribosomes promoted ~3-fold lower affinity for ternary complex and aminoacyl-tRNA (aa-tRNA), and ~3-fold increased affinity for eEF2, both of which are ligands that specifically interact with the ribosomal A-site (Figures 50 and 51). Similar to other rpL10 loop mutants, rpL10-R98S ribosomes did not affect binding of acetylated-aa-tRNA (Ac-aa-tRNA) to the ribosomal P-site. Also similar to other *rpl10* mutants, R98S mutant ribosomes had ~2.5-fold lower affinity for Sdo1p. Notably, none of the biochemical defects were suppressed by expression of *NMD3-Y379D* (Figure 50). This indicates that, while *NMD3-Y379D* can suppress the ribosome biogenesis defect, it does not correct the underlying biochemical defect conferred by the *rpl10-R98S* mutation. This allows us to separate the effects of R98S on biogenesis from those on translation fidelity.
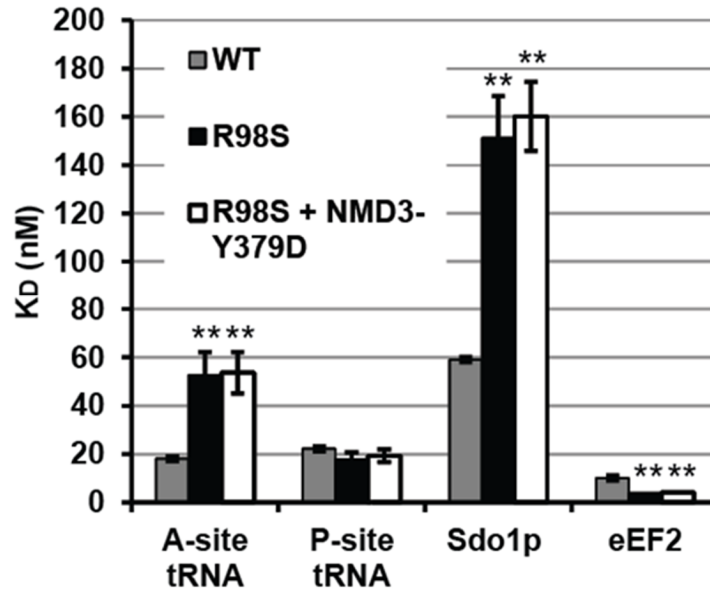
Figure 50. Co-expression of *NMD3-Y379D* does not suppress the *rpl10-R98S* biochemical defects.

Steady state binding of indicated ligands to ribosomes isolated from cells expressing wild-type, *rpl10-R98S*, and *rpl10-R98S + NMD3-Y379D*. Dissociation constants were obtained from binding assays of Ac-aa-tRNA to the P-site and ternary complex to the A-site as monitored by filter binding, eEF2 as monitored by extent of ribosylation of unbound protein, and Sdo1p as monitored by levels of radiolabel detection in ribosomes. Bars indicate s.e.m. (n=4), * $P < 0.05$, ** $P < 0.01$.
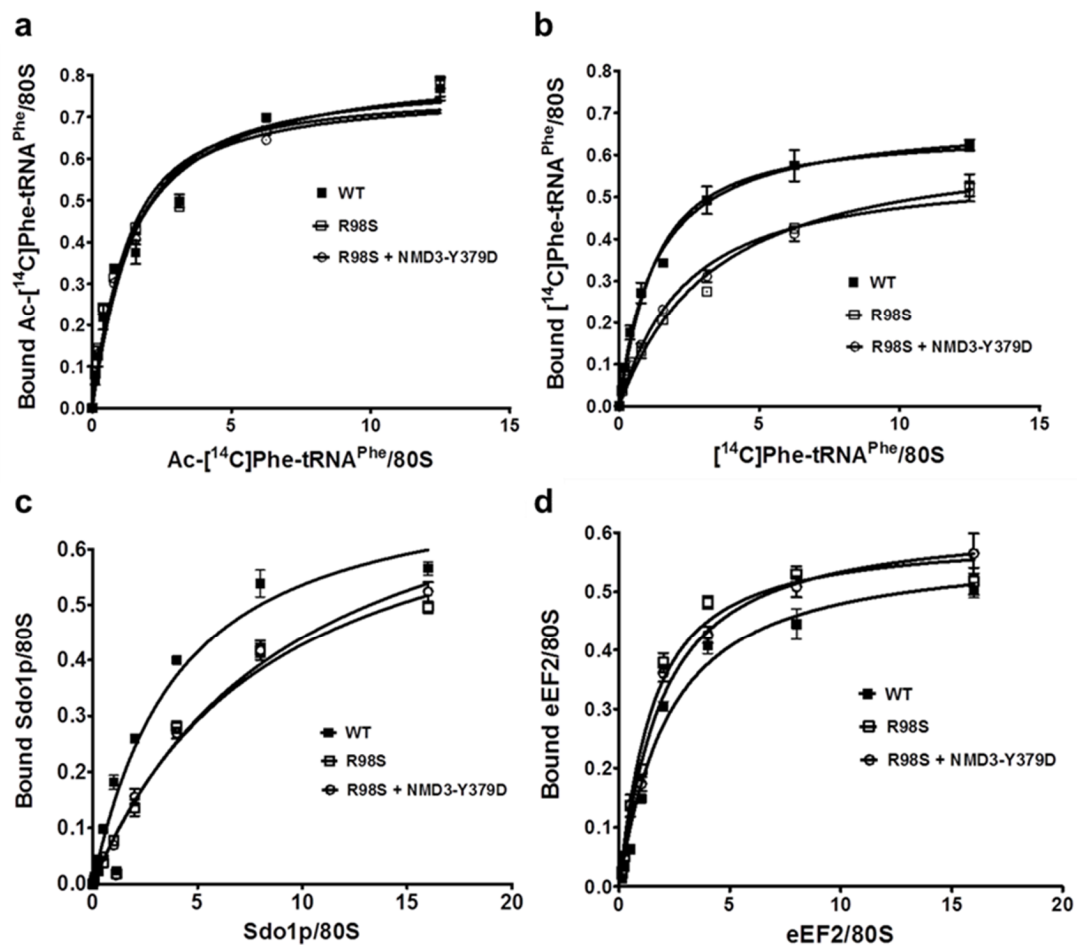
Figure 51. Primary ligand binding data related to Figure 50.

Single site binding isotherms for ribosomes and various ligands. Binding of Ac-aa-tRNA to the P-site (panel a), ternary complex the A-site (panel b), and eEF2 (panel c) and Sdo1p (panel d) to ribosomes isolated from cells expressing wild-type, *rpl10-R98S*, and *rpl10-R98S + NMD3-Y379D*. 5 pmoles of ribosomes in 120 µl total volume were used at each dilution throughout. Bars indicated standard error of the mean (n=4).

Translational fidelity defects of the *rpl10-R98S* mutant are not suppressed by *NMD3-Y379D*. In general, ribosomes must maintain translational reading frame in order to faithfully translate the genetic code. However, there are a growing number of examples of *cis*-acting mRNA sequences that direct elongating ribosomes to shift reading frame: this is called Programmed Ribosomal Frameshifting (PRF). Different sequences direct ribosomes to slip by 1 base in either the 5' (-) or 3' (+) direction, i.e. -1 PRF and +1 PRF, respectively. Numerous studies have revealed mechanistic differences between the two: most -1 PRF events require slippage of both A- and P-site tRNA [151,222], while only the P-site tRNA is involved in +1 PRF, for example, in translation of the retrotransposon Ty*1* from yeast [166]. Consistent with the biochemical data indicating a large subunit A-site specific defect, the *rpl10-R98S* mutation stimulated -1 PRF by ~2.6-fold while +1 PRF remained unchanged (Figure 52). Similarly, *rpl10-R98S* cells were defective for recognition of a termination codon (~2-fold increased readthrough) which requires efficient recruitment of the eRF1/eRF3 complex to the ribosomal A-site [117]. Discrimination between sense and missense tRNAs during elongation, a process that occurs in the A-site of the small subunit, was only slightly affected in *rpl10-R98S* mutant cells. Consistent with the structural and biochemical findings, co-expression of *NMD3-Y379D* did not suppress either the -1 PRF or termination codon misreading defects. To determine whether or not the genetic and biochemical trends we observed were unique to the R98S mutant, we assayed the effects of a second *trans*-acting suppressor of a different *rpl10* mutant that exhibits similar phenotypic, biochemical and functional defects. Similar to the results described above, the *TIF6-Y192F* suppressor of the growth and biogenesis defect of *rpl10-S104D* mutant cells [187] (Chapter 2) did not suppress the

ternary complex binding or -1 PRF defects (Figure 53). Additionally *SDO1-V36A*, also previously shown to suppress the growth defect of *rpl10-S104D*, exhibited a 2-fold higher binding affinity to ribosomes isolated from *rpl10-S104D* cells as compared to wild-type (Figure 54). This indicates that the suppressing activity of *trans*-acting biogenesis factors is likely driven by their increased (i.e. Sdo1) or decreased (i.e. Tif6/Nmd3) affinity to ribosomes.
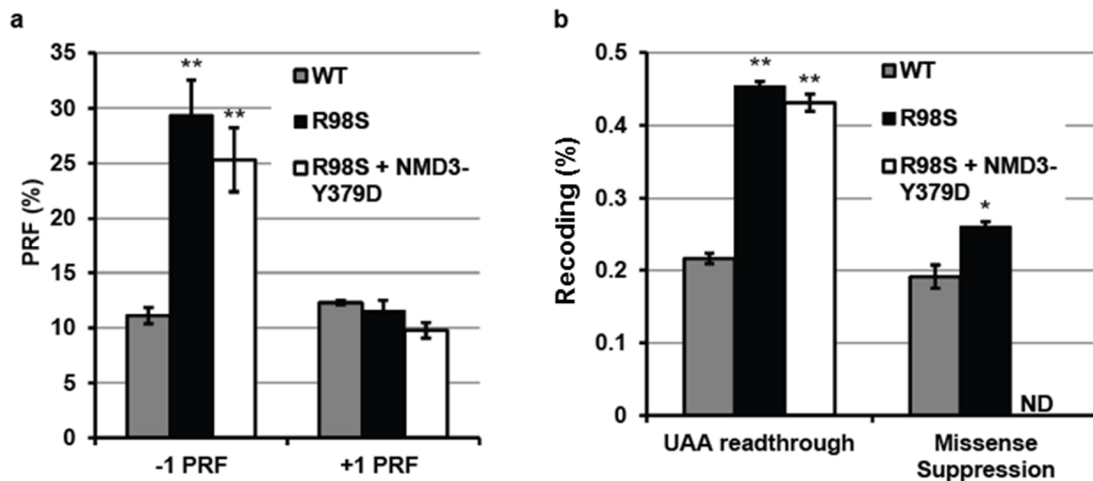
Figure 52. Co-expression of *NMD3-Y379D* does not suppress the *rpl10-R98S* translational fidelity defects.

a. Programmed -1 and +1 ribosomal frameshifting values obtained using dual-luciferase reporters. **b.** Misincorporation of a UAA stop codon and a near-cognate amino acid (missense) in mutants compared to wild-type levels as monitored using dual-luciferase reporters. ND = not determined. Bars indicate s.e.m. (n=4), * $P < 0.05$, ** $P < 0.01$.
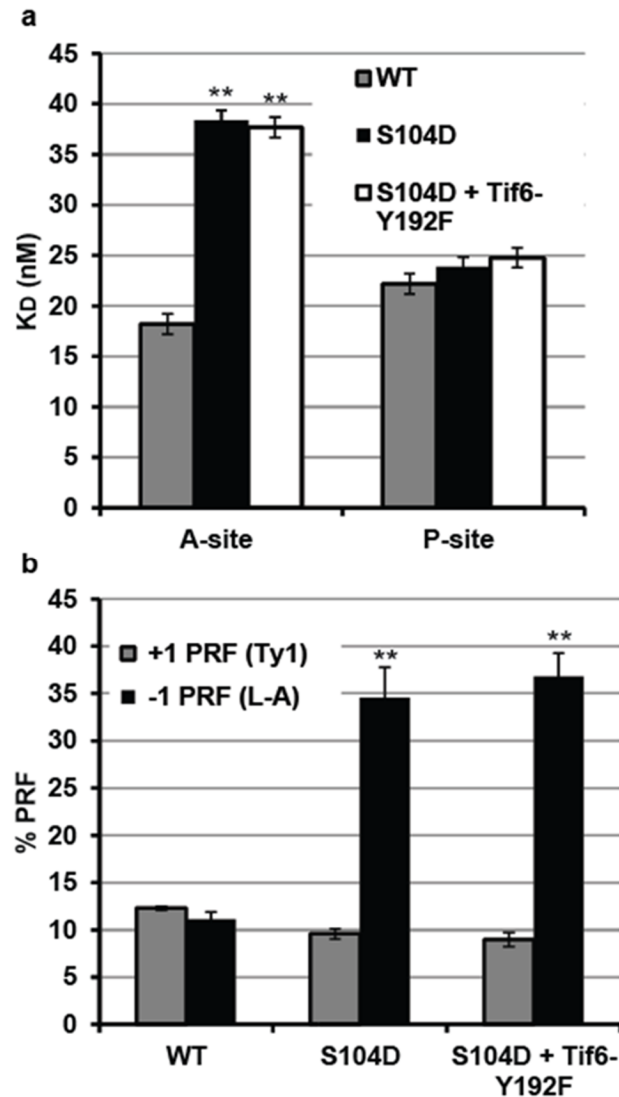
Figure 53. Co-expression of *TIF6-Y192F* does not suppress the *rpl10-S104D* biochemical and translational fidelity defects.

a. Steady state binding of indicated ligands for ribosomes. Dissociation constants obtained from assays of binding of ternary complex to the A-site and Ac-aa-tRNA to the P-site in ribosomes isolated from cells expressing wild-type, *rpl10-S104D*, and *rpl10-S104D + TIF6-Y192F* as monitored by filter binding. **b.** Programmed -1 and +1 ribosomal frameshifting values obtained using dual-luciferase reporters. Bars indicate s.e.m. (n=4), $* P < 0.05$, $** P < 0.01$.
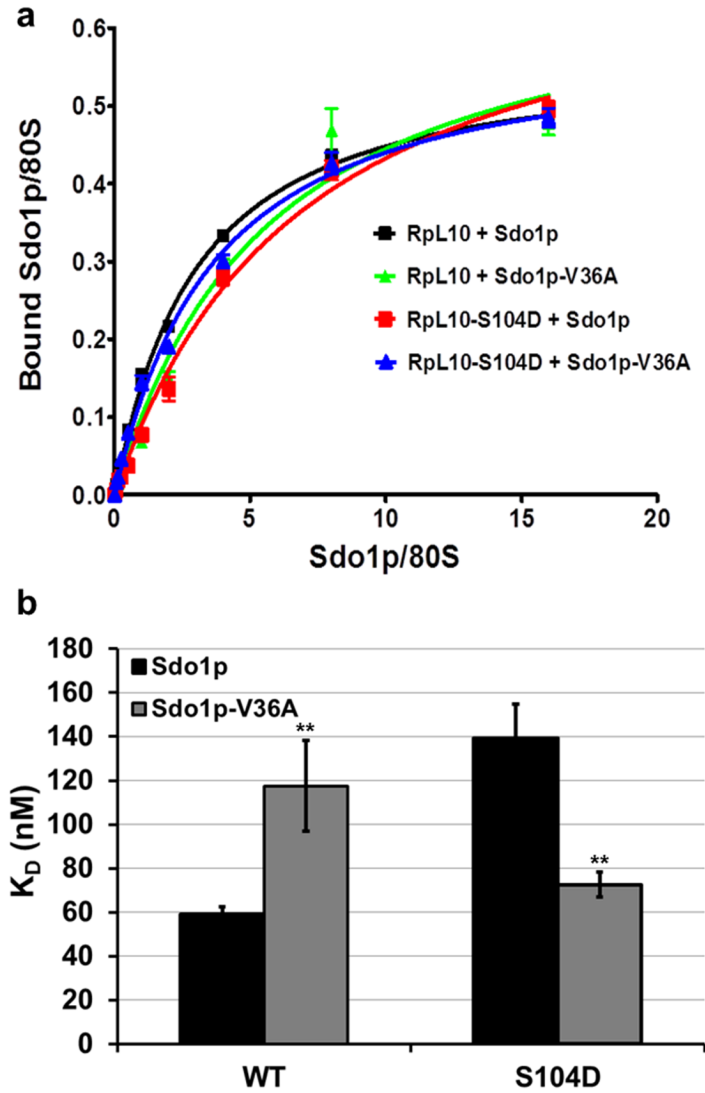
Figure 54. Sdo1p-V36A has a higher affinity to rpL10-S104D ribosomes.

Dissociation constants obtained from assays of binding of Sdo1p and Sdo1p-V36A to ribosomes isolated from cells expressing wild-type or *rpl10-S104D*. Bars indicate s.e.m. (n=3), * P < 0.05, ** P < 0.01.

Yeast telomere maintenance and length defects promoted by the *rpl10-R98S* mutant are not suppressed by *NMD3-Y379D*. Computational analyses suggest that ~10% of eukaryotic cellular mRNAs harbor operational -1 PRF signals. Over 95% of these are predicted to function as mRNA destabilizing elements through the nonsense-mediated mRNA decay pathway by directing translating ribosomes to premature termination codons [155]. More recently, -1 PRF was implicated in telomere maintenance in yeast [161]. To test if *rpl10-R98S*-promoted changes in -1 PRF also lead to changes in gene expression, we used dual luciferase reporter-based assays of -1 PRF directed by elements located in the yeast EST1, EST2, STN1 and CDC13 mRNAs. The *rpl10-R98S* mutant stimulated -1 PRF promoted by *cis*-acting elements located in these mRNAs by 2 to 3-fold as compared to isogenic wild-type controls. Consistent with the biochemical findings, *NMD3-Y379D* did not suppress these -1 PRF defects (Figure 55a). Similar to results observed with other yeast mutants that promoted changes in -1 PRF [159,161], the steady-state abundances of endogenous EST1, EST2, STN1 and CDC13 mRNAs were significantly reduced in *rpl10-R98S* cells, as monitored by qRT-PCR (Figure 55b). Consistent with previous data, the *NMD3-Y379D* mutant did not affect the abundance of these mRNAs in *rpl10-R98S* mutant cells. Furthermore, *rpl10-R98S* cells exhibited significantly shortened telomeres as assessed by PCR, and this defect was not ameliorated by co-expression of *NMD3-Y379D* (Figure 56).
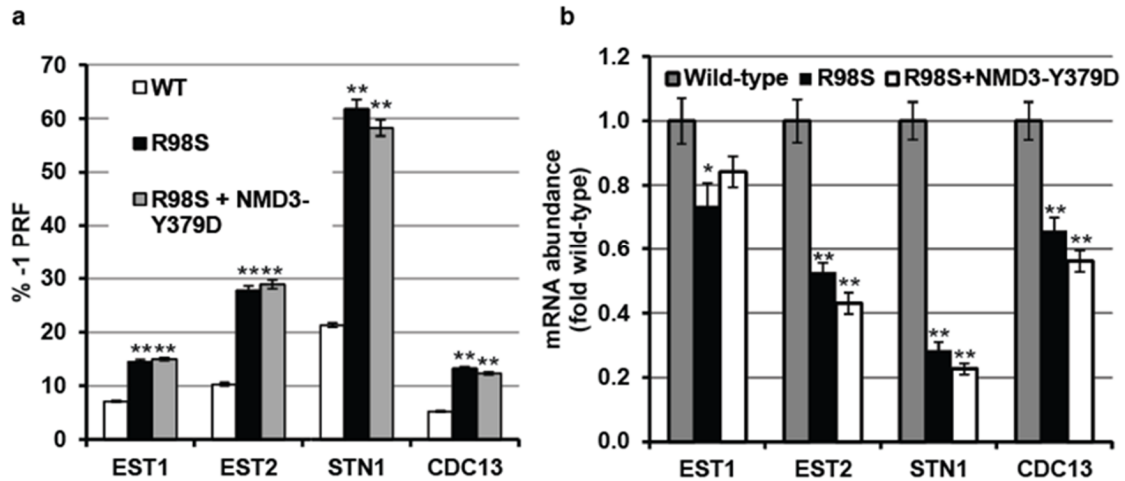
Figure 55. Co-expression of *NMD3-Y379D* does not suppress the *rpl10-R98S* telomere maintenance defects.

a. Programmed -1 ribosomal frameshifting directed by sequences in the following yeast genes: *EST1* (signal beginning at nt 1272); *EST2* (signal beginning at nt 1251); *STN1* (signal beginning at nt 1203); and *CDC13* (signal beginning at nt 1272). **b.** Expression of endogenous EST1, EST2, STN1 and CDC13 mRNAs was monitored by qRT-PCR. Bars indicate s.e.m. (n=4), * P < 0.05, ** P < 0.01.
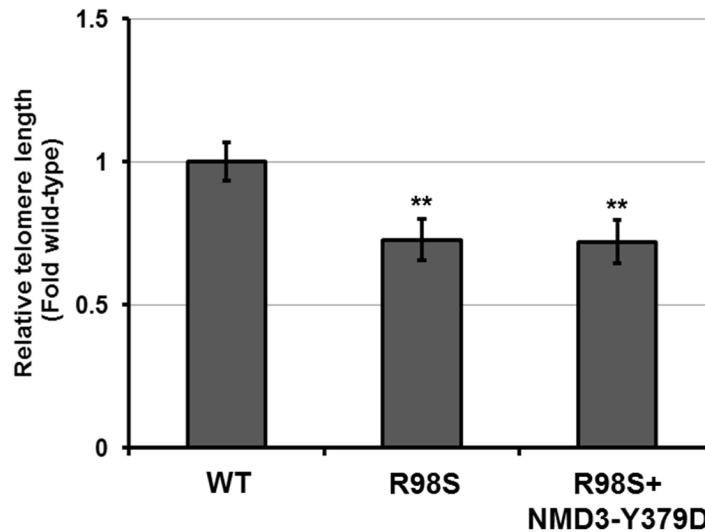
Figure 56. Co-expression of *NMD3-Y379D* does not suppress the *rpl10-R98S* telomere length defects.

Abundance of telomere repeat sequences were quantified by PCR, with the single copy reference gene *SGS1* as the loading control. Bars indicate s.e.m. (n=9), ** P < 0.01.

114

Discussion

It is currently unclear how and by what mechanisms defects in a crucial cellular process like translation can lead to carcinogenesis. In particular, how a mutation that negatively impacts cell growth can promote a hyper-proliferative disease presents a paradox. While this is not the first time that defects in the translation machinery have been linked to cancer, the molecular mechanism of how a mutation in a specific ribosomal protein can promote a specific type of cancer is highly novel. Furthermore, the evidence presented above suggests that the acquisition of defects in ribosomal proteins throughout life may represent yet another unexplored mechanism to deregulate the translation machinery in cancer cells.

Our findings reveal that the malfunction of the rpL10 internal loop is at the heart of T-ALL. In particular, while the mutations described in Chapter 2 were located at the tip of the loop (much like fingers on a hand), thereby impairing its "sensitivity", the T-ALL mutations localize to the base of the loop (wrist of the hand), thereby possibly changing the general flexibility and dynamic nature of the structure and its ability to influence ribosomal rotational status. *NMD3-Y379D* suppresses the ribosome biogenesis defects but not the intrinsic biochemical defects conferred by the *rpl10-R98S* mutant, the most frequent acquired mutation in T-ALL patients. An identical trend applies to a different suppressor, *TIF6-Y192F*, which suppresses the ribosome biogenesis defects of the *rpl10-S104D* mutant but not the downstream translational functions. The observed suppression is possibly achieved due to a lower affinity of such mutant biogenesis factors to the ribosome, resulting higher rates of dissociation and hence passing of the pre-60S quality check point. These observations lead us to propose a novel model for

carcinogenesis offering an explanation for the apparent link between hypo-and hyper-proliferation seen in ribosomopathies (depicted in Figure 57). Given the importance of rpL10 in ribosome biogenesis, mutations that arise in this protein lead to defects in ribosome assembly. As the mutant ribosomes are prevented from entering the active pool of ribosomes because of a failed "test drive", the translational capacity of the cell is greatly diminished, resulting in a severe proliferation defect (hypo-proliferation). Such mutants are under selective pressure to select for mutations that suppress the biogenesis defects, which is sensed by the NRD apparatus. Once acquired, these suppressing mutations can subvert the quality control process and allow utilization of defective ribosomes. However, the continued use of defective ribosomes in translation ultimately drives altered gene expression patterns, evidenced by decreased abundances of -1 PRF signal containing mRNAs, including those implicated in telomere length maintenance (Figures 55 and 56). Thus, we suggest that suppression of the ribosome biogenesis defects represents a critical event in the progression of these cells to T-ALL (hyper-proliferation). As such, while providing a temporary fix by bypassing the primary quality check point in ribosome assembly, suppressing mutations are ultimately themselves the drivers of disease.
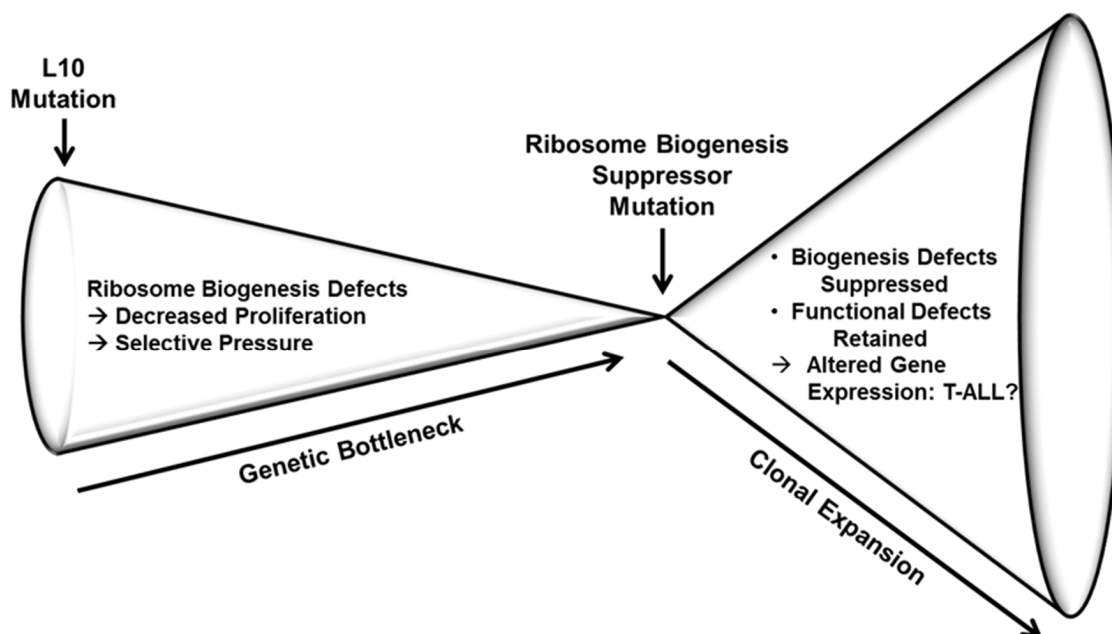
Figure 57. Model of T-ALL progression.

A mutation in L10 results in the inability of the pre-60S subunits to pass the quality control checkpoint, leading to decreased ribosome assembly and proliferation. A ribosome biogenesis suppressor can arise due to selective pressure allowing the bypass the quality "test drive" thereby boosting production of defective ribosomes. Continued defective translation ultimately leads to an altered gene expression profile and the onset of T-ALL.

Mutant ribosomes such as described here represent an attractive novel drug target. As detailed in Chapter 1, many clinically used antibiotics inhibit the proliferation of pathogenic bacteria by binding their ribosomes and interfering with translation. Although these drugs specifically target the prokaryotic ribosome, the presence of a ribosome mutation and resulting impaired ribosome function in eukaryotic cells may sensitize these cells to the effect of such antibiotics directly or in a synthetically lethal way. As such, clinically approved drugs could serve a second life as anti-cancer agents for ribosome defective cancer.

Although this study employed yeast as a model system to probe the molecular defects of T-ALL associated ribosome mutations, the function of the ribosome and the pathway of its assembly are highly conserved between yeast and humans. In fact, human rpL10 and Nmd3 can functionally replace their yeast counterparts [180,234]. Consequently, the mechanisms of bypassing these defects are also likely to be conserved. Using the yeast work described in this chapter as a foundation, we are currently performing similar studies in mouse and human cells, including T-ALL patient T-lymphoblasts. While this work was focused on one suppressor, identifying additional suppressing mutations in yeast should uncover the pathways that cancer cells exploit to avoid the growth inhibition of mutations in *RPL10*. This knowledge will identify new cellular targets for novel drug therapies. In addition, a more complete mechanistic understanding of the ribosome defects contributing to T-ALL will direct the search for additional genes that are mutated in pediatric T-ALL to improve molecular diagnostics and will also improve prognostics for this heterogeneous disease. Importantly, because patients with congenital ribosome defects develop various tumor types [235], the acquired ribosome mutations described in T-ALL may only represent 'the tip of the iceberg': acquired ribosome defects may represent a novel general concept involved in pathogenesis of many tumor types.

Chapter 4

Work in progress: the rpL10 C-terminal tail and autism

Introduction

The previous two chapters describe the importance of the ribosomal protein L10 internal loop, which approaches the peptidyltransferase center (PTC) and acts as the primary sensor of activity in this ribosomal core. Here, we explore the remaining regions of the protein and their functions. These regions comprise the "body" of L10 which lies in a plane along the face of the protein just above the tRNA accommodation corridor, and the C-terminal "tail" which is unique to eukaryotes (Figure 57).

The C-terminal tail of rpL10 is essential in yeast, as even small truncations of this structure are lethal. Mutations in the tail, as well as at the tip of the body of rpL10, resulted in profound defects in general growth, sensitivity to temperatures and antibiotics, and ribosome biogenesis. The locations of these mutations face and closely approach the factor binding site, suggesting that these regions of rpL10 play an important role in ligand binding. This hypothesis is currently being tested through binding experiments assaying the affinity of several *trans*-acting factors to ribosomes containing mutations in the C-terminus of L10.

Importantly, both mutations previously identified in rpL10 (L206M and H213Q) in children affected by autism in two independent families are located in the C-terminus of the protein [180]. One of these mutations, L206M, affects the last amino acid that is conserved between yeast and humans, and almost completely conserved in the whole eukaryotic tree (Figure 58). We introduced this mutation, as well as additional amino acid

substitutions at the rpL10-L206 position covering a range of chemical properties, into

yeast to assay their effects on ribosome structure and function.
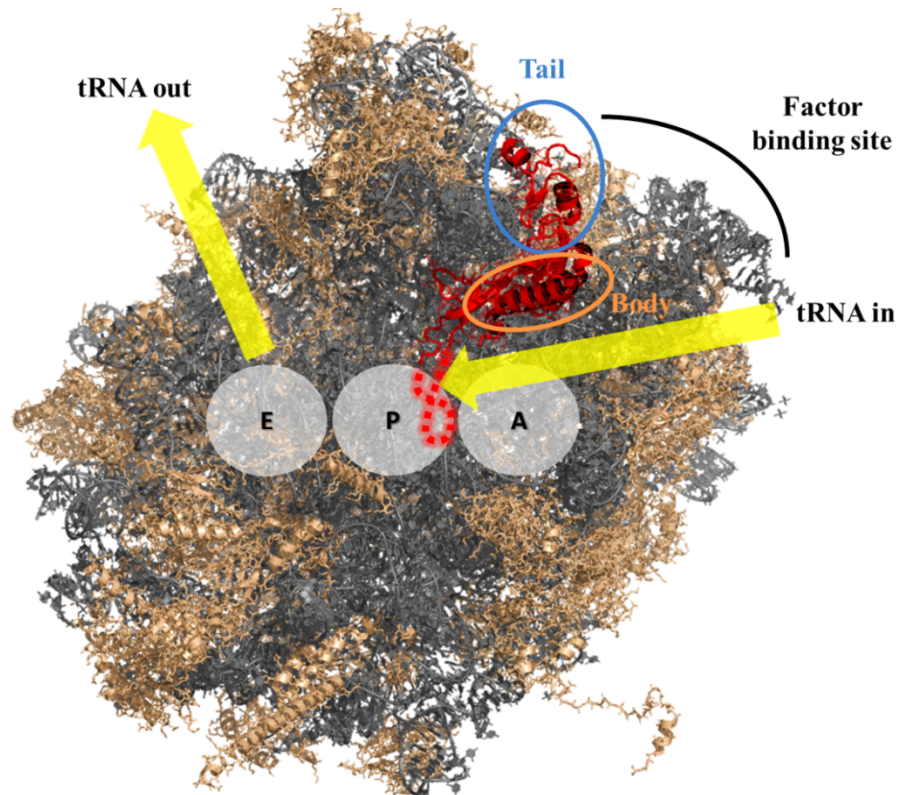
Figure 57. Location of L10 regions in the LSU.

The crown view is shown, and the path taken by tRNAs through the ribosome and the three binding pockets are indicated. L10 is red, with the loop sensing ligand arrival at the ribosomal A-site indicated by dashed lines. Other ribosomal proteins are shown in brown, and rRNA is grey.
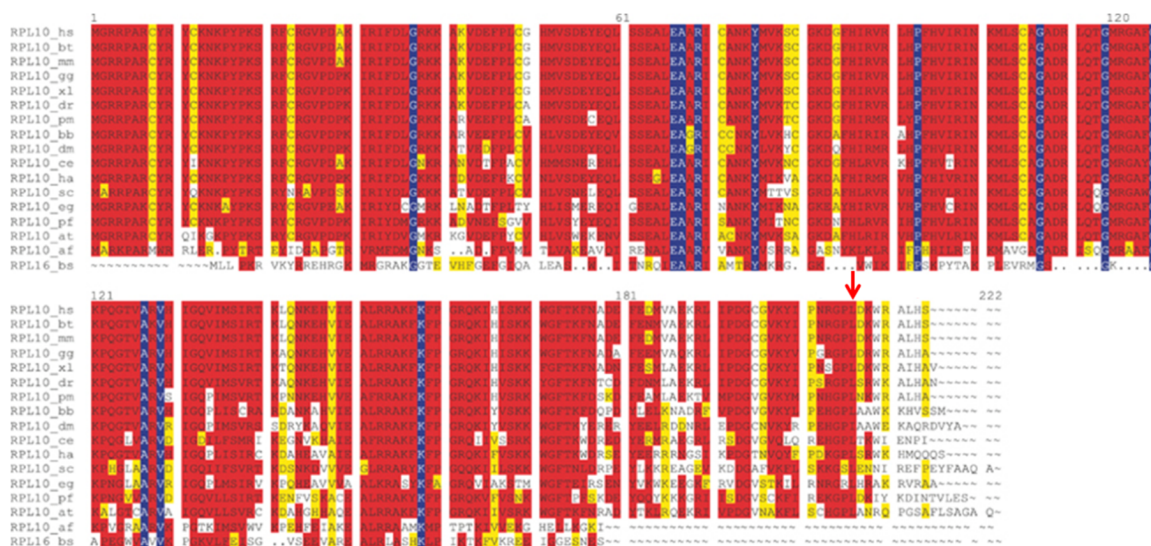
Figure 58. Multiple sequence alignment of L10.

Alignment of RPL10/RPL16 protein sequences. Sequences are abbreviated as follows: hs Homo sapiens; bt Bos taurus; mm Mus musculus; gg Gallus gallus; xl Xenopus laevis; dr Danio rerio; pm Petromyzon marinus; bb Branchiostoma belcheri; dm Drosophila melanogaster; ce Caenorhabditis elegans; ha Hydra attenuate; sc Saccharomyces cerevisiae; eg Euglena gracilis; pf Plasmodium falciparum; at Arabidopsis thaliana af Archaeoglobus fulgidus; bs Bacillus subtilis. Exon 7 is representing the C-terminal domain spanning aa 165–214 of human RPL10. Red arrows: position of the highly conserved aa 206 changed through mutations (L206M) in families with autism. The figure display is shown with clustalW colors. Image modified from Klauck [180].

Results

The "body" and "tail" mutants of rpL10 show general growth defects, and sensitivity to temperature and antibiotics. As ribosome-associated defects commonly result in growth deficiencies, 10-fold dilution spot assays were performed on previously generated mutants having lost the "killer" phenotype [236] on rich medium at the optimal temperature of 30°C (Figure 59). Many mutant cells assayed displayed significant growth defects, particularly those in the C-terminal tail (shown in blue in Fig. 59) or at the tip of the rpL10 body near the C-terminal tail (G81D, N144D, K145E, K145R). Because changes in ribosome structure and function also alter the growth characteristics of cells at various non-optimal temperatures, the same mutants were assayed with regard to their sensitivity or resistance to low (15°C) or high (37°C) temperatures. Almost all of the mutants with growth defects at 30°C also showed slow growth phenotypes on both of these restrictive temperatures. Wild type and mutant cells were also spotted onto medium containing small molecule protein synthesis inhibitors. Anisomycin is a competitive inhibitor at the ribosomal A-site [237], while paromomycin induces the utilization of near-cognate codons due to the stabilization of the mini helix required for GTP hydrolysis by eEF1A [238]. Sensitivity or resistance to these antibiotics suggests defects in the ribosomal A-site and the decoding center, respectively. As seen in Figure 59, several mutants displayed strong resistance to anisomycin, while others showed sensitivity to paromomycin. Notably, the most profound growth defects under all these conditions were seen in mutants of the C-terminal tail and also at the tip of the rpL10 body. One such mutant in the body of rpL10, G81D, was explored in more detail in Chapter 2 and was

shown to contact the elongation factor binding site and to participate in the required

allosteric communication pathways initiated by rpL10 during ribosomal rotation.
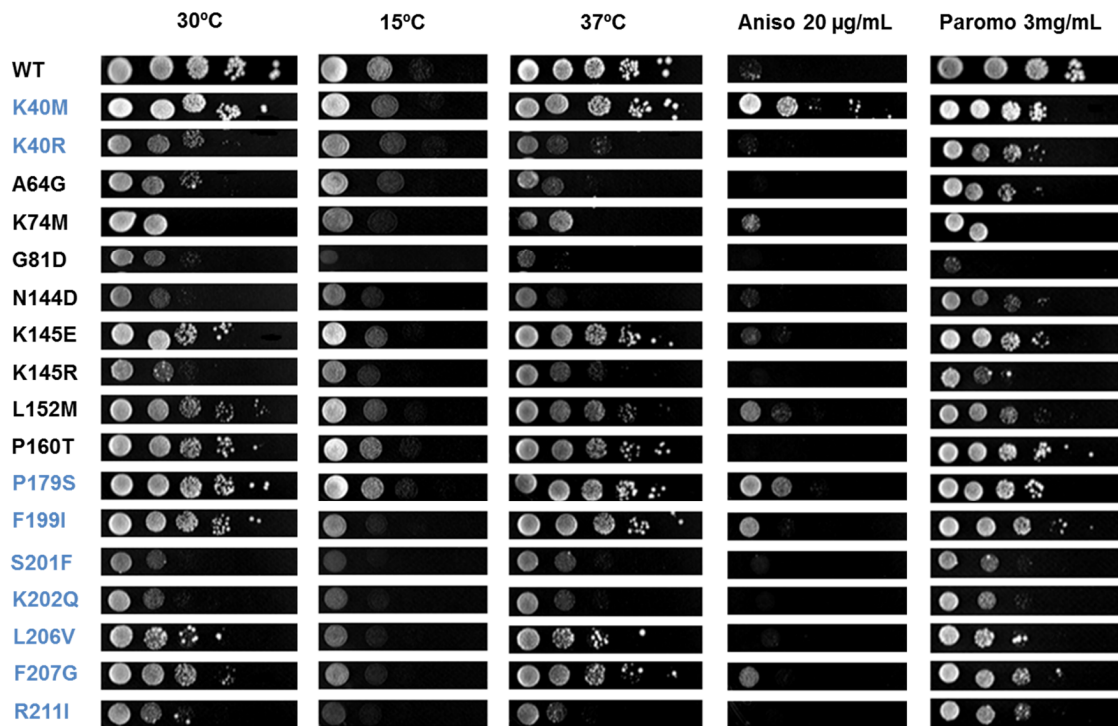
Figure 59. Genetic analysis of rpL10 "body" and "tail" mutants.

Dilution spot assays at indicated temperature and in the presence of the antibiotic anisomycin or paromomycin. Mutants of the C-terminal tail are highlighted in blue. Figure modified from the thesis of Alexey Petrov[236].

The "body" and "tail" mutants of rpL10 show defects in translational fidelity and ribosome biogenesis. As described in the previous chapters, defects in the translational apparatus frequently result in changes in -1 PRF efficiencies. These changes in turn can interfere with virus propagation by altering the ratio of structural to enzymatic proteins available for viral particle assembly, possibly leading to the observed loss the "killer" phenotype of the *rpl10* mutants. The dual luciferase assay was used to quantitatively assess rates of -1 PRF and the inability of ribosomes to correctly recognize termination codons (nonsense suppression). Consistent with the genetic analysis above, mutants in the C-terminal tail and at the tip of the body of rpL10 generally displayed elevated levels of -1 PRF and stop codon read-through, with several mutants displaying lower levels of -1 PRF as compared to wild-type (Figure 60). Five of these mutants also displayed profound defects in subunit biogenesis as assayed by polysome profiling (Figure 61). Of these, three (G81D, K145E, K145R) are located at the tip of the rpL10 body, and two (K40M, L206V) are located in the C-terminal tail. All these mutants displayed strong "halfmer" defects in the polysome profiles, indicative of defects in 40S and 60S subunit joining on the mRNA. In addition, all of these polysome profiles are also marked by a significantly elevated 40S/60S ratio, indicative of defects in 60S maturation. Importantly, the mutation at the position previously shown to play a role in autism (L206V) results in significant changes in both -1 PRF efficiency and ribosome biogenesis. Mutants in the rest of the rpL10 body did not show any significant phenotypic or functional defects.
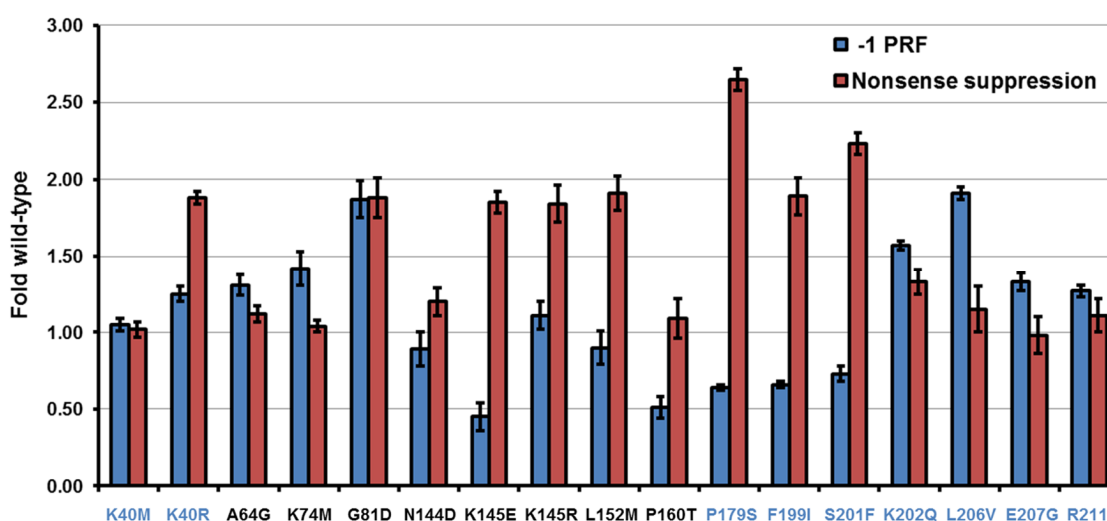
Figure 60. Translation fidelity analysis of rpL10 "body" and "tail" mutants.

Programmed -1 ribosomal frameshifting (L-A) and stop codon misincorporation (UAG) values compared to wild-type levels as monitored using dual-luciferase reporters. Wild-type level of -1 PRF: 8.1% +/- 0.17%. Wild-type level of nonsense suppression: 0.22% +/- 0.01%. Bars indicate s.e.m. (n=4). Mutants of the C-terminal tail are highlighted in blue.
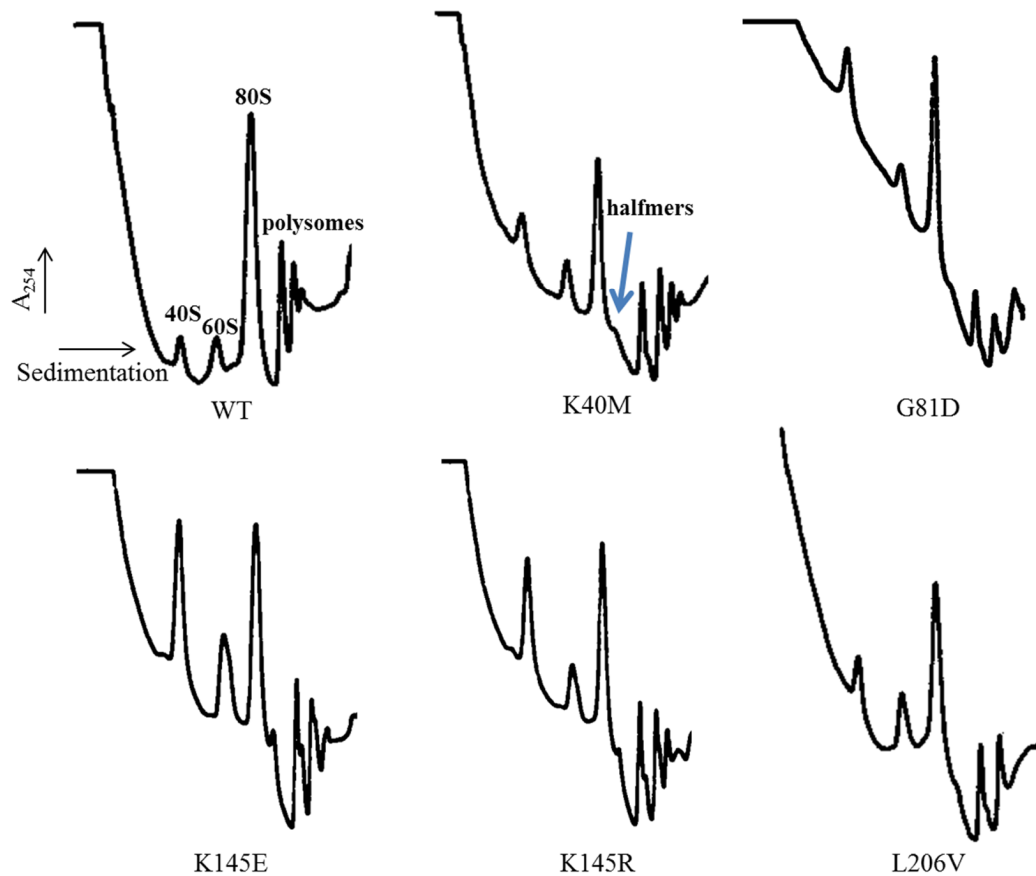
Figure 61. Polysome profiling of rpL10 "body" and "tail" mutants.

Sucrose density gradient analysis. Indicated strains of L10 were grown in glucose to repress genomic *RPL10* for 6 hrs before cells were harvested. Extracts were prepared and 9 A_{260} units were sedimented through 7–47% sucrose gradients.

Discussion

The studies presented here reveal that, in addition to the loop of ribosomal protein L10 described previously, the eukaryotic C-terminal domain of the protein is an additional important ribosomal control element. Mutations in this element at the L206 position have been reported in autism patients [180]. Deletion of the entire C-terminus (aa 170-221) or just the tip of the structure (aa 200-221) which interacts with the 5S rRNA (Figure 62), is lethal (data not shown). This suggests that its interaction with 5S rRNA plays an important role in ribosome function. In particular, examination of the location of the L206 and S201 residues of rpL10 in high resolution structures reveals an apparent interaction with A65 of the 5S rRNA (Figure 62). 5S rRNA is known to be important in translational fidelity in yeast [239], and mutants of A65 are always lethal [240]. Additionally, 5S rRNA is hypothesized to act as a physical transducer of information [241]: it is strategically positioned to link various functional centers of the ribosome and provides a connection to the small subunit. Thus, we hypothesize that the rpL10-L206/S201/5S-A65 "sandwich" interaction is an important component of the allosteric communication pathway initiated by the rpL10 loop in response to ligand binding at the A-site (Chapter 2). Disruption of this interaction likely results in an "uncoordinated" ribosome and translational fidelity defects. This is supported by the fact that these two mutations, particularly S201F, display some of the more profound growth and function defects (Figures 59-61). To test this hypothesis, we have generated additional mutations at the L206 position spanning a range of side-chain properties (L206A/C/E/F/K/M/T). Notably this includes the exact L206M mutation found in autistic patients. As of the time of this writing, shuttle vectors containing these mutants have been generated, and the

corresponding yeast strains are being prepared. It is likely that most of these substitutions will be lethal: very significant changes in phenotype and fidelity seen in *rpl10-L206V* (Figures 59-61) despite minimal changes in side chain chemistry suggests that a very particular delicate type of interaction is needed at that position.

Biochemical, translational fidelity, and gene expression analyses of the viable mutant strains will be performed and will provide insight into their hypothesized modulating effects on ribosome function, which might constitute a leading cause of the distinct neurodevelopmental syndrome autism. This disorder is a most often associated with mental retardation, and is caused mainly by genetic factors with at least three and possibly up to 100 genes [242]. However, more than a hundred candidate genes have been investigated without conclusive evidence for involvement in autistic disorders [243], and functional insight into the mechanism of the disorder is missing. Because there is a high sequence conservation in rpL10 between humans and yeast (65% protein identity), and the amino acid at position 206 is invariably a leucine, these results should provide a solid foundation for future studies in regards to ribosome dysfunction and the onset of autism.

Additionally, biochemical and structural analysis of the *rpl10-L206* mutants will provide a more complete view of how the protein is able to sense ligand binding at the ribosomal A-site, and then communicate this information to distally located functional centers. Mutants in the body region of L10 show far smaller phenotypic and functional defects, except those at the very tip most closely approaching the factor binding site, and most C-terminal mutants show similar profound defects (Figure 62). Because the more deleterious mutations face the factor binding site, it is likely that they also influence ligand binding in this region. In particular, non-enzymatic binding experiments using

128

elongation ternary complex will reveal the role of the C-terminal end in biochemical function: for instance, amelioration of binding defects at the A-site seen in non-enzymatic binding would indicate that the C-terminal tail is a structure that is required for binding the protein component of the ternary complex. This would point to rpL10 participating in the interaction and coordination of the entire ternary complex: the loop senses the tRNA arrival at the A-site, while the C-terminal may act as a docking site for the elongation factor. Such results would likely indicate that the body of rpL10 provides a platform on which the two more dynamic structures, the loop and C-terminus, are attached. In this model, the body of rpL10 functions akin to a piston that is physically linked to multiple functional centers of the machine. The dynamic structures are involved in ligand binding and transduction of information and are sensitive to mutations as a result, while the robust β-sheet foundation is much more tolerant to single amino acid substitutions. Additionally, chemical probing of 5S RNA in L206 mutants will unravel the role of the L206/S201/A65 "sandwich" or "hook" and the structural changes that need to take place at this position to ensure proper allosteric communication within the ribosome.
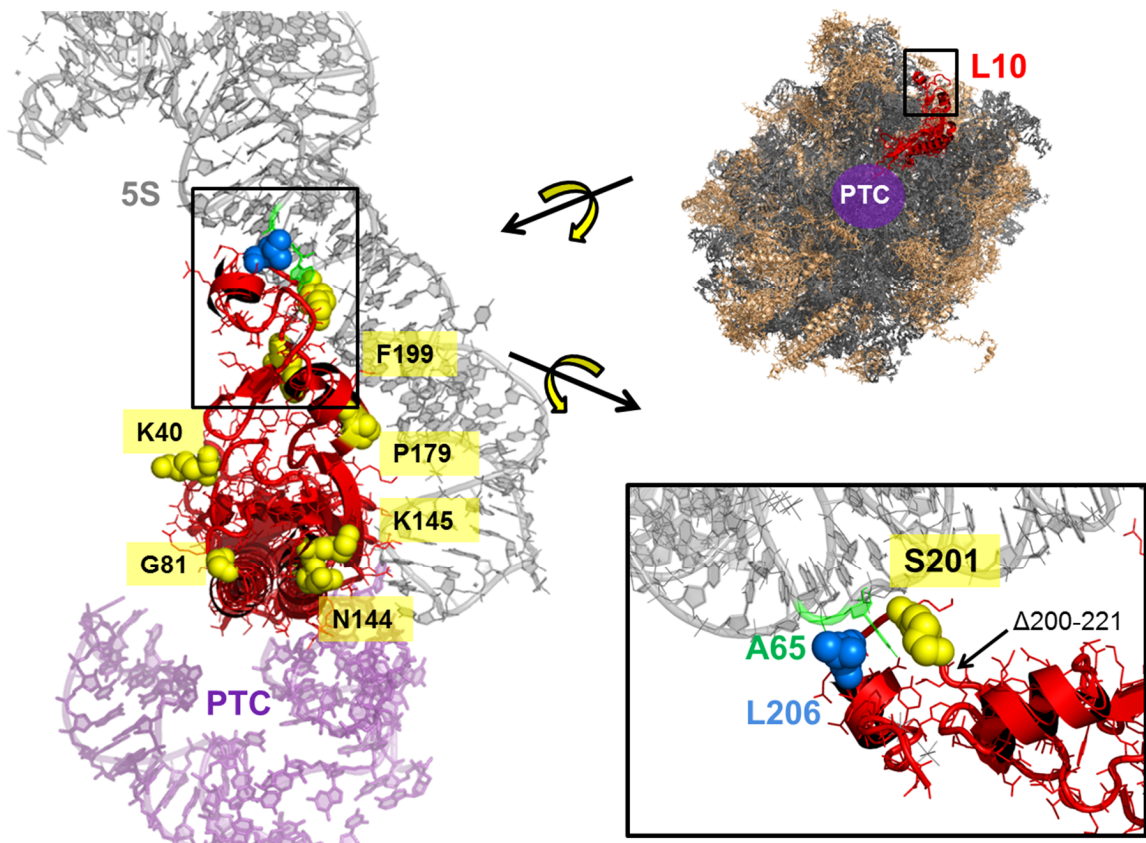
Figure 62. The rpL10 C-terminal tail and location of the L206 "autism residue."

The location of L10 in the "crown view" of the LSU is shown on the top right. Indicated rotation of this structure and zooming in yields the view on the left, showing the backside of L10 composed of the C-terminal tail and the tip of the body of the protein. Location of some of the mutations causing profound growth, fidelity, and biogenesis defects are shown in yellow. Further indicated rotation and zooming in yields the structure on the bottom right. Location of L206 is indicated in blue, A65 of the 5S rRNA is shown in green. The first amino acid that is part of the C-terminal truncation (Δaa200-221) in the lethal mutant is indicated with a black arrow.

Chapter 5

Conclusion and future directions

At the fundamental level, this thesis endeavors to answer a basic biological question: how do ribosomes work? Particularly, how are unidirectionality, order, and quality control achieved during the process of translation? Chapters 2-5 describe the discovery of a central ribosomal control element participating in the coordination of all these parameters. Malfunction of this element contributes to promoting the neoplastic disease acute lymphoblastic T-cell leukemia (T-ALL).

Summary and significance

A flexible loop of the essential ribosomal protein L10 is strategically positioned near the ribosomal peptidyltransferase center, and is the first sensor of arrival of ligands at the ribosomal A-site. The ligand occupancy information is first transduced locally by movement of the protein platform as a result of dynamic changes in loop positioning, to ultimately all important functional centers of the ribosome through rRNA networks, setting the ribosome rotational mechanism in motion. While many other ribosomal proteins are also essential, L10 is a primary sensor and thus an essential initiator of allosteric communication pathways necessary for ribosome dynamics. As a result, any defects in this initial step get amplified through the subsequent series of outward radiating allosteric networks, ultimately leading to biologically significant ribosome dysfunction. This is a very significant finding in the field: contrary to the current view

that rotation can only be achieved through GTP hydrolysis of *trans*-acting factors, this shows that the ribosome alone can actively influence its own rotational status through this mobile loop element. Throughout this thesis and in the field in general, the ribosome is frequently referred to as a "molecular machine". And while translation does require tremendous sophistication and accuracy, this terminology perhaps stereotypes the view of the ribosome as a passive participant. The studies of the L10 loop and its involvement in ribosome structure and function throughout its lifecycle have shown that the ribosome is a more capable "nanomachine" than previously thought, and such knowledge can be applied in nanotechnology. Concerns of machine design center around how structure of each component contributes to function, and how these components interact dynamically to ensure proper function. As one of the primary goals of nanotechnology is to create increasingly smaller machines that operate at the nanometer range, studies as this provide the foundation for the design of new classes of nanodevices, and are crucial complements to the structural work that has been revolutionizing our knowledge of the ribosome. While these studies offer a detailed description of the L10 loop function, they ultimately also provide a wealth of new information to the efforts to form a "big picture" regarding information exchange in the ribosome. For example, this work for the first time identifies landmarks of rotated and non-rotated yeast ribosomes at single nucleotide resolution, as well as several long-range interactions between distally located functional centers - information that will be tremendously useful to future researchers of ribosome mechanics.

Despite more than a half-century of intensive research on the ribosome, the exact roles of many ribosomal components in its biogenesis, and the link between ribosome

biogenesis and translation, are still poorly understood. The findings presented in this project improve our understanding of this link between ribosome biogenesis and translational fidelity. The L10 flexible loop was found to also be involved in a 60S quality control point during ribosome biogenesis, generating the first model of a "test drive" of the large subunit. Indeed, bypassing of this test drive can promote suppression of slow-growing phenotypes.

Medical relevance and future avenues

Because of the essential broad roles played by L10 in biogenesis and translation, defects in the loop are linked to ribosome dysfunction and disease as exemplified by T-ALL. Analysis of such defective ribosomes and cells led to a possible description of the molecular mechanism of this disease, from the underlying structural changes to the biochemical and functional defects, and out to biological function. This illuminates a pathway from genotype to phenotype and in so doing identifies critical control nodes that can be targeted for therapeutic intervention (Figure 63). For example, this knowledge coupled with future small-drug screens could be used to identify new drugs and drug targets that can be exploited to specifically eliminate cells with acquired ribosome defects. Such drugs should cause minimal side effects, because they will leave the healthy cells without ribosome defects untouched. -1 PRF also represents an attractive drug target, as unpublished work from our lab has revealed that levels of frameshifting can be attenuated with miRNAs. Nonsense-mediated decay (NMD) could be altered by knock-down of components of the NMD machinery, though effects of such a treatment are unknown and could be severe, and knockout of NMD components is lethal in

embryonic mice [244]. However, siRNA knockdown levels of specific NMD components could be controlled which could significantly decrease the degradation of target messages of interest. Alternatively, NMD could be controlled by miRNA-mediated stabilization of specific -1 PRF containing messages, leaving global NMD intact.

The presence of acquired ribosome defects in T-ALL cancer cells is a novel finding and it is likely that this mechanism is of general relevance in cancer. For example, cancer risks have been documented in much detail in patients with the ribosomopathy Diamond-Blackfan anemia (DBA). Although DBA patients have a 5-fold higher incidence to develop cancer in general, the cancers they are most predisposed to are colon cancer (36-fold higher incidence than in the general population), osteosarcoma (33-fold higher) and acute myeloid leukemia (28-fold higher) [235]. It is thus not unlikely that acquired ribosome defects may also be present in these cancer types. Therefore, public datasets could be used to analyze these particular tumor types first. Similar analyses can be extended to all other possible tumor types for which data are available afterwards. Such work should pave the way towards the development of diagnostic tests allowing the early identification of patients with acquired ribosome defects. Over the longer term, it may also lead to the development of innovative diagnostic tests for cancers associated with acquired ribosome defects. Development of this class of tests will enable earlier intervention using therapies tailored to specifically target the translation defect specific to the individual patient - personalized medicine.

While mutations in several ribosomal proteins can lead to the onset of DBA, patients also exhibit tissue-specific defects including limb defects, cleft palate, abnormalities in heart development, growth failure and a predisposition for cancer [245].

Interestingly, mutations in different ribosomal proteins also give rise to different types of birth defects. For instance, most patients with rpL5 mutations have a cleft palate, whereas most individuals with rpL11 mutations do not have any craniofacial defects [246]. As such, patients with genetic disorders that are linked to mutations in ribosomal proteins show remarkably specific phenotypes, suggesting that ribosomal proteins have unique functions in different tissues. Studying the molecular mechanism of these defective ribosomes can contribute to the exciting emerging field of "specialized ribosomes" – ribosomes whose specificity may be controlled and fine-tuned by tissue-specific and developmentally regulated signals [247]. The hypothesis that despite the constitutive nature of the ribosome, several components could also give rise to divergent regulation of the molecular machine can be compared to the combustion engine: many subtle variations of the engine exist which are fine-tuned to a diversity of machines and applications, but the fundamental underlying mechanism remains the same. Direct proof supporting the existence of such specialized ribosomes would surely impact the field in a manner similar to the first ribosomal electron microscopy images of the 1970s and the first high resolution structures of the early 2000s.

Final words

The above examples illustrate that there are multiple exciting avenues for future studies on L10 as well as other ribosomal proteins in both yeast and mammals. Similar to scientists who have come before me, particularly Dr. Alexey Petrov who left behind a great platform to initiate my own PhD project, I am grateful and happy to have provided

a solid foundation for future graduate students. To borrow from the thesis title of the former lab member Dr. Michael Rhodin [248] – we are all "cogs in the nanomachine."
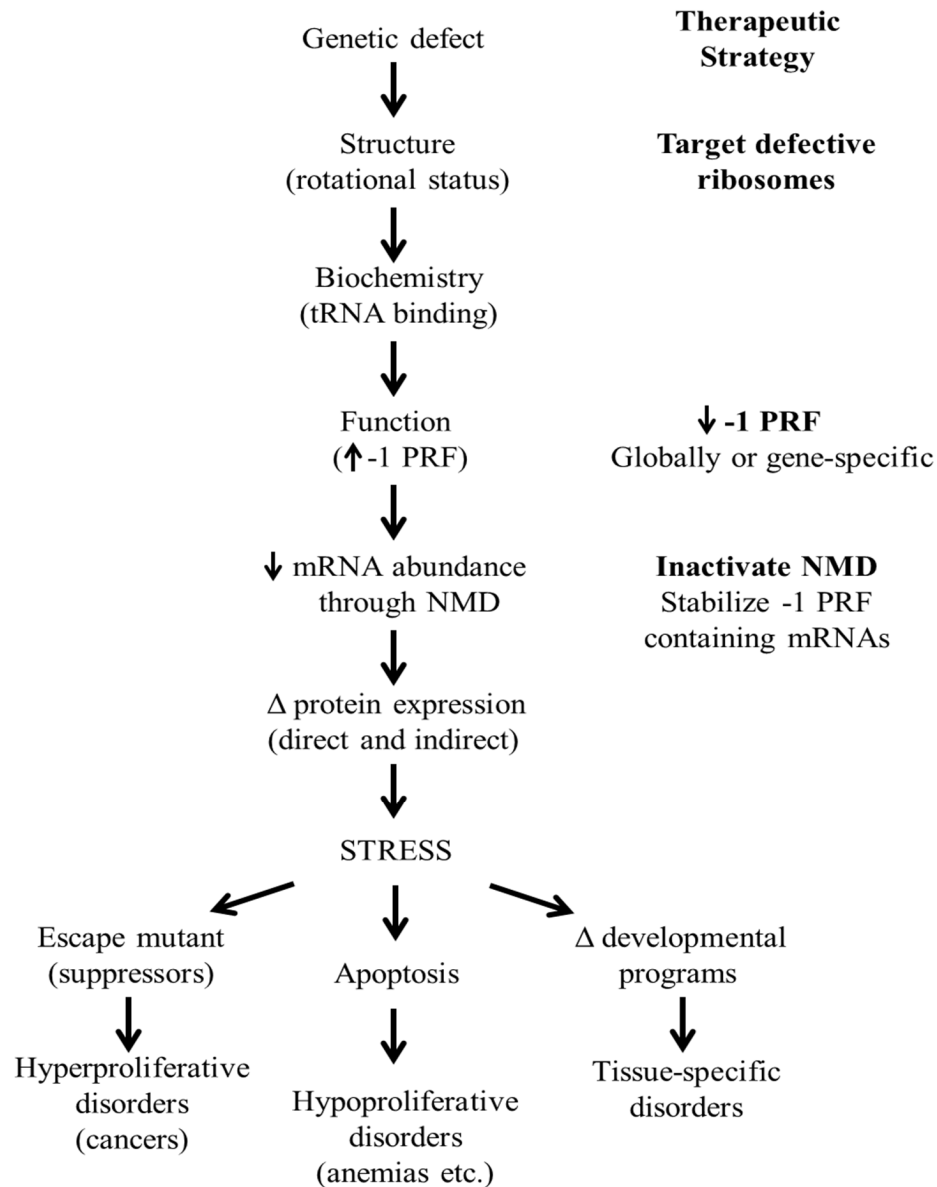
Figure 63. Ribosomopathies: proposed chain of causality.

An acquired mutation in L10 causes ribosomes to distribute more towards a rotated state. This affects the binding of ligands, which in turn drives elevated levels of - 1PRF and the resulting change in mRNA abundances. A changed protein expression profile induces cellular stress, which can lead to three possible mutually non-exclusive pathways.

Chapter 6

Materials and Methods

Media, strains, plasmids, and genetic manipulation.

E. coli DH5α was used to amplify plasmid DNA. Transformation of *E. coli* and yeast, and preparation of yeast growth media (YPAD and synthetic drop out medium) were as reported earlier [249]. Restriction enzymes were obtained from Promega (Madison, WI, USA) and Roche Applied Science (Indianapolis, IN, USA). DNA sequencing was performed by Genewiz (Germantown, MD, USA).

The haploid *S. cerevisiae* strain AJY1437 (*MATα rpl10::Kan lysΔ0 met15Δ0 leu2Δ0 ura3Δ0 his3Δ0* pAJ392) containing wild-type *RPL10* on a centromeric *URA3* vector (pAJ392) has previously been described [187]. In AJY3222, the wild type vector was replaced by wild type *RPL10* on a centromeric *LEU2* vector (pAJ2522) through standard 5-fluoroorotic acid (5-FOA) shuffling techniques [250]. AJY3209 harbors pAJ2609, a centromeric *LEU2* vector expressing the *rpl10-S104D* allele. Similarly, AJY3212 contains pAJ2612, which expresses the *rpl10-A106R* mutant from a centromeric *LEU2* vector; AJY2784 contains pAJ2726, which expresses the *rpl10-R98S* mutant from a centromeric *LEU2* vector. Generation of the *rpl10-F94I* and *rpl10-G81D* expressing strains, JD1308.F94I (*MATα rpl10::Kan met15Δ0 leu2Δ0 ura3Δ0 his3Δ0* pJD589.F94I.HIS) and JD1308.G81D (*MATα rpl10::Kan met15Δ0 leu2Δ0 ura3Δ0 his3Δ0* pJD589.G81D.HIS), was previously described [178]. Identification of suppressing factors has previously been described [187]. In suppression studies, AJY3209 was transformed with pAJ2240, which expresses *TIF6-Y192F* from

138

a centromeric *URA3* vector; AJY2784 was transformed with pAJ2805, which expresses *NMD3-Y379D* from a centromeric *URA3* vector. AJY2104 [186] was transformed with pAJ2522 or pAJ2609 and *RPL3* or *rpl3-W255C* expressed from 2 micron *TRP1* vectors. Standard molecular biology techniques were used to subclone *RPL3* and *rpl3-W255C* into the *HIS3* selectable pRS423 [251]. AJY3209 was subsequently transformed with pRS423-*RPL3* and pRS423-*rpl3-W255C*.

Mutations of the *RPL10* C-terminal domain were generated using the mega-oligo mutagenesis method as previously described [252] (primers listed in Table 6) using pJD589 as the template. The generated plasmids (see Appendix 2) were transformed into JD1293 expressing *RPL10* from a 2 micron *URA3* maintenance plasmid, grown on selective (- his) medium, after which viable cells having lost the wild-type *RPL10*-containing vector were selected by replica plating on 5-FOA.

Dilution spot assays were performed by growing yeast to mid-log growth phase in liquid culture, and spotting them in tenfold serial dilutions from 10^5 to 10^1 colony-forming units per spot on appropriate media, followed by a two day incubation at 30°C or as appropriate.

Translational fidelity and polysome analyses.

The dual luciferase reporter plasmids pYDL-control, pYDL-LA, pYDL-Ty*1,* pYDL-UAA [213], and pYDL-AGC$_{218}$ and pYDL-TCT$_{218}$ [212] were employed to monitor programmed -1 ribosomal frameshifting, programmed +1 ribosomal frameshifting, suppression of UAA, and suppression of an AGC near-cognate serine codon and a TCT non-cognate serine codon in place of the cognate AGA codon in the firefly

luciferase catalytic site, respectively. The reporters were expressed from high-copy *URA3/LEU2*-based plasmids (pJD375, pJD376, pJD376, pJD431, pJD642, pJD643). Assays were performed as previously described [253]. Sample readings were collected using a GloMax Multi-Microplate luminometer (Promega). All assays were repeated 4 times. Sucrose density gradient analysis was carried out as described [187].

mRNA abundance and telomere length analyses.

qRT-PCR experiments to assay mRNA abundance were carried out as described [161]. Similar methods were used to quantify telomere length in yeast cells. Genomic DNA was isolated from mid-logarithmic cell cultures using the 'Smash & Grab' yeast DNA preparation method as described [254]. Each DNA sample was diluted serially. The telomere PCR (T) and the single copy reference gene *SGS1* PCR (S) were performed using the Bio-Rad iTaqTM Universal SYBR Green system using primer pairs complementary to telomere repeats (listed in Table 7), and cycle threshold (Ct) values were determined. The T/S ratios were calculated from three experimental replicates at each of three DNA concentrations (100, 200 and 400 ng).

Peptidyltransferase activity.

Single turnover peptidylpuromycin reactions were performed to assay apparent rates of peptidyltransfer as described [255] with the following modification. Ribosomes pre-bound with Ac-[^{14}C]Phe-tRNA^{Phe} and polyuridylic acid (polyU) were loaded onto pre-wetted Millipore HA (0.45 micron) filters and washed with binding buffer. The

filters were placed into 15 mL scintillation vials and 2.4 mL of binding buffer + 0.05% Zwittergent (EMD BioScience), followed by a 30 min incubation on a rocker at 4°C. Aliquots (1 mL) were taken from each vial, incubated for 5 min at 30°C to activate ribosomes, reactions were initiated by adding pH-neutralized puromycin to 10 mM final concentrations, and the procedure completed as described [255]. Reactions were repeated 4 times.

Sdo1p cloning, purification and labeling.

Sdo1p was cloned into a modified pET-21a, expressing Sdo1p with a C-terminal 6xhistidine tag and a phosphorylatable kemptide (the resulting amino acid sequence beyond the last residue of Sdo1: LEHHHHHHLRRASLG. The S gets phosphorylated). The protein was expressed in Codon Plus bacteria (Stratagene) and purified by Ni-NTA (Invitrogen) chromatography followed by gel filtration on sephacryl S200 (GE Healthcare). Labeling reactions containing 10 μg of Sdo1p, 5x molar excess of $[^{32}P]$-γ-ATP, 1 μl PKA (NEB) in 100 μl 1x kinase buffer (NEB) were incubated for 15 minutes at 30°C, passed through G25 columns (GE) to remove unincorporated ATP, and flow-through was measured by scintillation counting. Flow-through values from control mixtures lacking PKA were subtracted from values of the labeling reactions to determine the specific activity of ^{32}P-labeled Sdo1p, yielding 40-60% label incorporation.

Ribosome preparation.

Purification of active 80S ribosomes using cysteine-charged sulfolink columns was performed as described [256], with the following modifications: after elution from the column, ribosomes were treated with 1 mM final concentration GTP and 1 mM final concentration pH-neutralized puromycin at 30°C for 30 min to remove endogenous tRNAs. After a 100,000 x g 16 -20 hr spin through a high salt glycerol cushion (20 mM HEPES-KOH pH 7.6, 60 mM NH_4Cl, 500mM KCl, 10 mM $Mg(OAc)_2$, 2 mM DTT, 25% glycerol), ribosomes were resuspended in elution buffer and passed through a low salt cushion (20 mM HEPES-KOH pH 7.6, 50 mM NH_4Cl, 5 mM $Mg(OAc)_2$, 1 mM DTT, 25% glycerol) to increase purity.

Ribosome/tRNA interactions.

eEF1A preparation, purification of aminoacyl-tRNA synthetases, charging of $tRNA^{Phe}$ (Sigma) with $[^{14}C]$-phenylalanine (PerkinElmer) and purification of aminoacyl-tRNA and acetylated aminoacyl-tRNA were carried out as described [218,257]. To assay steady-state dissociation rates (K_D) of aa-tRNA to the ribosomal A-site, 2 sets of reactions were set up in parallel. A mix containing 100 μg of polyU, 50 pmoles of ribosomes, a 4-fold molar excess of $tRNA^{Phe}$, all in binding buffer (80 mM Tris-HCl, pH 7.4 at 30° C, 160 mM NH_4Cl, 15 mM $Mg(CH_3COOH)_2$, 2 mM spermidine, 0.5 mM spermine, 6 mM β-mercaptoethanol) in 150 μl total volume was prepared and incubated for 30 min at 30°C to block the P-site. To prepare the ternary complex ($[^{14}C]Phe-tRNA^{Phe} \cdot eEF1A \cdot GTP$), 100 μg of soluble protein factors, 1 mM final concentration of GTP, 125 pmoles $[^{14}C]$-Phe-$tRNA^{Phe}$ were mixed in in 50 μl total

volume binding buffer and incubated for 30 min at 30^0C. After incubation, serial 2-fold dilutions of the ternary complex reaction mix were prepared, resulting in 8 fractions containing decreasing amounts of ternary complex (62.5 - 1 pmoles), in 105 µl each. An equal amount of the ribosome mix (5 pmoles of ribosomes, 15 µl) was added to each dilution, followed by incubation for 30 min at 30^oC. The mixtures were applied onto pre-wetted nitrocellulose Millipore HA (0.45 micron) filters, washed with binding buffer, and radioactivity was measured via scintillation counting. Background control reactions without ribosomes were performed at each ligand dilution and subtracted from experimental ones. K_D values were calculated using GraphPad Prism software fitted to single binding site with ligand depletion models:

$$Y = (-b+\sqrt{(b*b-4*a*c)})/(2*a)$$

Bmax initial Ymax value set to 1.0; a = -1; b = K_D + X + Bmax; c = -1*X*Bmax

X is total ligand added. Y is total binding (X and Y must be expressed in the same units).

Non-enzymatic binding studies were performed likewise, but without eEF1A or by using 50 µg of soluble protein factors (half maximum activity). To test binding of tRNA to the P-site, Ac-[^{14}C]-Phe-tRNA^{Phe} was used as the ligand, there was no need to pre-block with tRNA^{Phe}, and 11 mM Mg($CH_3COOH)_2$ was used in the binding buffer. All reactions were repeated 4 times.

Ribosome/protein interactions.

6x-His-tagged eEF2 was purified from TKY675 yeast cells (a generous gift from Dr. T. Kinzy) as described [258]. Aliquots containing ribosomes (2 pmoles) were first pre-incubated with increasing concentrations of eEF2 (0.25 – 32 pmoles), 100 µg of polyU, 0.1 mM final concentration GDPNP (Sigma), and 4x molar excess of [^{14}C] NAD (PerkinElmer) over ribosomes in 50 µl total volume binding buffer at 30°C for 20 minutes. Diphtheria toxin (0.2 µg, Sigma) was added, and reactions were incubated for 30 min at 30°C. After precipitation with TCA (final concentration 15%) and 15 min incubation on ice, reaction mixtures were applied onto GF/C filters, washed with 5% TCA, and the amount of [^{14}C]-ADP ribosylated eEF2 was determined by scintillation counting. Readings reflect unbound eEF2 and were subtracted from total eEF2 to obtain values bound. Sdo1p binding assays were performed by incubating ribosomes (2 pmoles) with increasing concentrations of Sdo1p (0.25 – 32 pmoles) and 100 µg of polyU in binding buffer (50 mM Tris-(OAc)$_2$ pH 7.5 RT, 50 mM NH4(OAc)$_2$, 10 mM Mg(OAc)$_2$, 2 mM DTT) in 50 µl total volume at 30°C for 20 minutes. The reaction mixtures were then applied onto pre-equilibrated 1 mL polyethylene filter spin columns (Pierce) containing 0.3 mL cysteine-charged sulfolink resin and incubated on ice for 5 minutes. The columns were spun and flow-through measured via scintillation counting. Readings reflect unbound Sdo1p and were subtracted from total loaded to obtain Sdo1p bound. Background control reactions without ribosomes were performed at each ligand dilution. eEF2 assays were repeated 4 times, Sdo1p assays were performed in triplicate.

Ribosome binding competition.

To monitor effects of Sdo1p on tRNA binding to the A-site, wild-type ribosomes (270 pmoles) primed with polyU (0.35 mg), were first mixed with a 4-fold molar excess of uncharged tRNA^{Phe}, 2.8 nmoles GTP, and 5 µg of soluble protein factors (including eEF1A) in 700 µl total volume of ribosome binding buffer. After 10 min incubation at 30ºC, ribosome/tRNA complexes (50 µl aliquots) were added to 10 µl aliquots of 2-fold dilutions of purified Sdo1p (500 pmol – 31 pmol, plus a no-Sdo1p control) and incubated at 30ºC for 10 min. Subsequently, 25 pmol of [^{14}C]Phe-tRNA was added to each ribosome/Sdo1p complex, and incubated at 30ºC for 10 min. The reaction mixtures were applied onto pre-wetted nitrocellulose Millipore HA (0.45 micron) filters, washed with binding buffer, and radioactivity was measured via scintillation counting. Background control reaction values from samples without ribosomes were subtracted from experimental ones. To monitor the ability of Sdo1p to compete for binding at the P-site, the same conditions were employed except that binding reactions were performed in 11 mM magnesium, and [^{14}C]Ac-Phe-tRNA^{Phe} was used. Assays of peptidyltransferase activity were performed as described above in the presence of Sdo1p. All assays were performed twice in triplicate.

Preparation of complexes for chemical probing.

Fifty pmoles 80S ribosomes isolated from isogenic strains were incubated with 100 µg polyU in binding buffer (80 mM HEPES pH 7.5, 50 mM NaCl, 11 mM Mg(OAc)$_2$, 6 mM β-mercaptoethanol) at 30°C for 10 minutes. One set of ribosomes so prepared ("empty 80S" wild-type, rpL10-S104D, rpL10-A106R) was employed for

chemical protection assays. To prepare control "non-rotated" ribosomes, 200 pmoles N-acetyl-phenylalanyl tRNA[Phe] were added and incubations continued for 20 minutes. To prepare "rotated" wild-type ribosomes, empty 80S ribosomes were first incubated with 200 pmoles of deacylated tRNA[Phe]. eEF2 (400 pmoles) and GDPNP (final concentration of 1 mM) were then added to the deacylated tRNA[Phe] - ribosome mixture and incubated for an additional 20 minutes. These conditions were based on results of binding assays as above.

rRNA structure probing.

hSHAPE of rRNA with 1M7 was performed as described [199] using the following substrates: empty ribosomes isolated from isogenic wild type cells, cells expressing mutant ribosomes, and wild-type ribosomes containing acetylated-aa-PhetRNA[Phe] in the P-site (non-rotated control), and deacylated-tRNA[Phe] + eEF2-GDPNP (rotated control). The following primers were employed: 969 and 1780 in the SSU; 25-2, 1466, 2632, 2836, 25-7, and 3225 in the LSU. Data were analyzed using SHAPEFinder [197]. For kethoxal studies, 25 pmoles of ribosomes in a 50 µl volume were treated with 1 µl of a 4% kethoxal solution (in pure ethanol), or 1 µl of ethanol as control, and incubated for 10 min at 30°C. Reactions were stopped by addition of one half volume of stop solution (150 mM sodium acetate, 250 mM potassium borate), followed by analysis as above using primer 969.

Statistical analyses.

Student's t test for two-tailed *p*-value calculations was used throughout. Data analysis of dual-luciferase assays and rRNA probing was carried out as described [199,253]. After generation of rRNA chemical modification data using ShapeFinder [197] the median reactivities of each primer region were used to normalize the raw integrated peak values.

Acknowledgments

Appendix 1: Yeast strain list

Table 4. Yeast strains generated.

Strain Name	Description
JD1586	JD1293*; Δ200-221 in L10
JD1587	JD1293; Δ170-221 in L10
JD1588	JD1293; L206C in L10
JD1589	JD1293; L206E in L10
JD1590	JD1293; L206F in L10
JD1591	JD1293; L206K in L10
JD1592	JD1293; L206M in L10
JD1593	JD1293; L206T in L10

* 1293: (aka AJY1437) MATα rpl10::Kan met15Δ0 leu2Δ0 ura3Δ0 his3Δ0 RPL10.URA3.2μ, K+

Appendix 2: Yeast plasmid list

Table 5. Plasmids generated.

Plasmid Name	Backbone Plasmid	Insertion	Bacterial Marker	Yeast Marker
pJD1932	pRS423	Wild type L3	AmpR	HIS3
pJD1933	pRS423	L3-W255C	AmpR	HIS3
pJD1934	pJD589	L10-Δ200-221	AmpR	HIS3
pJD1935	pJD589	L10-Δ170-221	AmpR	HIS3
pJD1936	pJD589	L10-L206C	AmpR	HIS3
pJD1937	pJD589	L10-L206E	AmpR	HIS3
pJD1938	pJD589	L10-L206F	AmpR	HIS3
pJD1939	pJD589	L10-L206K	AmpR	HIS3
pJD1940	pJD589	L10-L206M	AmpR	HIS3
pJD1941	pJD589	L10-L206T	AmpR	HIS3

Appendix 3: Oligonucleotide primer list

Table 6. Oligonucleotides used in directed mutagenesis.

Strain	Mutation	Forward and Reverse 5' to 3' Oligonucleotide sequence
JD1586	L10-Δ200-221	CGGTGCTTTCGTTAAGTTCTTGTCCAAGAAGGTgttcttttcaaacatttgaactaac * (forward)
		CAGGAAACAGCTATGAC (reverse)
JD1587	L10-Δ170-221	CCCAGGTCAACAAAAGATTATTTTGTCTAAGAAGTGGGGgttcttttcaaacatttgaactaac *
		CAGGAAACAGCTATGAC
JD1588	L10-L206C	CCAAGAAGGGTTCTGTGAAAACAACATCAGAGAATTCCCAGAATACTTTGC
		CCTGCGTTATCCCCTGATTCTGTGGATAACCGTATTACCGCC
JD1589	L10-L206E	CCAAGAAGGGTTCGAAGAAAACAACATCAGAGAATTCCCAGAATACTTTGC
		CCTGCGTTATCCCCTGATTCTGTGGATAACCGTATTACCGCC
JD1590	L10-L206F	CCAAGAAGGGTTCTTTGAAAACAACATCAGAGAATTCCCAGAATACTTTGCTGC
		CCTGCGTTATCCCCTGATTCTGTGGATAACCGTATTACCGCC
JD1591	L10-L206K	CCAAGAAGGGTTCAAAGAAAACAACATCAGAGAATTCCCAGAATACTTTGCTGC
		CCTGCGTTATCCCCTGATTCTGTGGATAACCGTATTACCGCC
JD1592	L10-L206M	CCAAGAAGGGTTCTATGGAAAACAACATCAGAGAATTCCCAGAATACTTTGC
		CCTGCGTTATCCCCTGATTCTGTGGATAACCGTATTACCGCC
JD1593	L10-L206T	CCAAGAAGGGTTCACTGAAAACAACATCAGAGAATTCCCAGAATACTTTGC
		CCTGCGTTATCCCCTGATTCTGTGGATAACCGTATTACCGCC

* Bases at the 5' end of the deleted region are capitalized; bases at the 3' end of the deletion region are written in lower case.

Table 7. Oligonucleotides used in telomere length assays.

Oligonucleotide purpose	Oligonucleotide name	5' to 3' Oligonucleotide sequence
Yeast telomere repeat probe	yTel_Fwd	CAGTGGTGTGGGTGTGCATGGTGGTGT GGGTGTGTGGAC
	yTel_Rev	GCCCACAACCACACCCAACACATCCCA CACCACCTA
Single copy reference gene probe	ySGS1_Fwd	GGCTCTCGTACACTGCCACATCGAATC AATATGCTGACGTACCC
	ySGS1_Rev	CATGTGGAGATGCGGGAATGCGGGAGA ATGTGGAGC

References

1.   Claude, A. The constitution of protoplasm. *Science* **97,** 451–456 (1943).

2.   Claude, A. The constitution of mitochondria and microsomes. *J. Exp. Med.* **80,** 19–29 (1944).

3.   Allfrey, V., Daly, M. M. & Mirsky, A. E. Synthesis of protein in the pancreas. II. The role of ribonucleoprotein in protein synthesis. *J. Gen. Physiol.* **37,** 157–175 (1953).

4.   Hultin, T. Incorporation in vivo of 15N-labeled glycine into liver fractions of newly hatched chicks. *Experim. Cell. Res.* **1,** 372–376 (1950).

5.   Keller, E. B. Turnover of proteins of cell fractions of adult rat liver in vivo. *Fed. Proc.* **10,** 206–210 (1951).

6.   Zamecnik, P. C. & Keller, E. B. Relation between phosphate energy donors and incorporation of labelled amino acids into proteins. *J. Biol. Chem* **209,** 337–354 (1954).

7.   Palade, G. E. A small particulate component of the cytoplasm. *J. Biophys. Biochem. Cyt.* **1,** 59–68 (1955).

8.   Palade, G. E. & Siekevitz, P. Liver microsomes; an integrated morphological and biochemical study. *J. Biophys. Biochem. Cyt.* **2,** 171–200 (1956).

9.   Roberts, R. B. *Microsomal particles and protein synthesis.* vii–viii (Pergamon Press, 1958).

10.   Wittmann, H. G. Architecture of prokaryotic ribosomes. *Ann. Rev. Biochem.* **52,** 35–65 (1983).

11.   Ban, N., Nissen, P., Hansen, J., Moore, P. B. & Steitz, T. A. The complete atomic structure of the large ribosomal subunit at 2.4 Å resolution. *Science* **289,** 905–20 (2000).

12.   Schluenzen, F. *et al.* Structure of functionally activated small ribosomal subunit at 3.3 angstroms resolution. *Cell* **102,** 615–623 (2000).

13.   Carter, A. P. *et al.* Structure of the 30S ribosomal subunit. *Nature* **407,** 327–339 (2000).

14.   Ben-Shem, A., Jenner, L., Yusupova, G. & Yusupov, M. Crystal structure of the eukaryotic ribosome. *Science* **330,** 1203–1209 (2010).

15.   Ben-Shem, A. *et al.* The structure of the eukaryotic ribosome at 3.0 Å resolution. *Science* **334,** 1524–9 (2011).

16.   Anger, A. M. *et al.* Structures of the human and Drosophila 80S ribosome. *Nature* **497,** 80–85 (2013).

17.   Lomakin, I. B. & Steitz, T. A. The initiation of mammalian protein synthesis and mRNA scanning mechanism. *Nature* **500,** 1–6 (2013).

18.   Sharma, M. R., Booth, T. M., Simpson, L., Maslov, D. A. & Agrawal, R. K. Structure of a mitochondrial ribosome with minimal RNA. *PNAS* **106,** 9637–9642 (2009).

19.   Agrawal, R. K. & Sharma, M. R. Structural aspects of mitochondrial translational apparatus. *Curr. Opin. Struct. Biol.* **22,** 797–803 (2012).

20.   Jack, K. *et al.* rRNA pseudouridylation defects affect ribosomal ligand binding and translational fidelity from yeast to human cells. *Mol. Cell* **44,** 660–666 (2011).

21.   Ruggero, D. *et al.* Dyskeratosis congenita and cancer in mice deficient in ribosomal RNA modification. *Science* **299,** 259–62 (2003).

22.   Noller, H. F. RNA structure: reading the ribosome. *Science* **309,** 1508–1514 (2005).

23.   Moore, P. B. Structural motifs in RNA. *Ann. Rev. Biochem.* **68,** 287–300 (1999).

24.   Nierhaus, K. H. & Schulze, H. Minimal set of ribosomal components for reconstitution of the peptidyltransferase activity. *EMBO J.* **1,** 609–13 (1982).

25.   Wilson, D. N. & Nierhaus, K. H. Ribosomal proteins in the spotlight. *Crit. Rev. Biochem. Mol. Biol.* **40,** 243–267 (2005).

26.   DeLano, W. L. The PyMOL molecular graphics system. (2002). at <http://www.pymol.org>

27.   Giege, R., Sissler, M. & Florentz, C. Universal rules and idiosyncratic features in tRNA identity. *Nucleic Acids Res.* **26,** 5017–5035 (1998).

28.   Yusupov, M. M. *et al.* Crystal structure of the ribosome at 5.5 Å resolution. *Science* **292,** 57883–869 (2001).

29.   Griffiths-Jones, S. *et al.* Rfam: annotating non-coding RNAs in complete genomes. *Nucleic Acids Res.* **33,** D121–D124 (2005).

30.   Warner, J. R. The economics of ribosome biosynthesis in yeast. *Trends Biochem.Sci.* **24,** 437–440 (1999).

31.   Cohlberg, J. A. & Nomura, M. Reconstitution of Bacillus stearothermophilus 50S ribosomal subunits from purified molecular components. *J. Biol. Chem.* **251,** 209–21 (1976).

32.   Held, W. A., Ballou, B., Mizushima, S. & Nomura, M. Assembly mapping of 30S ribosomal proteins from Escherichia coli. *J. Biol. Chem.* **249,** 3103–11 (1974).

33.   Held, W. A., Mizushima, S. & Nomura, M. Reconstitution of Escherichia coli 30S ribosomal subunits from purified molecular components. *J. Biol. Chem.* **248,** 5720–30 (1973).

34.   Hosokawa, K., Fujimura, R. K. & Nomura, M. Reconstitution of functionally active ribosomes from inactive subparticles and proteins. *PNAS* **55,** 198–204 (1966).

35.   Fromont-Racine, M., Senger, B., Saveanu, C. & Fasiolo, F. Ribosome assembly in eukaryotes. *Gene* **313,** 17–42 (2003).

36.   Kressler, D., Linder, P. & De La Cruz, J. Protein trans-acting factors involved in ribosome biogenesis in Saccharomyces cerevisiae. *Mol. Cell. Biol.* **19,** 7897–912 (1999).

37.   Granneman, S. & Baserga, S. J. Ribosome biogenesis: of knobs and RNA processing. *Exp. Cell. Res.* **296,** 43–50 (2004).

38.   Henras, A. K. *et al.* The post-transcriptional steps of eukaryotic ribosome biogenesis. *Cell. Mol. Life Sci.* **65,** 2334–2359 (2008).

39.   Kressler, D., Hurt, E. & Bassler, J. Driving ribosome assembly. *Biochim. Biophys. Acta* **1803,** 673–683 (2010).

40.   Lo, K.-Y. *et al.* Defining the pathway of cytoplasmic maturation of the 60S ribosomal subunit. *Mol. Cell* **39,** 196–208 (2010).

41.   Strunk, B. S. & Karbstein, K. Powering through ribosome assembly. *RNA* **15,** 2083–2104 (2009).

42.   Strunk, B. S., Novak, M. N., Young, C. L. & Karbstein, K. A translation-like cycle is a quality control checkpoint for maturing 40S ribosome subunits. *Cell* **150,** 111–21 (2012).

43.   Narla, A. & Ebert, B. L. Ribosomopathies: human disorders of ribosome dysfunction. *Blood* **115,** 3196–205 (2010).

44. Draptchinskaia, N. *et al.* The gene encoding ribosomal protein S19 is mutated in Diamond-Blackfan anaemia. *Nature Genet.* **21,** 169–175 (1999).

45. Liu, J. M. & Ellis, S. R. Ribosomes and marrow failure: coincidental association or molecular paradigm? *Blood* **107,** 4583–4588 (2006).

46. Ebert, B. L. *et al.* Identification of RPS14 as a 5q- syndrome gene by RNA interference screen. *Nature* **451,** 335–339 (2008).

47. Finch, A. J. *et al.* Uncoupling of GTP hydrolysis from eIF6 release on the ribosome causes Shwachman-Diamond syndrome. *Genes & Dev.* **25,** 917–929 (2011).

48. Constantinou, C., Elia, A. & Clemens, M. J. Activation of p53 stimulates proteasome-dependent truncation of eIF4E-binding protein 1 (4E-BP1). *Biol. Cell* **100,** 279–289 (2008).

49. Dai, M.-S. & Lu, H. Inhibition of MDM2-mediated p53 Ubiquitination and Degradation by Ribosomal Protein L5. *J. Biol. Chem.* **279,** 44475 –44482 (2004).

50. Teng, T., Thomas, G. & Mercer, C. A. Growth control and ribosomopathies. *Curr. Opin. Gen. Dev.* **23,** 63–71 (2013).

51. Zaher, H. S. & Green, R. Fidelity at the Molecular Level : Lessons from Protein Synthesis. *Cell* **136,** 746–762 (2009).

52. Laughrea, M. Speed-accuracy relationships during in vitro and in vivo protein biosynthesis. *Biochimie* **63,** 145–68 (1981).

53. Nobel Prize. at <http://www.nobelprize.org/educational/medicine/dna/a/translation/polysome_em.html>

54. Sonenberg, N. & Hinnebusch, A. G. Regulation of translation initiation in eukaryotes: mechanisms and biological targets. *Cell* **136,** 731–45 (2009).

55. Rabl, J., Leibundgut, M., Ataide, S. F. F., Haag, A. & Ban, N. Crystal structure of the eukaryotic 40S ribosomal subunit in complex with initiation factor 1. *Science* **331,** 730 (2011).

56. Asano, K., Clayton, J., Shalev, A. & Hinnebusch, A. G. A multifactor complex of eukaryotic initiation factors, eIF1, eIF2, eIF3, eIF5, and initiator tRNA(Met) is an important translation initiation intermediate in vivo. *Genes & Dev.* **14,** 2534–2546 (2000).

57. Gingras, A. C., Raught, B. & Sonenberg, N. eIF4 initiation factors: effectors of mRNA recruitment to ribosomes and regulators of translation. *Ann. Rev. Biochem.* **68,** 913–63 (1999).

58. Lomakin, I. B., Kolupaeva, V. G., Marintchev, A., Wagner, G. & Pestova, T. V. Position of eukaryotic initiation factor eIF1 on the 40S ribosomal subunit determined by directed hydroxyl radical probing. *Genes & Dev.* **17,** 2786–97 (2003).

59. Pestova, T. V. & Kolupaeva, V. G. The roles of individual eukaryotic translation initiation factors in ribosomal scanning and initiation codon selection. *Genes & Dev.* **16,** 2906–22 (2002).

60. Pestova, T. V. *et al.* Molecular mechanisms of translation initiation in eukaryotes. *PNAS* **98,** 7029–36 (2001).

61. Unbehaun, A. *et al.* Position of eukaryotic initiation factor eIF5B on the 80S ribosome mapped by directed hydroxyl radical probing. *EMBO J.* **26,** 3109–3123 (2007).

62. Wilson, J. E., Pestova, T. V., Hellen, C. U. T. & Sarnow, P. Initiation of protein synthesis from the A site of the ribosome. *Cell* **102,** 511–520 (2000).

63. Hinnebusch, A. G. Molecular mechanism of scanning and start codon selection in eukaryotes. *Microbiol. Mol. Biol. Rev.* **75,** 434–467 (2011).

64. Dias, A. *et al.* The cap-snatching endonuclease of influenza virus polymerase resides in the PA subunit. *Nature* **458,** 914–918 (2009).

65. Flanegan, J. B., Petterson, R. F., Ambros, V., Hewlett, N. J. & Baltimore, D. Covalent linkage of a protein to a defined nucleotide sequence at the 5'-terminus of virion and replicative intermediate RNAs of poliovirus. *PNAS* **74,** 961–965 (1977).

66. Goodfellow, I. *et al.* Identification of a cis-acting replication element within the poliovirus coding region. *J. Virol.* **74,** 4590–600. (2000).

67. Thompson, S. R. Tricks an IRES uses to enslave ribosomes. *Trends Microbiol.* **20,** 1–9 (2012).

68. Costantino, D. A., Pfingsten, J. S., Rambo, R. P. & Kieft, J. S. tRNA–mRNA mimicry drives translation initiation from a viral IRES. *Nat. Struct. Mol. Biol.* **15,** 57–64 (2007).

69. Thompson, S. R., Gulyas, K. D. & Sarnow, P. Internal initiation in Saccharomyces cerevisiae mediated by an initiator tRNA/eIF2-independent internal ribosome entry site element. *PNAS* **98,** 12972–7 (2001).

70. Hellen, C. U. & Sarnow, P. Internal ribosome entry sites in eukaryotic mRNA molecules. *Genes & Dev.* **15,** 1593–1612 (2001).

71. López-Lastra, M., Rivas, A. & Barría, M. I. Protein synthesis in eukaryotes: the growing biological relevance of cap-independent translation initiation. *Biol. Res.* **38,** 121–146 (2005).

72. Thakor, N. & Holcik, M. IRES-mediated translation of cellular messenger RNA operates in eIF2alpha- independent manner during stress. *Nucleic Acids Res.* **40,** 1–12 (2011).

73. Mendez, R. & Richter, J. D. Translational control by CPEB: a means to the end. *Nature Rev. Mol. Cell. Biol.* **2,** 521–529 (2001).

74. Filbin, M. E. Toward a structural understanding of IRES RNA function. *Curr. Opin. Struct. Biol.* **19,** 267–276 (2009).

75. Eriani, G., Delarue, M., Poch, O., Gangloff, J. & Moras, D. Partition of tRNA synthetases into two classes based on mutually exclusive sets of sequence motifs. *Nature* **347,** 203–206 (1990).

76. Fersht, A. R. & Kaethner, M. M. Enzyme hyperspecificity. Rejection of threonine by the valyl-tRNA synthetase by misacylation and hydrolytic editing. *Biochem.* **15,** 3342–3346 (1976).

77. Ling, J., Reynolds, N. & Ibba, M. Aminoacyl-tRNA synthesis and translational quality control. *Ann. Rev. Microbiol.* **63,** 61–78 (2009).

78. Nureki, O. *et al.* Enzyme structure with two catalytic sites for double-sieve selection of substrate. *Science* **280,** 578–582 (1998).

79. Dock-Bregeon, A.-C. *et al.* Achieving error-free translation; the mechanism of proofreading of threonyl-tRNA synthetase at atomic resolution. *Mol. Cell* **16,** 375–386 (2004).

80. Berg, J. M., Tymoczko, J. L. & Stryer, L. *Biochemistry, 5th edition.* (New York: W. H. Freeman, 2002).

81. Rodnina, M. V. & Wintermeyer, W. Fidelity of aminoacyl-tRNA selection on the ribosome: kinetic and structural mechanisms. *Ann. Rev. Biochem.* **70,** 415–435 (2001).

82. Rodnina, M. V., Gromadski, K. B., Kothe, U. & Wieden, H. J. Recognition and selection of tRNA in translation. *FEBS Letters* **579,** 938–942 (2005).

83. Valle, M. *et al.* Cryo-EM reveals an active role for aminoacyl-tRNA in the accommodation process. *EMBO J.* **21,** 3557–3567 (2002).

84. Ogle, J. M. *et al.* Recognition of cognate transfer RNA by the 30S ribosomal subunit. *Science* **292,** 897–902 (2001).

85. Schmeing, T. M. & Ramakrishnan, V. What recent ribosome structures have revealed about the mechanism of translation. *Nature* **461,** 1234–42 (2009).

86. Schuette, J.-C. *et al.* GTPase activation of elongation factor EF-Tu by the ribosome during decoding. *EMBO J.* **28,** 755–65 (2009).

87. Pape, T., Wintermeyer, W. & Rodnina, M. V. Complete kinetic mechanism of elongation factor Tu-dependent binding of aminoacyl-tRNA to the A site of the E. coli ribosome. *EMBO J.* **17,** 7490–7497 (1998).

88. Rodnina, M. V. Long-range signalling in activation of the translational GTPase EF-Tu. *EMBO J.* **28,** 619–620 (2009).

89. Gromadski, K. B., Daviter, T. & Rodnina, M. V. A uniform response to mismatches in codon-anticodon complexes ensures ribosomal fidelity. *Mol. Cell* **21,** 369–377 (2006).

90. Gromadski, K. B. & Rodnina, M. V. Kinetic determinants of high-fidelity tRNA discrimination on the ribosome. *Mol. Cell* **13,** 191–200 (2004).

91. Mittelstaet, J., Konevega, A. L. & Rodnina, M. V. Distortion of tRNA upon near-cognate codon recognition on the ribosome. *J. Biol. Chem.* **286,** 8158–64 (2011).

92. Demeshkina, N., Jenner, L., Westhof, E., Yusupov, M. & Yusupova, G. A new understanding of the decoding principle on the ribosome. *Nature* **484,** 256–259 (2012).

93. Pape, T., Wintermeyer, W. & Rodnina, M. V. Induced fit in initial selection and proofreading of aminoacyl-tRNA on the ribosome. *EMBO J.* **18,** 3800–3807 (1999).

94. Sievers, A., Beringer, M., Rodnina, M. V & Wolfenden, R. The ribosome as an entropy trap. *PNAS* **101,** 7897–7901 (2004).

95. Trobro, S. & Åqvist, J. Mechanism of peptide bond synthesis on the ribosome. *PNAS* **102,** 12395–400 (2005).

96. Rodnina, M. V., Beringer, M. & Wintermeyer, W. How ribosomes make peptide bonds. *Trends Biochem.Sci.* **32,** 20–26 (2007).

97. Beringer, M. & Rodnina, M. V. The ribosomal peptidyl transferase. *Mol. Cell* **26,** 311–321 (2007).

98. Radzicka, A. & Wolfenden, R. A proficient enzyme. *Science* **267,** 90–93 (1995).

99. Woese, C. R. R. Translation: in retrospect and prospect. *RNA* **7,** 1055–1067 (2001).

100. Krupkin, M. *et al.* A vestige of a prebiotic bonding machine is functioning within the contemporary ribosome. *Phil. Trans. R. Soc. Lond. B* **366,** 2972–8 (2011).

101. Fischer, N., Konevega, A. L., Wintermeyer, W., Rodnina, M. V. & Stark, H. Ribosome dynamics and tRNA movement by time-resolved electron cryomicroscopy. *Nature* **466,** 329–333 (2010).

102. Spahn, C. M. T. *et al.* Structure of the 80S ribosome from Saccharomyces cerevisiae–tRNA-ribosome and subunit-subunit interactions. *Cell* **107,** 373–386 (2001).

103. Agirrezabala, X. *et al.* Visualization of the hybrid state of tRNA binding promoted by spontaneous ratcheting of the ribosome. *Mol. Cell* **32,** 190–197 (2008).

104. Valle, M. *et al.* Locking and unlocking of ribosomal motions. *Cell* **114,** 123–134 (2003).

105. Spahn, C. M. T. *et al.* Domain movements of elongation factor eEF2 and the eukaryotic 80S ribosome facilitate tRNA translocation. *EMBO J.* **23,** 1008–1019 (2004).

106. Frank, J., Gao, H., Sengupta, J., Gao, N. & Taylor, D. J. The process of mRNA-tRNA translocation. *PNAS* **104,** 19671–19678 (2007).

107. Noller, H. F., Yusupov, M. M., Yusupova, G. Z., Baucom, A. & Cate, J. Translocation of tRNA during protein synthesis. *FEBS Letters* **514,** 11–16 (2002).

108. Cornish, P. V., Ermolenko, D. N., Noller, H. F. & Ha, T. Spontaneous intersubunit rotation in single ribosomes. *Mol. Cell* **30,** 578–588 (2008).

109. Dunkle, J. A. *et al.* Structures of the bacterial ribosome in classical and hybrid states of tRNA binding. *Science* **332,** 981–4 (2011).

110. Frank, J. & Agrawal, R. K. A ratchet-like inter-subunit reorganization of the ribosome during translocation. *Nature* **406,** 318–322 (2000).

111. Taylor, D. J. *et al.* Comprehensive molecular structure of the eukaryotic ribosome. *Structure* **17,** 1591–1604 (2009).

112. Zhang, W., Dunkle, J. A. & Cate, J. H. D. Structures of the Ribosome in Intermediate States of Ratcheting. *Science* **325,** 1014–1017 (2009).

113. Spiegel, P. C., Ermolenko, D. N. & Noller, H. F. Elongation factor G stabilizes the hybrid-state conformation of the 70S ribosome. *RNA* **13,** 1473–1482 (2007).

114. Uemura, S. *et al.* Real-time tRNA transit on single translating ribosomes at codon resolution. *Nature* **464,** 1012–1017 (2010).

115. Chen, J., Tsai, A., O'Leary, S. E., Petrov, A. & Puglisi, J. D. Unraveling the dynamics of ribosome translocation. *Curr. Opin. Struct. Biol.* **22,** 804–814 (2012).

116. Song, H. W. *et al.* The crystal structure of human eukaryotic release factor eRF1 - Mechanism of stop codon recognition and peptidyl-tRNA hydrolysis. *Cell* **100,** 311–321 (2000).

117. Zhouravleva, G. *et al.* Termination of translation in eukaryotes is governed by two interacting polypeptide chain release factors, eRF1 and eRF3. *EMBO J.* **14,** 4065–72 (1995).

118. Nakamura, Y. & Ito, K. tRNA mimicry in translation termination and beyond. *RNA* **2,** 647–668 (2011).

119. Mora, L. *et al.* The essential role of the invariant GGQ motif in the function and stability in vivo of bacterial release factors RF1 and RF2. *Mol. Micro.* **47,** 267–275 (2003).

120. Seit-Nebi, A., Frolova, L., Justesen, J. & Kisselev, L. Class-1 translation termination factors: invariant GGQ minidomain is essential for release activity and ribosome binding but not for stop codon recognition. *Nucleic Acids Res.* **29,** 3982–3987 (2001).

121. Frolova, L. Y. *et al.* Mutations in the highly conserved GGQ motif of class 1 polypeptide release factors abolish ability of human eRF1 to trigger peptidyl-tRNA hydrolysis. *RNA* **5,** 1014–1020 (1999).

122. Chavatte, L., Seit-Nebi, A., Dubovaya, V. & Favre, A. The invariant uridine of stop codons contacts the conserved NIKSR loop of human eRF1 in the ribosome. *Euro. Mol. Biol. Org. J.* **21,** 5302–5311 (2002).

123. Karimi, R., Pavlov, M. Y., Buckingham, R. H. & Ehrenberg, M. Novel roles for classical factors at the interface between translation termination and initiation. *Mol. Cell* **3,** 601–609 (1999).

124. Becker, T. *et al.* Structural basis of highly conserved ribosome recycling in eukaryotes and archaea. *Nature* **482,** 501–6 (2012).

125. Shoemaker, C. J., Eyler, D. E. & Green, R. Dom34:Hbs1 promotes subunit dissociation and peptidyl-tRNA drop-off to initiate no-go decay. *Science* **330,** 369–72 (2010).

126. Khoshnevis, S., Hauer, F., Milón, P., Stark, H. & Ficner, R. Novel insights into the architecture and protein interaction network of yeast eIF3. *RNA* **18,** 2306–19 (2012).

127. Uchida, N., Hoshino, S.-I., Imataka, H., Sonenberg, N. & Katada, T. A novel role of the mammalian GSPT/eRF3 associating with poly(A)-binding protein in Cap/Poly(A)-dependent translation. *J. Biol. Chem.* **277,** 6700–6707 (2002).

128. Auerbach, T., Bashan, A. & Yonath, A. Ribosomal antibiotics: structural basis for resistance, synergism and selectivity. *Trends Biotech.* **22,** 570–576 (2004).

129. Bulkley, D., Innis, C. A., Blaha, G. & Steitz, T. A. Revisiting the structures of several antibiotics bound to the bacterial ribosome. *PNAS* **107,** 17158–17163 (2010).

130. Hansen, J. L., Moore, P. B. & Steitz, T. A. Structures of five antibiotics bound at the peptidyl transferase center of the large ribosomal subunit. *J. Mol. Biol.* **330,** 1061–1075 (2003).

131. Schlunzen, F. *et al.* Inhibition of peptide bond formation by pleuromutilins: the structure of the 50S ribosomal subunit from Deinococcus radiodurans in complex with tiamulin. *Mol. Micro.* **54,** 1287–1294 (2004).

132. Schlunzen, F. *et al.* Structural basis for the interaction of antibiotics with the peptidyl transferase centre in eubacteria. *Nature* **413,** 814–821 (2001).

133. Tenson, T. & Mankin, A. Antibiotics and the ribosome. *Mol. Micro.* **59,** 1664–1677 (2006).

134. Lambert, T. Antibiotics that affect the ribosome. *Rev. Sci. Tech.* **31,** 57–64 (2012).

135. Zhou, J. *et al.* Design at the atomic level: generation of novel hybrid biaryloxazolidinones as promising new antibiotics. *Bioorg. Med. Chem. Lett.* **18,** 6179–83 (2008).

136. Long, K. S. & Vester, B. Resistance to linezolid caused by modifications at its binding site on the ribosome. *Antimicrob. Agents Chemoth.* **56,** 603–12 (2011).

137. Kannan, K., Vazquez-Laslop, N. & Mankin, A. S. Selective protein synthesis by ribosomes with a drug-obstructed exit tunnel. *Cell* **151,** 508–520 (2012).

138. Sohmen, D., Harms, J. M., Schlunzen, F. & Wilson, D. N. SnapShot: Antiobiotic inhibition of protein synthesis I. *Cell* **18,** 1248.e1 (2009).

139. Eyler, D. E. & Green, R. Distinct response of yeast ribosomes to a miscoding event during translation. *RNA* **17,** 925–932 (2011).

140. Atkins, J., Gesteland, R., Dinman, J. D., Connor, M. O. & Farabaugh, P. J. *Recoding: expansion of decoding rules enriches gene expression. Nucleic Acids and Molecular Biology* **24,** 221–247 (Springer New York, 2010).

141. Dinman, J. D. Programmed Ribosomal Frameshifting Goes Beyond Viruses: Organisms from all three kingdoms use frameshifting to regulate gene expression, perhaps signaling a paradigm shift. *Microbe (Washington, D.C.)* **1,** 521–527 (2006).

142. Biswas, P., Jiang, X., Pacchia, A. L., Dougherty, J. P. & Peltz, S. W. The human immunodeficiency virus type 1 ribosomal frameshifting site is an invariant sequence determinant and an important target for antiviral therapy. *J. Virol.* **78,** 2082–7 (2004).

143. Jacks, T. *et al.* Characterization of ribosomal frameshifting in HIV-1 gag-pol expression. *Nature* **331,** 280–283 (1988).

144. Marra, M. A. *et al.* The genome sequence of the SARS-associated coronavirus. *Science* **300,** 1399–1404 (2003).

145. Schwartz, D. E., Tizard, R. & Gilbert, W. Nucleotide sequence of Rous sarcoma virus. *Cell* **32,** 853–869 (1983).

146. Brierley, I. A., Digard, P. & Inglis, S. C. Characterization of an efficient coronavirus ribosomal frameshifting signal: requirement for an RNA pseudoknot. *Cell* **57,** 537–547 (1989).

147. Harger, J. W., Meskauskas, A. & Dinman, J. D. An "integrated model"of programmed ribosomal frameshifting. *Trends Biochem. Sci.* **27,** 448–454 (2002).

148. Lopinski, J. D., Dinman, J. D. & Bruenn, J. A. Kinetics of ribosomal pausing during programmed-1 translational frameshifting. *Mol. Cell. Biol.* **20,** 1095–1103 (2000).

149. Plant, E. P. *et al.* The 9-Å solution: How mRNA pseudoknots promote efficient programmed- 1 ribosomal frameshifting. *RNA* **9,** 168–174 (2003).

150. Cho, C.-P., Lin, S.-C., Chou, M.-Y., Hsu, H.-T. & Chang, K.-Y. Regulation of programmed ribosomal frameshifting by co-translational refolding RNA hairpins. *PloS ONE* **8,** e62283 (2013).

151. Liao, P. Y., Choi, Y. S., Dinman, J. D. & Lee, K. H. The many paths to frameshifting: kinetic modelling and analysis of the effects of different elongation steps on programmed -1 ribosomal frameshifting. *Nucleic Acids Res.* **39,** 300–312 (2010).

152. Plant, E. P., Rakauskaite, R., Taylor, D. R. & Dinman, J. D. Achieving a golden mean: mechanisms by which coronaviruses ensure synthesis of the correct stoichiometric ratios of viral proteins. *J. Virol.* **84,** 4330–40 (2010).

153. Dinman, J. D. & Wickner, R. B. Ribosomal frameshifting efficiency and gag/gag-pol ratio are critical for yeast M1 double-stranded RNA virus propagation. *J. Virol.* **66,** 3669–76 (1992).

154. Dinman, J. D. Mechanisms and implications of programmed translational frameshifting. *RNA* **3,** 661–73 (2012).

155. Belew, A. T., Hepler, N. L., Jacobs, J. L. & Dinman, J. D. PRFdb: A database of computationally predicted eukaryotic programmed -1 ribosomal frameshift signals. *BMC Genomics* **9,** 339–47 (2008).

156. Jacobs, J. L., Belew, A. T., Rakauskaite, R. & Dinman, J. D. Identification of functional, endogenous programmed -1 ribosomal frameshift signals in the genome of Saccharomyces cerevisiae. *Nucleic Acids Res.* **35,** 165–174 (2007).

157. Manktelow, E., Shigemoto, K. & Brierley, I. Characterization of the frameshift signal of Edr, a mammalian example of programmed -1 ribosomal frameshifting. *Nucleic Acids Res.* **33,** 1553–63 (2005).

158. Wills, N. M., Moore, B., Hammer, A., Gesteland, R. F. & Atkins, J. F. A functional -1 ribosomal frameshift signal in the human paraneoplastic Ma3 gene. *J. Biol. Chem.* **281,** 7082–8 (2006).

159. Belew, A. T., Advani, V. M. & Dinman, J. D. Endogenous ribosomal frameshift signals operate as mRNA destabilizing elements through at least two molecular pathways in yeast. *Nucleic Acids Res.* **39,** 2799–2808 (2011).

160. Plant, E. P., Wang, P., Jacobs, J. L. & Dinman, J. D. A programmed -1 ribosomal frameshift signal can function as a cis-acting mRNA destabilizing element. *Nucleic Acids Res.* **32,** 784–90 (2004).

161. Advani, V., Belew, A. T. & Dinman, J. D. Yeast telomere maintenance is globally controlled by programmed ribosomal frameshifting and the nonsense-mediated mRNA decay pathway. *Translation* **1,** 1–10 (2013).

162. Hulo, C. *et al.* ViralZone: a knowledge resource to understand virus diversity. *Nucleic Acids Res.* **39,** D576–D582 (2011).

163. Craigen, W. J. & Caskey, C. T. Expression of peptide chain release factor 2 requires high-efficiency frameshift. *Nature* **322,** 273–275 (1986).

164. Matsufuji, S. *et al.* Autoregulatory frameshifting in decoding mammalian ornithine decarboxylase antizyme. *Cell* **80,** 51–60 (1995).

165. Farabaugh, P. J., Zhao, H. & Vimaladithan, A. A novel programed frameshift expresses the POL3 gene of retrotransposon Ty3 of yeast: frameshifting without tRNA slippage. *Cell* **74,** 93–103 (1993).

166. Belcourt, M. F. & Farabaugh, P. J. Ribosomal frameshifting in the yeast retrotransposon Ty: tRNAs induce slippage on a 7 nucleotide minimal site. *Cell* **62,** 339–352 (1990).

167. Adamski, F. M., Donly, B. C. & Tate, W. P. Competition between frameshifting, termination and suppression at the frameshift site in the Escherichia coli release factor-2 mRNA. *Nucleic Acids Res.* **21,** 5074–5078 (1993).

168. Liao, P. Y., Gupta, P., Petrov, A. N., Dinman, J. D. & Lee, K. H. A new kinetic model reveals the synergistic effect of E-, P-and A-sites on+ 1 ribosomal frameshifting. *Nucleic Acids Res.* **36,** 2619–2629 (2008).

169. Beier, H. & Grimm, M. Misreading of termination codons in eukaryotes by natural nonsense suppressor tRNAs. *Nucleic Acids Res.* **29,** 4767–82 (2001).

170. Wills, N. M., Gesteland, R. F. & Atkins, J. F. Evidence that a downstream pseudoknot is required for translational read-through of the Moloney murine leukemia virus gag stop codon. *PNAS* **88,** 6991–95 (1991).

171. Yoshinaka, Y., Katoh, I., Copeland, T. D. & Oroszlan, S. Murine leukemia virus protease is encoded by the gag-pol gene and is synthesized through suppression of an amber termination codon. *PNAS* **82,** 1618–1622 (1985).

172. Leibundgut, M., Frick, C., Thanbichler, M., Böck, A. & Ban, N. Selenocysteine tRNA-specific elongation factor SelB is a structural chimaera of elongation and initiation factors. *EMBO J.* **24,** 11–22 (2005).

173. Schomburg, L., Schweizer, U. & Köhrle, J. Selenium and selenoproteins in mammals: extraordinary, essential, enigmatic. *Cell. Mol. Life Sci.* **61,** 1988–1995 (2004).

174. Hao, B. *et al.* A new UAG-encoded residue in the structure of a methanogen methyltransferase. *Science* **296,** 1462–6 (2002).

175. Tron, T., Yang, M., Dick, F. A., Schmitt, M. E. & Trumpower, B. L. QSR1, an essential yeast gene with a genetic relationship to a subunit of the mitochondrial cytochrome bc1 complex, is homologous to a gene implicated in eukaryotic cell differentiation. *J. Biol. Chem.* **270,** 9961–9970 (1995).

176. Dick, F. A. & Trumpower, B. L. Heterologous complementation reveals that mutant alleles of QSR1 render 60S ribosomal subunits unstable and translationally inactive. *Nucleic Acids Res.* **26,** 2442–48 (1998).

177. Eisinger, D. P., Dick, F. A. & Trumpower, B. L. Qsr1p, a 60S ribosomal subunit protein, is required for joining of 40S and 60S subunits. *Mol. Cell. Biol.* **17,** 5136–42 (1997).

178. Petrov, A. N., Meskauskas, A. M., Roshwalb, S. C. & Dinman, J. D. Yeast ribosomal protein L10 helps coordinate tRNA movement through the large subunit. *Nucleic Acids Res.* **36,** 6187–98 (2008).

179. De Keersmaecker, K. *et al.* Exome sequencing identifies mutation in CNOT3 and ribosomal genes RPL5 and RPL10 in T-cell acute lymphoblastic leukemia. *Nature Genet.* **45,** 186–190 (2012).

180. Klauck, S. M. *et al.* Mutations in the ribosomal protein gene RPL10 suggest a novel modulating disease mechanism for autism. *Mol. Psych.* **11,** 1073–1084 (2006).

181. Kirsch, J., Siekevitz, P. & Palade, G. E. Amino acid incorporation in vitro by ribonucleoprotein particles detached from guinea pig liver microsomes. *J. Biol. Chem.* **235,** 1419–1425 (1960).

182. Dinman, J. D. & Kinzy, T. G. Expanding the ribosomal universe. *Structure* **17,** 1547–8 (2009).

183. West, M., Hedges, J. B., Chen, A. & Johnson, A. W. Defining the order in which Nmd3p and Rpl10p load onto nascent 60S ribosomal subunits. *Mol. Cell. Biol.* **25,** 3802–13 (2005).

184. Hedges, J., West, M. & Johnson, A. W. Release of the export adapter, Nmd3p, from the 60S ribosomal subunit requires Rpl10p and the cytoplasmic GTPase Lsg1p. *EMBO J.* **24,** 567–79 (2005).

185. Menne, T. F. *et al.* The Shwachman-Bodian-Diamond syndrome protein mediates translational activation of ribosomes in yeast. *Nature Genet.* **39,** 486–495 (2007).

186. Hofer, A., Bussiere, C. & Johnson, A. W. Mutational analysis of the ribosomal protein Rpl10 from yeast. *J. Biol. Chem.* **282,** 32630–9 (2007).

187. Bussiere, C., Hashem, Y., Arora, S., Frank, J. & Johnson, A. W. Integrity of the P-site is probed during maturation of the 60S ribosomal subunit. *J. Cell Biol.* **197,** 747–59 (2012).

188. Armache, J.-P. *et al.* Localization of eukaryote-specific ribosomal proteins in a 5.5-Å cryo-EM map of the 80S eukaryotic ribosome. *PNAS* **107,** 19754–9 (2010).

189. Voorhees, R. M., Weixlbaumer, A., Loakes, D., Kelley, A. C. & Ramakrishnan, V. Insights into substrate stabilization from snapshots of the peptidyl transferase center of the intact 70S ribosome. *Nat. Struct. Mol. Biol.* **16,** 528–33 (2009).

190. Shammas, C. *et al.* Structural and mutational analysis of the SBDS protein family. Insight into the leukemia-associated Shwachman-Diamond Syndrome. *J. Biol. Chem.* **280,** 19221–9 (2005).

191. Chen, J., Petrov, A., Tsai, A., O'Leary, S. E. & Puglisi, J. D. Coordinated conformational and compositional dynamics drive ribosome translocation. *Nat. Struct. Mol. Biol.* **20,** 718–27 (2013).

192. Agrawal, R. K. *et al.* Visualization of tRNA movements on the Escherichia coli 70S ribosome during the elongation cycle. *J. Biol. Chem.* **150,** 447–60 (2000).

193. Cate, J. H., Yusupov, M. M., Yusupova, G. Z., Earnest, T. N. & Noller, H. F. X-ray crystal structures of 70S ribosome functional complexes. *Science* **285,** 2095–104 (1999).

194. Gao, H. *et al.* Study of the structural dynamics of the E. coli 70S ribosome using real-space refinement. *Cell* **113,** 789–801 (2003).

195. Moazed, D. & Noller, H. F. Intermediate states in the movement of transfer RNA in the ribosome. *Nature* **342,** 142–148 (1989).

196. Stern, S., Moazed, D. & Noller, H. F. Structural analysis of RNA using chemical and enzymatic probing monitored by primer extension. *Methods Enzymol.* **164,** 481–9 (1988).

197. Vasa, S. M., Guex, N., Wilkinson, K. A., Weeks, K. M. & Giddings, M. C. ShapeFinder: a software system for high-throughput quantitative analysis of nucleic acid reactivity information resolved by capillary electrophoresis. *RNA* **14,** 1979–90 (2008).

198. Wilkinson, K. A., Merino, E. J. & Weeks, K. Selective 2'-hydroxyl acylation analyzed by primer extension (SHAPE): quantitative RNA structure analysis at single nucleotide resolution. *Nat. protoc.* **1,** 1610–1616 (2006).

199. Leshin, J., Heselpoth, R., Belew, A. & Dinman, J. D. High throughput structural analysis of yeast ribosomes using hSHAPE. *RNA Biol.* **8,** 478–487 (2011).

200. Rakauskaite, R. & Dinman, J. D. Mutations of highly conserved bases in the peptidyltransferase center induce compensatory rearrangements in yeast ribosomes. *RNA* **17,** 855–64 (2011).

201. Rakauskaite, R. & Dinman, J. D. rRNA mutants in the yeast peptidyltransferase center reveal allosteric information networks and mechanisms of drug resistance. *Nucleic Acids Res.* **36,** 1497–507 (2008).

202. Sanbonmatsu, K. Y., Joseph, S. & Tung, C. S. Simulating movement of tRNA into the ribosome during decoding. *PNAS* **102,** 15854–60 (2005).

203. Schmeing, T. M., Huang, K. S., Strobel, S. A. & Steitz, T. A. An induced-fit mechanism to promote peptide bond formation and exclude hydrolysis of peptidyl-tRNA. *Nature* **438,** 520–524 (2005).

204. Remacha, M. *et al.* Proteins P1, P2, and P0, components of the eukaryotic ribosome stalk. New structural and functional aspects. *Biochem. Cell Biol.* **73,** 959–968 (1995).

205. Nierhaus, K. H. The allosteric three-site model for the ribosomal elongation cycle: features and future. *Biochem.* **29,** 4997–5008 (1990).

206. Rhodin, M. H. J. & Dinman, J. D. A flexible loop in yeast ribosomal protein L11 coordinates P-site tRNA binding. *Nucleic Acids Res.* **38,** 8377–8389 (2010).

207. Rhodin, M. H. J. & Dinman, J. D. An Extensive Network of Information Flow through the B1b/c Intersubunit Bridge of the Yeast Ribosome. *PLoS ONE* **6,** e20048 (2011).

208. Selmer, M. *et al.* Structure of the 70S ribosome complexed with mRNA and tRNA. *Science* **313,** 1935–42 (2006).

209. Ratje, A. H. *et al.* Head swivel on the ribosome facilitates translocation by means of intra-subunit tRNA hybrid sites. *Nature* **468,** 713–6 (2010).

210. Rakauskaite, R. & Dinman, J. D. An arc of unpaired" hinge bases" facilitates information exchange among functional centers of the ribosome. *Mol. Cell. Biol.* **26,** 8992–9002 (2006).

211. Meskauskas, A. & Dinman, J. D. Ribosomal protein L3: gatekeeper to the A site. *Mol. Cell* **25,** 877–888 (2007).

212. Plant, E. P. *et al.* Differentiating between near-and non-cognate codons in Saccharomyces cerevisiae. *PloS ONE* **2,** e517 (2007).

213. Harger, J. W. & Dinman, J. D. An in vivo dual-luciferase assay system for studying translational recoding in the yeast Saccharomyces cerevisiae. *RNA* **9,** 1019–1024 (2003).

214. Kavran, J. M. & Steitz, T. A. Structure of the base of the L7/L12 stalk of the Haloarcula marismortui large ribosomal subunit: analysis of L11 movements. *J. Mol. Biol.* **371,** 1047–1059 (2007).

215. Korostelev, A., Trakhanov, S., Laurberg, M. & Noller, H. F. Crystal structure of a 70S ribosome-tRNA complex reveals functional interactions and rearrangements. *Cell* **126,** 1065–1077 (2006).

216. Gao, Y.-G. *et al.* The structure of the ribosome with elongation factor G trapped in the posttranslocational state. *Science* **326,** 694–699 (2009).

217. Dunkle, J. & Cate, J. H. Ribosome structure and dynamics during translocation and termination. *Annu. Rev. Biophys.* **39,** 227–44 (2010).

218. Meskauskas, A. & Dinman, J. D. A molecular clamp ensures allosteric coordination of peptidyltransfer and ligand binding to the ribosomal A-site. *Nucleic Acids Res.* **38,** 7800–13 (2010).

219. Meskauskas, A. & Dinman, J. D. Ribosomal protein L3 functions as a "rocker switch" to aid in coordinating of large subunit-associated functions in eukaryotes and Archaea. *Nucleic Acids Res.* **36,** 6175–86 (2008).

220. Meskauskas, A. & Dinman, J. D. Ribosomal protein L5 helps anchor peptidyl-tRNA to the P-site in Saccharomyces cerevisiae. *RNA* **7,** 1084–1096 (2001).

221. Meskauskas, A., Russ, J. R. & Dinman, J. D. Structure/function analysis of yeast ribosomal protein L2. *Nucleic Acids Res.* **36,** 1826–35 (2008).

222. Jacks, T., Madhani, H. D., Masiarz, F. R. & Varmus, H. E. Signals for ribosomal frameshifting in the Rous sarcoma virus gag-pol region. *Cell* **55,** 447–458 (1988).

223. Carter, A. P. *et al.* Crystal structure of an initiation factor bound to the 30S ribosomal subunit. *Science* **291,** 498–501 (2001).

224. Lebaron, S. *et al.* Proofreading of pre-40S ribosome maturation by a translation initiation factor and 60S subunits. *Nat. Struct. Mol. Biol.* **19,** 744–53 (2012).

225. Rheinberger, H. J., Sternbach, H. & Nierhaus, K. H. Three tRNA binding sites on Escherichia coli ribosomes. *PNAS* **78,** 5310–14 (1981).

226. Ng, C. L. *et al.* Conformational flexibility and molecular interactions of an archaeal homologue of the Shwachman-Bodian-Diamond syndrome protein. *BMC Struct. Biol.* **9,** 32–40 (2009).

227. Lariviere, F. J., Cole, S. E., Ferullo, D. J. & Moore, M. J. A late-acting quality control process for mature eukaryotic rRNAs. *Molecular cell* **24,** 619–626 (2006).

228. Ruggero, D. & Pandolfi, P. P. Does the ribosome translate cancer? *Nat. Rev. Cancer* **3,** 179–92 (2003).

229. Stumpf, C. R. & Ruggero, D. The cancerous translation apparatus. *Curr. Opin. Gen. Dev.* **21,** 474–83 (2011).

230. Amsterdam, A. *et al.* Many ribosomal protein genes are cancer genes in zebrafish. *PLoS Biol.* **2,** E139 (2004).

231. Van Vlierberghe, P. & Ferrando, A. The molecular basis of T cell acute lymphoblastic leukemia. *J. Clin. Invest.* **122,** 3398–406 (2012).

232. Ho, J. H., Kallstrom, G. & Johnson, A. W. Nascent 60S ribosomal subunits enter the free pool bound by Nmd3p. *RNA* **6,** 1625–1634 (2000).

233. Trotta, C. R., Lund, E., Kahan, L., Johnson, A. W. & Dahlberg, J. E. Coordinated nuclear export of 60S ribosomal subunits and NMD3 in vertebrates. *EMBO J.* **22,** 2841–2851 (2003).

234. Hedges, J., Chen, Y.-I., West, M., Bussiere, C. & Johnson, A. W. Mapping the functional domains of yeast NMD3, the nuclear export adapter for the 60 S ribosomal subunit. *J. Biol. Chem.* **281,** 36579–87 (2006).

235. Vlachos, A., Rosenberg, P. S., Atsidaftos, E., Alter, B. P. & Lipton, J. M. Incidence of neoplasia in Diamond Blackfan anemia: a report from the Diamond Blackfan Anemia Registry. *Blood* **119,** 3815–9 (2012).

236. Petrov, A. N. Wiring the ribosome: Functions of ribosomal proteins L3 and L10, and 5S rRNA (Doctoral dissertation). 132–135 (2006).

237. Grollman, A. P. Inhibitors of protein biosynthesis. II. Mode of action of anisomycin. *J. Biol. Chem.* **242,** 3226–33 (1967).

238. Carter, A. P. *et al.* Functional insights from the structure of the 30S ribosomal subunit and its interactions with antibiotics. *Nature* **407,** 340–8 (2000).

239. Dinman, J. D. & Wickner, R. B. 5S rRNA is involved in fidelity of translational reading frame. *Genetics* **141,** 95–105 (1995).

240. Kiparisov, S. *et al.* Structural and functional analysis of 5S rRNA in Saccharomyces cerevisiae. *Mol. Genet. Gen.* **274,** 235–247 (2005).

241. Dinman, J. D. 5S rRNA: Structure and Function from Head to Toe. *Int. J. Biomed. Sci.* **1,** 2–7 (2005).

242. Volkmar, F. R. & Pauls, D. Autism. *Lancet* **362,** 1133–41 (2003).

243. Klauck, S. M. Genetics of autism spectrum disorder. *Eur. J. Hum. Genet.* **14,** 714–20 (2006).

244. Medghalchi, S. M. *et al.* Rent1, a trans-effector of nonsense-mediated mRNA decay, is essential for mammalian embryonic viability. *Hum. Mol. Genet.* **10,** 99–105 (2001).

245. Boria, I. *et al.* The ribosomal basis of Diamond-Blackfan Anemia: mutation and database update. *Hum. Mut.* **31,** 1269–79 (2010).

246. Gazda, H. T. *et al.* Ribosomal protein L5 and L11 mutations are associated with cleft palate and abnormal thumbs in Diamond-Blackfan anemia patients. *Am. J. Hum. Gen.* **83,** 769–80 (2008).

247. Xue, S. & Barna, M. Specialized ribosomes: a new frontier in gene regulation and organismal biology. *Nat. Rev. Mol. Cell. Biol.* **13,** 355–69 (2012).

248. Rhodin, M. H. J. Ribosomal protein L11: a cog in the nanomachine (Doctoral dissertation). (2011).

249. Ito, H., Fukuda, Y., Murata, K. & Kimura, A. Transformation of intact yeast cells treated with alkali cations. *J. Bacteriol.* **153,** 163–168 (1983).

250. Boeke, J. D., LaCroute, F. & Fink, G. R. A positive selection for mutants lacking orotidine-5'-phosphate decarboxylase activity in yeast: 5-fluoro-orotic acid resistance. *Mol. Gen. Genet.* **197,** 345–6 (1984).

251. Christianson, T. W., Sikorski, R. S., Dante, M., Shero, J. H. & Hieter, P. Multifunctional yeast high-copy-number shuttle vectors. *Gene* **110,** 119–22 (1992).

252. Tseng, W.-C., Lin, J.-W., Wei, T.-Y. & Fang, T.-Y. A novel megaprimed and ligase-free, PCR-based, site-directed mutagenesis method. *Anal. Biochem.* **375,** 376–8 (2008).

253.   Jacobs, J. L. & Dinman, J. D. Systematic analysis of bicistronic reporter assay data. *Nucleic Acids Res.* **32,** e160 (2004).

254.   Rose, M. D., Winston, F. & Hieter, P. *Methods in Yeast Genetics: A Laboratory Course Manual.* 180 (Cold Spring Harbor Laboratory Press, 1987).

255.   Meskauskas, A., Harger, J. W., Jacobs, K. L. M. & Dinman, J. D. Decreased peptidyltransferase activity correlates with increased programmed -1 ribosomal frameshifting and viral maintenance defects in the yeast Saccharomyces cerevisiae. *RNA* **9,** 982–992 (2003).

256.   Leshin, J. A., Rakauskaitė, R., Dinman, J. D. & Meskauskas, A. Enhanced purity, activity and structural integrity of yeast ribosomes purified using a general chromatographic method. *RNA Biol.* **7,** 354–60 (2010).

257.   Meskauskas, A., Petrov, A. N. & Dinman, J. D. Identification of functionally important amino acids of ribosomal protein L3 by saturation mutagenesis. *Mol. Cell. Biol.* **25,** 10863–74 (2005).

258.   Ortiz, P. A., Ulloque, R., Kihara, G. K., Zheng, H. & Kinzy, T. G. Translation elongation factor 2 anticodon mimicry domain mutants affect fidelity and diphtheria toxin resistance. *J. Biol. Chem.* **281,** 32639–48 (2006).